博士論文

論文題目

Gelation process of homogeneous polymer network iongel and application to CO_2 separation membrane

（均一高分子網目イオンゲルの形成過程解析とその二酸化炭素分離膜への応用）

氏　　名

橋本　慧

Doctoral Dissertation

Department of Advanced Materials Science

Graduate School of Frontier Sciences, The University of Tokyo

Gelation process of homogeneous polymer network iongel and application to CO_2 separation membrane

2015

Kei Hashimoto

Contents

Chapter 1

General Introduction

1.1 Ionic Liquids and its Application

Room-temperature ionic liquids (ILs), i.e., salts composed of only ions with melting points lower than room-temperature, have attracted attentions as a new type of solvents in the scientific and industrial fields [1–4]. ILs have unique solvent properties including non-volatility, non-flammability, high thermal and electrochemical stabilities [5], which are essentially different from conventional molecular solvent or aqueous systems. These general properties of ILs mentioned above originate from the complicated interactions between cations and anions such as Coulombic interaction, hydrogen bond, π–π interaction and van der Waals interaction. These various cation–anion interactions in ILs also have an effect on its solubility to make specific affinities to target molecules (e.g. metal ions [6, 7], macromolecules [8], biomacromolecules [9] and gases [10–12]). That is, these novel solvent properties can be easily designed by controlling the interactions between anion and cation, i.e., the combination of cation and anion. This property, designability is one of the reason why intense number of research for ILs have been performed and reported until now.

The studies for application of ILs have been rapidly developing since 1992, when Wilkes et al. reported water/air-stable imidazolium-based ILs, for example, 1-ethyl-3-methyl imidazolium tetrafluoroborate ($[C_2mIm^+][BF_4^-]$) [13, 14]. Since this report, numerous ILs have been suggested and investigated in the wide application field such as electrochemistry [15], dissolution/separation studies [7, 16], synthetic organic and catalytic chemistry [17–19]. These applications are closely related to its dissolution ability. For example, ILs are used for applications as solvent for dissolution and conversion of cellulose into fuel or functionalized polymer [20–24]. Rogers et al. reported some ILs composed of imidazolium-based cation and chloride anion can dissolve cellulose with relatively low temperature ($\sim$100°C) [25] although

cellulose could not be dissolved by conventional organic liquids or water even with intense heat. Recently, Ohno et al. reported that some phosphonate-based ILs can easily dissolve cellulose under mild condition [26], for example, 1-ethyl-3-methylimidazolium methylphosphonate, $[C_2mIm^+][CH_3(H)PO_3^-]$, dissolves 2–4 wt% cellulose at room temperature with high dissolution rate as shown in Figure 1.1.

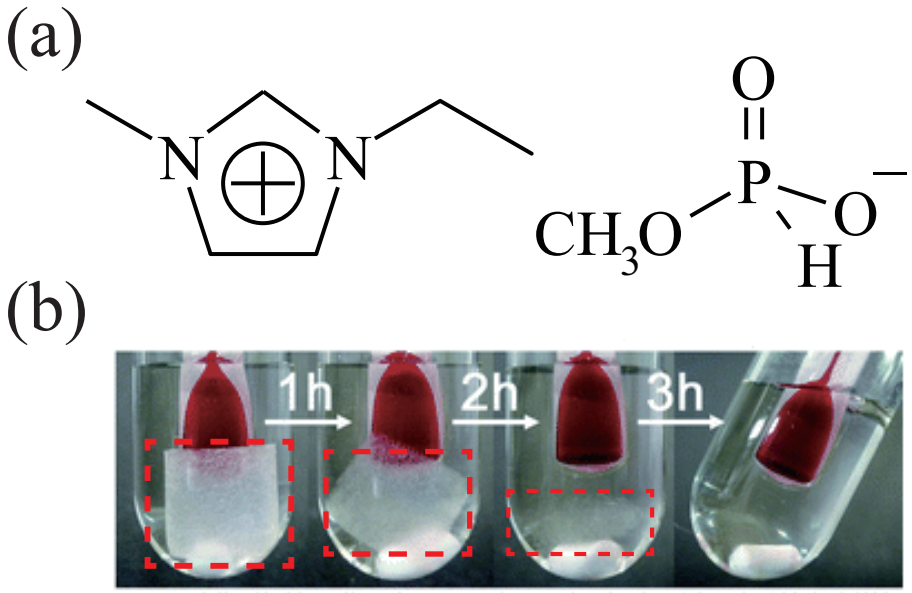

Figure 1.1. (a) The molecular formula of $[C_2mIm^+][CH_3(H)PO_3^-]$ and (b) cellulose dissolution in $[C_2mIm^+][CH_3(H)PO_3^-]$. The broken line indicates cellulose residual. This figure was reprinted from [26].

This cellulose solubility enables us to extract biomass energy from numerous types of plants composed of cellulose without complicated and large apparatus. In this way, ILs are applied as a task-specific solvent to show unique solubility by controlling its solvent properties.

One of the most popular research of ILs is application for electrolytes [27–29]. The high electrochemical stability and high ion conductivity of some cation and anion types enable application for electrochemical devices such as lithium-ion batteries [30–32], fuel cells [33, 34] and actuators [35, 36]. The advantages of IL-based electrolytes are negligible volatility and non-flammability, which offer longer life-time and more advanced safety than conventional organic solvents. In the application as lithium-ion batteries, the affinity to lithium-ion, i.e., high dissolution amount as well as high diffusion rate of the ion, is required. To develop ILs with more electrochemically stable and higher lithium-ion conductivity, numerous combinations of anion and cation have been suggested and investigated. Mat-

sumoto et al. reported that combination of pyrrolidinium cations and bis(fluorosulfonyl)imide ([FSI$^-$]) anion shows good charge-discharging cycling stability of a Li/$LiCoO_2$ with high transport rate [37]. Watanabe et al. reported lithium-ion-based IL by using balky borate salts containing two methoxy-oligo(ethylene oxide) groups and trifluoroacetyl groups as anion, which shows high ion conductivity and electrochemical stability [30, 38]. Many researchers have tried to develop ILs with high lithium-ion transport ability comparable to conventional electrolyte and it is one of the important research for energy application using ILs. On the other hand, the research for solid electrolyte using ILs has also attracted much attentions to prevent the leakage of liquid [38, 39]. Until now, various support materials for ILs including inorganic, organic and polymeric materials have been developed and investigated [40]. However, as the support materials for electrolyte, there are many requirements such as good compatibility with ILs, high mechanical toughness, thermal and electrochemical stabilities. Therefore, establishment of solidification method for ILs is still in progress.

Recently, CO_2 gas separation has attracted much attentions because excessive CO_2 production causes environmental problems such as global warming and air pollution. Blanchard et al. reported that an imidazolium-based ILs containing fluorine shows high CO_2 absorption ability [41], leading to application as CO_2 absorption media with non-volatility, thermal and chemical stability. In addition, CO_2 is highly soluble in ILs relative to other gases like N_2, H_2, and CH_4 [42], that is, ILs show CO_2 absorption selectivity to separate CO_2 gas from mixed gases. Therefore, a large number of investigations for CO_2 separation using ILs have been performed [43–46]. The pressure swing absorption method is mainly investigated to separate CO_2 gas from a mixed gases under pressure according to the affinity of IL to CO_2, as illustrated in Figure 1.2.

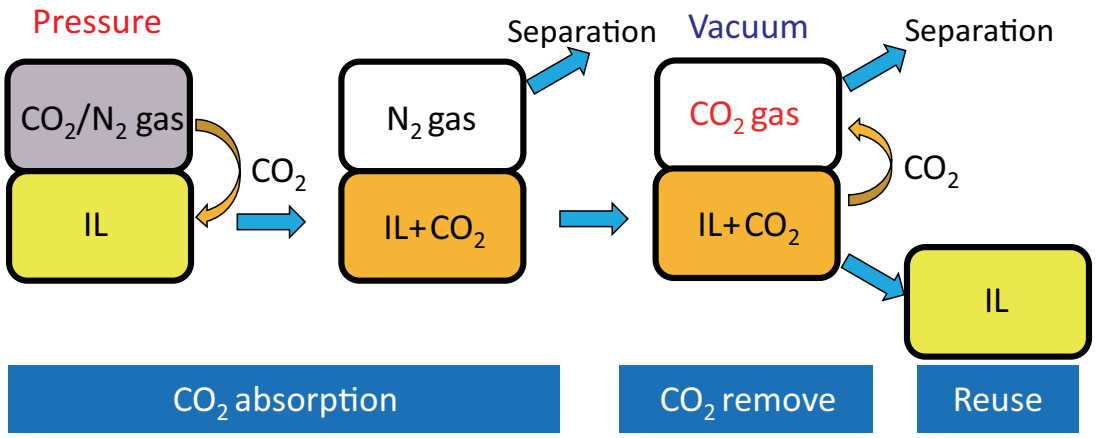

Figure 1.2. Illustration of the CO_2 separation process using pressure swing method.

Under high pressure, only CO_2 gas is dissolved and extracted to IL phase from mixed

gases. By separating liquid phase and gas phase, CO_2-removed gas and ILs which contains CO_2 can be obtained. After separation, ILs emit CO_2 under low pressure for reuse. Due to non-volatility of ILs, the loss of solvent can be negligible, which is one of the advantages of IL compared with conventional solvents (aqueous amine solution or organic solvent) in this method. However, this method needs pressure swing from high pressure to vacuum, thus a large and complicated apparatus with high energy consumption is required for separation.

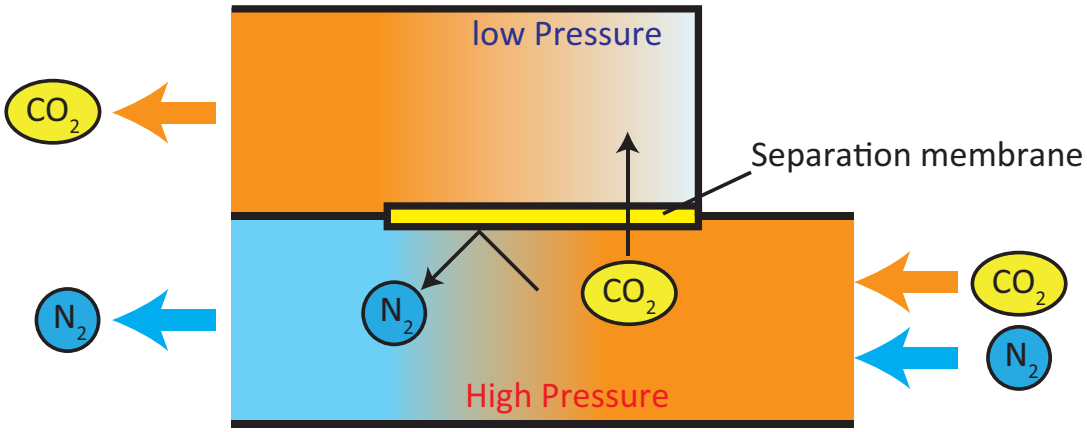

Figure 1.3. Illustration of the CO_2 separation process using separation membrane.

As an alternative separation method, a separation membrane method using ILs as illustrated in Figure 1.3 has attracted much attentions. Only CO_2 gas passes through the membrane due to selective affinity between ILs and CO_2 without pressure swing. Thus, this method generally requires smaller operational energy compared with conventional methods. In addition, due to non-volatility and thermal stability of ILs, the separation process can be performed in wide range of pressure and temperature unless the membrane does not break. Here, note that, it is essential to solidify ILs for application to separation membrane and thus the solidification of ILs is one of the important studies also in CO_2 separation [47, 48].

In this way, the solidification of ILs is one of the hottest topics because the liquid material has a serious disadvantage, the leakage of liquid. For the applications as not only CO_2 separation membranes but also electrolytes, leakage is inevitable problems in materials using ILs. To improve this property, some composite materials using ILs have been suggested to solidify ILs.

1.2 Composite Materials Using ILs

The composite materials with ILs are roughly classified to three types; supported IL membranes (SILMs), polymeric ILs and iongels, as illustrated in Figure 1.4. The SILMs,

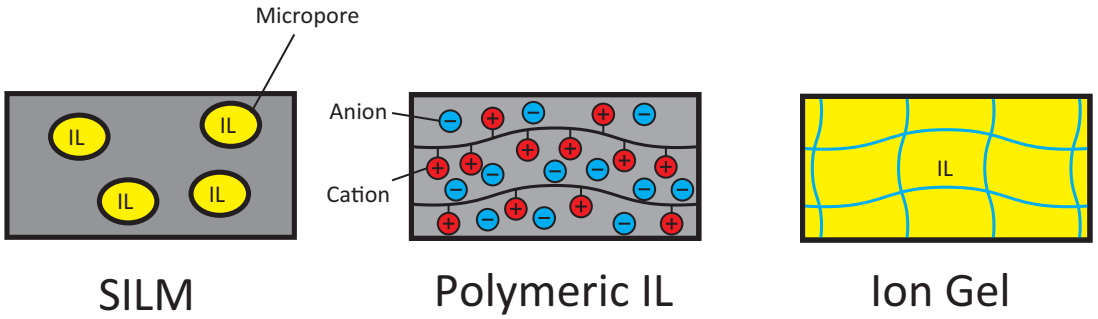

Figure 1.4. Illustration of three types of composite material using ILs, SILM, Polymeric IL and iongel.

i.e., polymeric or inorganic porous materials filled with ILs, are the most investigated ones, but they have a serious disadvantage. The supported materials cannot hold ILs under high pressure because they hold ILs with weak surface tension. Thus, SILM does not work under high pressure or at high temperature. Polymeric ILs, i.e., polymers made by cross-linking ILs themselves, which can strongly hold ILs, were also suggested for solidification of ILs. However, it was pointed out that the separation performances or ion conductivities are inferior to that of the SILM. In the polymeric ILs, ILs are bound to rigid polymer matrix, resulting in limited diffusion of gas molecules or ions. By contrast, iongels, which can strongly hold solvents in their polymer network structure, can hold ILs under high pressure and they contain "free" ILs. Thus, the iongels show inherent solvent properties of ILs comparable to SILMs or neat ILs.

However, a gel is generally brittle material. Watanabe et al. reported typical ion-gel composed of poly(methyl methacrylate) (PMMA) and 1-ethyl-3-methylimidazolium bis(trifluoromethanesulfonyl)amide($[C_2mIm^+][TFSA^-]$), which shows too small elastic modulus for application under high pressure (for example, iongel with 20 wt% polymer content shows only 10 Pa elastic modulus, i.e., one of the indicators for the mechanical toughness) [39]. To obtain free-standing iongel, they added high content of polymer (up to 60%), but the ionic conductivity decreases due to decrease of content of IL. Similar to this example, a low IL content leads to decrease in the inherent IL properties including CO_2 separation performances, which is a serious problem in the development of iongels as new soft materials. Therefore, iongels with both low polymer content and high mechanical toughness are required for application studies using iongels.

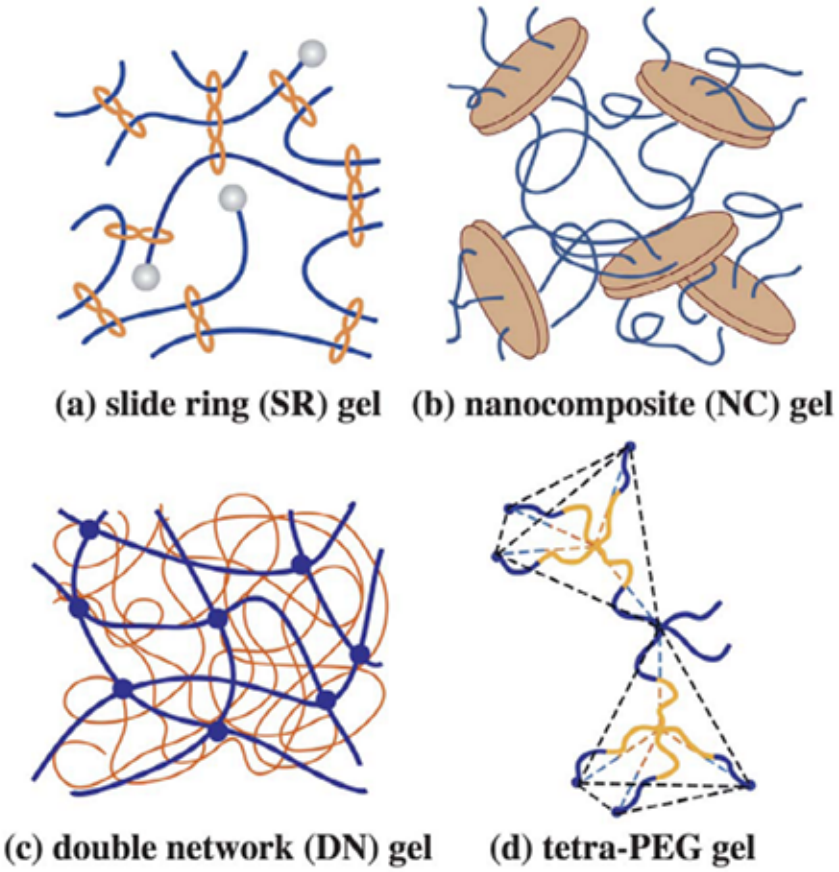

Figure 1.5. Schematic illustration of (a) slide-ring gel, (b) nano-composite (NC) gel, (c) double network (DN) gel and (d) tetra-PEG gel. These illustrations were reprinted from [49].

1.3 Previous Studies for TetraPEG Hydrogel and Iongel

In the hydrogel system, many tough hydrogels have been explored and investigated. Shibayama reviewed tough hydrogels, for example, nano-composite gel (NC gel), double-network gel (DN gel), slide-ring gel and TetraPEG gel (Figure 1.5), and pointed out that the mechanical properties of these gels deeply depend on the polymer network structure, especially, homogeneity of polymer network [49]. Among them, Tetra-PEG gels, which are prepared by cross-end-coupling of two kinds of tetra-arm poly(ethylene glycol) prepolymers of the same size, have ideal homogeneous polymer network, which have been studied by small-angle neutron scattering (SANS) measurements [50]. This homogeneous network results in homogeneous dispersion of tension to be the origin of the high mechanical toughness of TetraPEG gel [51, 52].

Here, note that, the homogeneity of TetraPEG gel originates in not only tetra-arm

structure of prepolymers but also reaction mechanism between two kinds of terminals, i.e., amide formation between NH_2- and *N*-hydroxysuccinimide- (activated ester) terminals. Our research group investigated the gelation kinetics of TetraPEG in water by using UV measurement and pointed out that the gelation of TetraPEG is not a diffusion-limited mechanism, but a reaction-limited mechanism [53, 54]. In a reaction-limited reaction, the reaction rate of prepolymers is much slower than their self-diffusion. Thus, prepolymers can sufficiently diffuse and homogeneously mix with each other, before the cross-end coupling reaction occurs. This results in formation of homogenous network structure and high reaction efficiency (>90%), leading to high mechanical toughness of TetraPEG hydrogel. We achieved this reaction-limited reaction by the control of the gelation reaction rate, which strongly depends on the concentration of H^+ ($[H^+]$ or pH). That is, the reaction rate depends on the acid-base reaction of the NH_2 terminal, $\text{-}NH_2 + H^+ \rightleftarrows \text{-}NH_3{}^+$, because the protonated $NH_3{}^+$ does not react with activated ester terminal. It has already been established that TetraPEG hydrogels with high toughness and a homogeneous polymer network can be prepared in aqueous solutions using a phosphate-type buffer with constant pH ($\sim$ 7) during the gelation reaction.

We previously proposed a iongel using tetra-armed poly(ethylene glycol) (TetraPEG) as a network polymer, which shows a high mechanical toughness (18 MPa of maximum breaking compression modulus at 83.5% strain) with extremely low polymer content ($\sim$6 wt%) [55]. From SANS measurement, it was suggested that TetraPEG iongel prepared in ILs has a homogeneous polymer network structure similar to the TetraPEG hydrogel [56]. The TetraPEG iongel has both high IL content and high mechanical toughness. Thus, it is a promising material for CO_2 separation membrane or solid electrolyte. However, the mechanical properties of TetraPEG iongels are inferior to the corresponding hydrogels.

Figure 1.6 shows stress-elongation curves for 6 wt% TetraPEG iongel and hydrogel. As can be clearly seen, both maximum breaking stretching ratio ($\lambda_{\max}$) and maximum breaking stretching stress ($\sigma_{\max}$) for the iongel are smaller than the values for hydrogel. The elastic modulus can be estimated from the initial slope of the curves in small deformation and the value for iongel is estimated to be 7.2 kPa although the value for hydrogel is approximately 11 kPa. This results might be ascribed to the connectivity defects (or low reaction efficiency) caused during the reaction in ILs because the gelation control, which is essential to produce homogeneous polymer networks, has not been established in IL system.

Therefore, in this doctoral dissertation, I elucidated the gelation mechanism of TetraPEG iongel on the basis of acid-base reaction and reaction kinetics to control the gelation reaction. By establishing the control of the gelation reaction, I successfully prepared a tough iongel

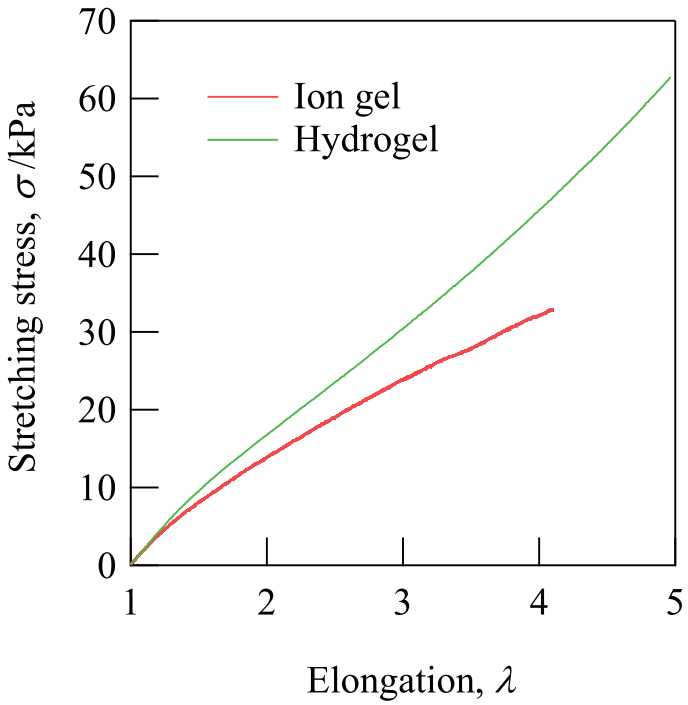

Figure 1.6. Stress-elongation curves for 6 wt% TetraPEG iongel together with corresponding data for TetraPEG hydrogel [55].

enough to be applied as solid electrolyte or CO_2 separation membrane. I confirmed that the solvent properties of the TetraPEG iongel is almost equivalent to composing IL from CO_2 separation experiment in this study.

1.4 Outline of the Dissertation

In the previous section, I pointed out that the control of NH_2/protonated NH_3^+ group fraction and reaction rate plays a key role in the preparation of homogeneous TetraPEG gel with high mechanical toughness. However, the acid-base reactions in ILs, which essentially differ from those in conventional solvents, have not been well investigated and established at the present stage.

In Chapter 2 and 3, I thus investigated the acid-base reactions in two types of ILs, protic ILs and aprotic ILs (the former have dissociative proton in cation and the latter have no dissociative proton) by direct pH measurement.

In Chapter 2, I investigated the acid-base property of protic IL, 1-alkylimidazolium bis(trifluoromethanesulfonyl)amide ($[C_nImH^+][TFSA^-]$, n: alkyl-chain length), by potentiometric titration. The equilibrium constant, $K_s = [C_nIm][HTFSA]$ on the autoprotolysis reaction ($C_nImH^+ + TFSA^- \rightleftarrows C_nIm + HTFSA$) was successfully determined for $n = 2$ and 4 systems and the validity of potentiometric titration using ion-sensitive field effect (ISFET) electrode was confirmed.

In Chapter 3, I investigated the acid-base reaction of NH_2 in typical aprotic IL $[C_2mIm^+][TFSA^-]$. The quantitative Brønsted basicity of butylamine ($BuNH_2$) in the $[C_2mIm^+][TFSA^-]$ was determined. The pK_a value of butylammonium ($BuNH_3^+$) was estimated by potentiometric titration to be 16.6(1), and it was found that the value is significantly larger than that in aqueous solution (pKa = 10.6). The large pK_a might be ascribed to solvation structures unique to IL system.

In Chapter 4, the solvation structures of $BuNH_2$ and $BuNH_3^+$ in $[C_2mIm^+][TFSA^-]$ were investigated by high-energy X-ray total scattering (HEXTS) experiments with the aid of molecular dynamics (MD) simulations from the viewpoint of protonation effect on solvation structures. The nearest-neighbor molecular distance for $BuNH_3^+$–$TFSA^-$ was smaller than that for $BuNH_2$–$TFSA^-$, which indicates strong interaction between solute and anions occurs by protonation. In both systems, a specific interaction between the anion and amine group, i.e., hydrogen bonding between oxygen atoms of $TFSA^-$ anion and hydrogen atoms of amine/ammonium group, was found. From the spatial distribution functions (SDFs) obtained from MD simulations, it was pointed out that the coordination number of $TFSA^-$ anion

increased from 2 to 3, resulting in large stabilization energy. This results indicate that the large pK_a value originates in drastic change in solvation structure by protonation.

In Chapter 5 and 6, I reported the gelation mechanism of tetra-armed prepolymer in $[C_2mIm^+][TFSA^-]$ on the basis of acid-base reaction discussed in the previous chapters.

In Chapter 5, I applied the protic IL, 1-ethylimidazolium $TFSA^-$ ($[C_2ImH^+][TFSA^-]$) as a nonvolatile H^+ source to control the gelation reaction rate. It was found that the gelation time of TetraPEG iongel can be successfully controlled, suggesting that the acid-base properties of NH_2 terminal also play a key role in the gelation process. However, the reaction efficiency of amide bond (cross-linked point) systematically decreased with increasing proton concentration, leading to a low mechanical toughness of the iongels. This results indicates that excess proton binds with NH_2 terminal to make unreactive terminal and thus it forms network defects due to low reaction efficiency. This result indicates that removal of excess protons by pH control can improve the reaction efficiency of TetraPEG iongel.

In Chapter 6, to control solution pH, I established a "pH-buffering IL" by adding protic IL (as a proton source) and its conjugated base to the solvent aprotic IL. I demonstrated that the pH-buffering IL exhibits a successful pH-buffering effect to maintain a constant pH during the gelation reaction. From a kinetic study, I found that the gelation reaction undergoes a simple second-order reaction of the two TetraPEGs in the pH-buffering IL. The gelation rate constant, k_{gel} in the present iongel system was two orders of magnitude smaller than that in the corresponding hydrogel system, which implies reaction-limited mechanism. The reaction efficiency at the cross-linking point was experimentally estimated to be 92% by spectroscopic measurements. I thus conclude that a defect-free polymer network can be prepared in the pH-buffering IL system.

In Chapter 7, TetraPEG iongel has been applied to CO_2 separation study. I evaluated the CO_2 separation performance of TetraPEG iongel which contains 6 wt% polymer. The iongel shows excellent CO_2 permselectivity equivalent to neat IL over the high temperature range up to 100°C. This remarkable CO_2 separation property of TetraPEG iongel originates in a large fraction of ionic liquid (94 wt%), owing to the homogeneous network structure of TetraPEG iongel.

Reference

[1] N. V. Plechkova and K. R. Seddon. *Chem. Soc. Rev.*, Vol. 37, pp. 123–150, 2008.

[2] M. J. Earle and K. R. Seddon. *Pure Appl. Chem.*, Vol. 72, pp. 1391–1398, 2000.

[3] M. C. Bubalo, S. Vidovic, I. R. Redovnikovic, and S. Jokic. *J. Chem. Technol. Biotechnol.*, Vol. 90, pp. 1631–1639, 2015.

[4] A. Farran, C. Cai, M. Sandoval, Y. Xu, J. Liu, M. J. Hernaiz, and R. J. Linhardt. *Chem. Rev.*, Vol. 115, pp. 6811–6853, 2015.

[5] N. De Vos, C. Maton, and C. V. Stevens. *Chemelectrochem*, Vol. 1, pp. 1258–1270, 2014.

[6] A. E. Visser, R. P. Swatloski, W. M. Reichert, R. Mayton, S. Sheff, A. Wierzbicki, J. H. Davis, and R. D. Rogers. *Chem. Commun.*, pp. 135–136, 2001.

[7] A. Rout, K. A. Venkatesan, T. G. Srinivasan, and P. R. V. Rao. *Desalin. Water. Treat.*, Vol. 38, pp. 179–183, 2012.

[8] T. Ueki and M. Watanabe. *Macromolecules*, Vol. 41, pp. 3739–3749, 2008.

[9] H. Zhao, C. L. Jones, and J. V. Cowins. *Green Chem.*, Vol. 11, pp. 1128–1138, 2009.

[10] C. Cadena, J. L. Anthony, J. K. Shah, T. I. Morrow, J. F. Brennecke, and E. J. Maginn. *J. Am. Chem. Soc.*, Vol. 126, pp. 5300–5308, 2004.

[11] M. Besnard, M. I. Cabaco, F. V. Chavez, N. Pinaud, P. J. Sebastiao, J. a. P. Coutinho, J. Mascetti, and Y. Danten. *J. Phys. Chem. A*, Vol. 116, pp. 4890–4901, 2012.

[12] J. Blath, N. Deubler, T. Hirth, and T. Schiestel. *Chem. Eng. J.*, Vol. 181, pp. 152–158, 2011.

[13] J. S. Wilkes and M. J. Zaworotko. *J. Chem. Soc., Chem. Commun.*, pp. 965–967, 1992.

[14] J. S. Wilkes. *Green Chem.*, Vol. 4, pp. 73–80, 2002.

[15] H. Ohno. *Electrochemical aspects of ionic liquids*. Wiley-Interscience, Inc. Hoboken, New Jersey, 2005.

[16] C. P. Kapnissi-Christodoulou, I. J. Stavrou, and M. C. Mavroudi. *J. Chromatogr. A*, Vol. 1363, pp. 2–10, 2014.

[17] H. Zhao and G. A. Baker. *Front. Chem. Sci. Eng.*, Vol. 9, pp. 262–279, 2015.

[18] M. K. Potdar, G. F. Kelso, L. Schwarz, C. Zhang, and M. T. W. Hearn. *Molecules*, Vol. 20, pp. 16788–16816, 2015.

[19] R. Sheldon. *Chem. Commun.*, pp. 2399–2407, 2001.

[20] H. Wang, G. Gurau, and R. D. Rogers. *Chem. Soc. Rev.*, Vol. 41, pp. 1519–1537, 2012.

[21] H. Miyafuji. *J. Wood Sci.*, Vol. 61, pp. 343–350, 2015.

[22] L. Feng and Z.-I. Chen. *J. Mol. Liq.*, Vol. 142, pp. 1–5, 2008.

[23] S. H. Lee, T. V. Doherty, R. J. Linhardt, and J. S. Dordick. *Biotechnol. Bioeng.*, Vol. 102, pp. 1368–1376, 2009.

[24] R. Rinaldi, R. Palkovits, and F. Schueth. *Angew. Chem. Int. Ed.*, Vol. 47, pp. 8047–8050, 2008.

[25] R. P. Swatloski, S. K. Spear, J. D. Holbrey, and R. D. Rogers. *J. Am. Chem. Soc.*, Vol. 124, pp. 4974–4975, 2002.

[26] Y. Fukaya, K. Hayashi, M. Wada, and H. Ohno. *Green Chem.*, Vol. 10, pp. 44–46, 2008.

[27] D. R. Macfarlane, N. Tachikawa, M. Forsyth, J. M. Pringle, P. C. Howlett, G. D. Elliott, J. H. Davis, M. Watanabe, P. Simon, and C. A. Angell. *Energy. Environ. Sci.*, Vol. 7, pp. 232–250, 2014.

[28] M. Armand, F. Endres, D. R. Macfarlane, H. Ohno, and B. Scrosati. *Nat. Mater.*, Vol. 8, pp. 621–629, 2009.

[29] M. Galinski, A. Lewandowski, and I. Stepniak. *Electrochim. Acta*, Vol. 51, pp. 5567–5580, 2006.

[30] H. Shobukawa, H. Tokuda, S. Tabata, and M. Watanabe. *Electrochim. Acta*, Vol. 50, pp. 305–309, 2004.

[31] H. Yoon, A. S. Best, M. Forsyth, D. R. Macfarlane, and P. C. Howlett. *PCCP*, Vol. 17, pp. 4656–4663, 2015.

[32] M. A. Navarra. *MRS Bull.*, Vol. 38, pp. 548–553, 2013.

[33] S. Y. Lee, A. Ogawa, M. Kanno, H. Nakamoto, T. Yasuda, and M. Watanabe. *J. Am. Chem. Soc.*, Vol. 132, pp. 9764–9773, 2010.

[34] H. Matsuoka, H. Nakamoto, M. Susan, and M. Watanabe. *Electrochim. Acta*, Vol. 50, pp. 4015–4021, 2005.

[35] J. Ding, D. Z. Zhou, G. Spinks, G. Wallace, S. Forsyth, M. Forsyth, and D. R. Macfarlane. *Chem. Mater.*, Vol. 15, pp. 2392–2398, 2003.

[36] T. Fukushima, K. Asaka, A. Kosaka, and T. Aida. *Angew. Chem. Int. Ed. Engl.*, Vol. 44, pp. 2410–2413, 2005.

[37] H. Matsumoto, H. Sakaebe, K. Tatsumi, M. Kikuta, E. Ishiko, and M. Kono. *J. Power Sources*, Vol. 160, p. 1308, 2006.

[38] H. Shobukawa, H. Tokuda, M. a. B. H. Susan, and M. Watanabe. *Electrochim. Acta*, Vol. 50, pp. 3872–3877, 2005.

[39] M. a. B. H. Susan, T. Kaneko, A. Noda, and M. Watanabe. *J. Am. Chem. Soc.*, Vol. 127, pp. 4976–4983, 2005.

[40] M. Diaz, A. Ortiz, and I. Ortiz. *J. Memb. Sci.*, Vol. 469, pp. 379–396, 2014.

[41] L. A. Blanchard, D. Hancu, E. J. Beckman, and J. F. Brennecke. *Nature*, Vol. 399, pp. 28–29, 1999.

[42] J. Jacquemin, P. Husson, V. Majer, and M. F. C. Gomes. *Fluid Phase Equilib.*, Vol. 240, pp. 87–95, 2006.

[43] F. Karadas, M. Atilhan, and S. Aparicio. *Energy & Fuels*, Vol. 24, pp. 5817–5828, 2010.

[44] M. Karaszova, M. Kacirkova, K. Friess, and P. Izak. *Sep. Purif. Technol.*, Vol. 132, pp. 93–101, 2014.

[45] J. E. Bara, T. K. Carlisle, C. J. Gabriel, D. Camper, A. A. Finotello, D. L. Gin, and R. D. Noble. *Ind. Eng. Chem. Res.*, Vol. 48, pp. 2739–2751, 2009.

[46] M. Hasib-Ur-Rahman, M. Siaj, and F. Larachi. *Chem. Eng. Process.*, Vol. 49, pp. 313–322, 2010.

[47] L. C. Tome, C. Florindo, C. S. R. Freire, L. P. N. Rebelo, and I. M. Marrucho. *PCCP*, Vol. 16, pp. 17172–17182, 2014.

[48] J. E. Bara, D. E. Camper, D. L. Gin, and R. D. Noble. *Acc. Chem. Res.*, Vol. 43, pp. 152–159, 2010.

[49] M. Shibayama. *Soft Matter*, Vol. 8, pp. 8030–8038, 2012.

[50] T. Matsunaga, T. Sakai, Y. Akagi, U. Chung, and M. Shibayama. *Macromolecules*, Vol. 42, pp. 6245–6252, 2009.

[51] T. Sakai, T. Matsunaga, Y. Yamamoto, C. Ito, R. Yoshida, S. Suzuki, N. Sasaki, M. Shibayama, and U. Chung. *Macromolecules*, Vol. 41, pp. 5379–5384, 2008.

[52] T. Sakai. *Polym. J.*, Vol. 46, pp. 517–523, 2014.

[53] K. Nishi, K. Fujii, Y. Katsumoto, T. Sakai, and M. Shibayama. *Macromolecules*, Vol. 47, pp. 3274–3281, 2014.

[54] K. Nishi, K. Fujii, M. Chijiishi, Y. Katsumoto, U. Chung, T. Sakai, and M. Shibayama. *Macromolecules*, Vol. 45, pp. 1031–1036, 2012.

[55] K. Fujii, H. Asai, T. Ueki, T. Sakai, S. Imaizumi, U. Chung, M. Watanabe, and M. Shibayama. *Soft Matter*, Vol. 8, pp. 1756–1759, 2012.

[56] H. Asai, K. Fujii, T. Ueki, T. Sakai, U. Chung, M. Watanabe, Y. S. Han, T. H. Kim, and M. Shibayama. *Macromolecules*, Vol. 45, pp. 3902–3909, 2012.

Chapter 2

Acid-base Property of Protic Ionic Liquid, 1-Alkylimidazolium Bis(trifluoromethanesulfonyl)amide Studied by Potentiometric Titration

2.1 Introduction

As mentioned in the Chapter 1, room-temperature ionic liquids (ILs) have attracted much attentions as novel solvents for electrolytes [1–5], catalytic and organic reactions [6–10] due to the unique solvent properties such as non-flammability, negligible vapor pressure [11], high ion conductivity [12–16], thermal and electrochemical stabilities [17]. Furthermore, their solvent properties can be easily designed by changing the combination of cation and anion to give specific solvent properties such as hydrophilicity, gas absorption capability [18–23], proton conductivity [24] and so on. Especially, protic ionic liquids (pILs, $[HB^+][A^-]$), prepared by mixing strong acid (HA) and base (B) [25, 26], show good conductivity of the protons because they contain dissociative protons within the cation, and thus pILs are applied as non-volatile electrolytes for fuel cells [27, 28]. In such applications, the behavior of proton dissociated from the cation plays a key role, and thus the acid-base properties of pILs have been widely investigated [8, 29–34].

It has been established that pILs show an autoprotolysis (or a self-dissociation reaction), $A^- + HB^+ \rightarrow HA + B$, and the autoprotolysis constant K_s, is defined as $K_s = [HA][B]$. Angell et al. proposed ΔpK_a that is given by two acid dissociation constants, K_as for HA and HB^+ in aqueous solutions, i.e., $\Delta pK_a = pK_a(HB^+) - pK_a(HA) = -\log([HA][B]/[A^-][HB^+])$, to

evaluate the acid-base properties of pIL as a first step [35]. The ΔpK_a is useful to understand the acidity/basicity of pIL. However, it was pointed out that the ΔpK_a value appreciably differs from the actual K_s, because solvation environments of acid and base are quite different in pIL and aqueous systems [36].

In the case of aqueous solutions, we can easily evaluate the acid-base properties such as pK_a or pK_s by direct pH measurement using a popular glass electrode. However, in non-aqueous solutions including pILs, it is often difficult because the glass electrode is generally not available. Kanzaki and Umebayashi et al. firstly reported a direct pH measurement by potentiometric titration experiment using an ion-selective field effect transistor (IS-FET) electrode to estimate the K_s of ethylammonium nitrate ($[C_2NH_3^+][NO_3^-]$) [37–39]. They also reported the K_s values of some typical pILs recently, however, the number of reported K_s values is still limited compared with the number of reported various pILs. That is, the knowledge of the acid-base property of pILs is still limited at the present stage and should be accumulated by determining equilibrium constant such as K_s and K_a.

In this work, direct determination of K_s value was performed on typical imidazolium-based pIL, 1-alkylimidazolium bis(trifluoromethanesulfonyl)amide, $[C_nImH^+][TFSA^-]$ (n = 2 and 4), by potentiometric titration using IS-FET electrode. Furthermore, temperature dependence of the K_s was also investigated to estimate Gibbs energy, enthalpy and entropy for the autoprotolysis reaction of the $[C_2ImH^+][TFSA^-]$.

2.2 Experiment

2.2.1 Materials

The pIL, $[C_nImH^+][TFSA^-]$ was prepared by mixing equimolar amounts of bis(trifluoromethanesulfonyl)amide (HTFSA) as an acid and 1-alkylimidazole (C_nIm) as a base (Wako Pure Chemical Industries, Japan) in a glove box filled with argon. The C_nIm was purified by distillation and dried with molecular sieves (3A). The HTFSA was kept in a glove box and used without further purification. The obtained solution was dried in vacuum at room-temperature during 1 day. Water content in the pIL was checked by Karl Fisher titration to be less than 200 ppm for both $[C_2ImH^+][TFSA^-]$ and $[C_4ImH^+][TFSA^-]$. Density measurements were performed for the pILs, and the values were 1.576 g cm^{-3} and 1.477 g cm^{-3} for $[C_2ImH^+][TFSA^-]$ and $[C_4ImH^+][TFSA^-]$, respectively.

2.2.2 Potentiometric titration

Using [C_nImH$^+$][TFSA$^-$] as the solvent, the acid HTFSA solution (0.35 mol dm^{-3}) and the base C_2Im solution (3.20 mol dm^{-3}) were prepared in a glove box. The HTFSA solution (7.3 cm^3) was titrated with the C_nIm solution in a vessel at 298 K. The electromotive force (emf) was measured by using IS-FET electrode (HORIBA 0040-10D), which is well established to show an excellent Nernstian response to [H$^+$] and quick response with 3 min in ILs and non-aqueous solvents. To confirm validity of my measurements, firstly, potentiometric titration was carried out for [$C_2NH_3^+$][NO_3^-]. The value of pK_s was estimated to be 9.7, which is in good agreement with the value (9.83) already reported by Kanzaki et al. [37].

2.2.3 Analysis

Autoprotolysis equilibrium of [C_nImH$^+$][TFSA$^-$] is described as

$$C_n\text{ImH}^+ + \text{TFSA}^- \rightleftarrows C_n\text{Im} + \text{HTFSA}, K_s = [C_n\text{Im}][\text{HTFSA}]. \tag{2.1}$$

Total concentrations of HTFSA and C_nIm, $C_{H,i}$ and $C_{B,i}$, respectively, at each titration point, i are

$$C_{H,i} = \frac{V_0[\text{HTFSA}]_0}{V_0 + V_i} = [\text{HTFSA}]_i + [C_n\text{ImH}^+]_i \text{ and} \tag{2.2}$$

$$C_{B,i} = \frac{V_i[C_2\text{Im}]_0}{V_0 + V_i} = [C_n\text{Im}]_i + [C_n\text{ImH}^+]_i. \tag{2.3}$$

where V_0, V_i, $[\text{HTFSA}]_0$ and $[C_n\text{Im}]_0$ are the initial volume, the volume at titration point i, the initial concentrations of acid and base (titrant) solutions, respectively. In $C_H - C_B > 0$ (acid region), it is plausible that all the C_nIm are protonated to exist C_nImH$^+$ in the solution because HTFSA is a strong acid, and thus we can obtain the simple equation: [HTFSA] = $C_{H,i} - C_{B,i}$. From a Nernstain equation, the observed electromotive force (emf), E_i at the titration point i is represented as

$$E_i = E^{\circ\prime} + (2.303RT/F)\log[\text{HTFSA}]_i = E^{\circ\prime} + (2.303RT/F)\log(C_{H,i} - C_{B,i}), \tag{2.4}$$

where $E^{\circ\prime}$, R, T and F denote standard electrode potential, gas constant, temperature and Faraday constant. The observed E_is were analyzed according to Gran's method as follows, which is well known as analysis for an acid-base reaction by potentiometric titration. The

$(V_0 + V_i)10^{E_i/(2.303RT/F)}$ is plotted against V_i based on the following eq. 2.5 to give a straight line, and the slope and intercept essentially correspond to the $[C_nIm]_0$ and $E^{\circ\prime}$, respectively.

$$(V_0 + V_i)10^{E_i/(2.303RT/F)} = 10^{E^{\circ\prime}/(2.303RT/F)}(V_0[\mathrm{HTFSA}]_0 - V_i[C_nIm]_0) \tag{2.5}$$

In $C_H - C_B < 0$ (base region), all protons in the solution bind to C_nIm, leading to a relationship; $C_{H,i} = [C_nImH^+]$. We can thus obtain the simple equation; $[HTFSA] = K_s/[C_2Im] = K_s/(C_{B,i} - C_{H,i})$. From a Nernstain equation, the following equation is obtained in the base region,

$$\begin{aligned}(V_0 + V_i)10^{-E_i/(2.303RT/F)} \\ = 10^{-[\log K_s + E^{\circ\prime}/(2.303RT/F)]}(V_i[C_nIm]_0 - V_0[\mathrm{HTFSA}]_0)\end{aligned} \tag{2.6}$$

and from the intercept in the left side vs. V_i plot and that in eq. 2.6, we can estimate the autoprotolysis constant, pK_s. The data obtained by potentiometric titration experiments were analyzed by Gran's method. The titration experiment was performed 3 times and averaged.

2.3 Results and discussion

2.3.1 Potentiometric titration for $[C_nImH^+][TFSA^-]$

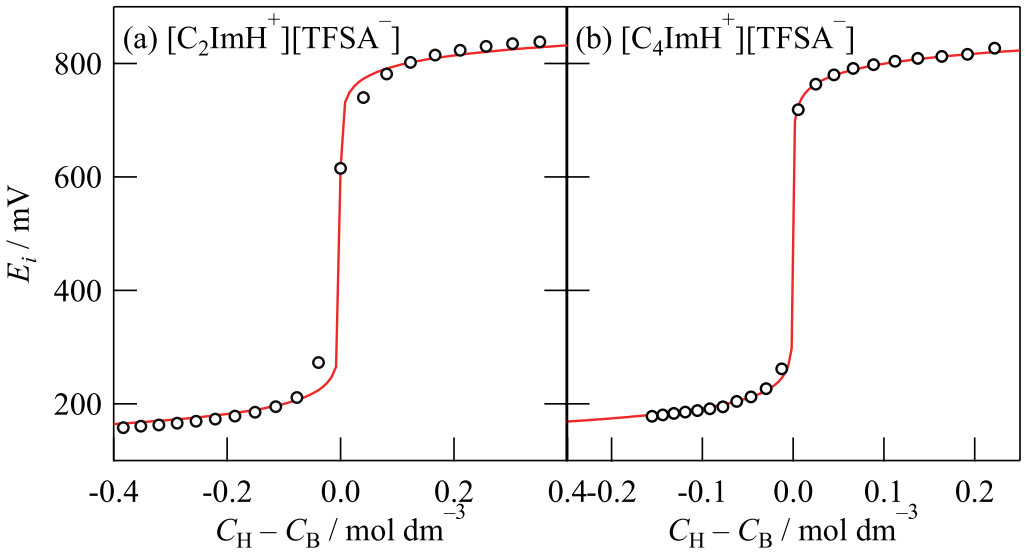

Figure 2.1. Potentiometric titration curve obtained for the acid HTFSA with the base C_nIm in $[C_nImH^+][TFSA^-]$ pILs with (a) $n = 2$ and (b) $n = 4$, respectively. The solid lines correspond to the theoretical curve calculated by using the K_s values obtained finally.

Figure. 2.1 (a) shows potentiometric titration curve observed for $[C_2ImH^+][TFSA^-]$ pIL. The value of E_i observed in the HTFSA solution slightly and gradually decreased with the

addition of the titrant C_2Im solution, and then sharply fell at the equivalent neutral point ([HTFSA] = [C_2Im]). Subsequently, it decreased slightly under excess base conditions. The large emf jump of approximately 600 mV indicates that the [C_2ImH^+][$TFSA^-$] has a large pK_s value. Similar potentiometric titration was applied to the [C_4ImH^+][$TFSA^-$] system, which can be seen in Figure 2.1 (b). The extent of the E_i jump is almost similar to n = 2 system, implying that the pK_s value for n = 4 system is close to that for n = 2. To estimate the pK_s value, I analyzed the observed titration data using Gran's method described in Experimental section in detail.

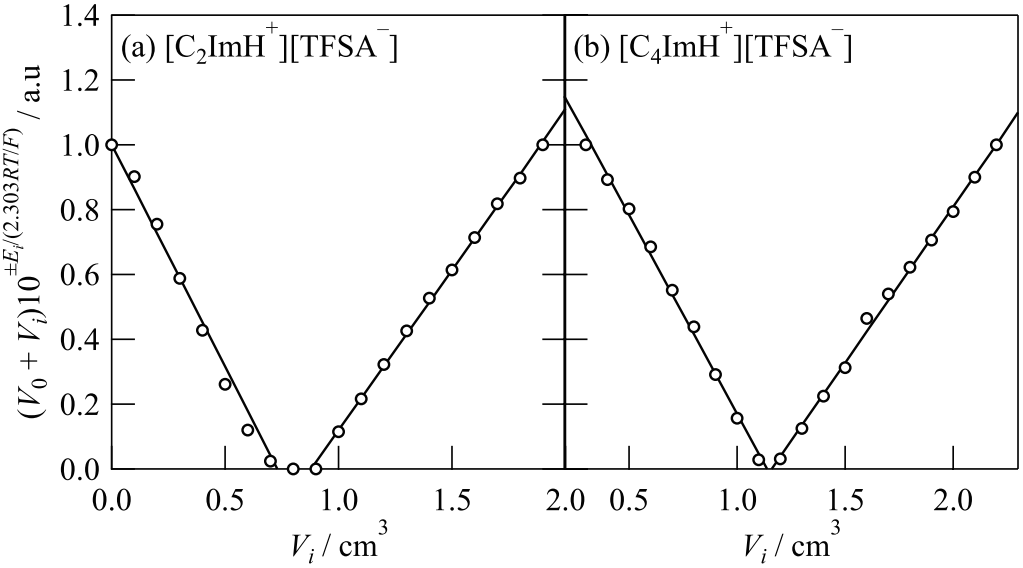

Figure 2.2. Gran's plot for the observed E_is in [C_nImH^+][$TFSA^-$] with (a) n = 2 and (b) n = 4. The straight solid lines show the theoretical lines calculated by a linear squared fitting method.

Figure 2.2 (a) shows the result of Gran's plots for [C_2ImH^+][$TFSA^-$] system. It was found that the experimental points fall on a straight line in both $C_H - C_B > 0$ (acid) and < 0 (base) regions, resulting in a successful determination of pK_s by using slope and intercept values. I thus estimated the pK_s value (and standard deviation) to be 12.3(2) for [C_2ImH^+][$TFSA^-$] at 298 K. This pK_s value means that both neutral C_2Im and HTFSA exist at the concentration of $10^{-6.2}$ mol dm^{-3} in [C_2ImH^+][$TFSA^-$] pIL. Similarly, the pK_s value for [C_4ImH^+][$TFSA^-$] was estimated from Gran's plots as shown in Figure 2.2 (b) to be 12.6(1) at 298 K. The obtained pK_s values are almost the same for both n = 2 and 4 systems, indicating that there is essentially no dependence of alkyl group on the pK_s. Kanzaki et al. recently reported the pK_s value of n = 1 system, [C_1ImH^+][$TFSA^-$] by potentiometric titration. In their work, the experiment was carried out for the melt [C_1ImH^+][$TFSA^-$] at 324 K because

$[C_1ImH^+][TFSA^-]$ is a solid at room temperature and the pK_s value was estimated to be 8.58 [34]. Although the result cannot be directly compared with those for $n = 2$ and 4 systems (this work) due to different temperature condition on the experiments, the pK_s seems to be enough small relative to those for $n = 2$ and 4 systems. This implies that the basicity of the neutral C_nIm in the $[C_nImH^+][TFSA^-]$ becomes stronger with increasing $n = 1$ up to 2, however, that is a constant even with further increasing n. Here, I note the acid-dissociation constant, pK_a of neutral C_nIm depending on n in aqueous solutions [40]. The K_a value does not show the dependence of the alkyl-chain length between C_2Im (7.3) and C_4Im (7.2) in aqueous solutions. Furthermore, the alkyl-chain length dependence of the pK_s was also reported for a series of alcohols in aqueous solution [41]. The pK_s is 16.7 for methanol ($n = 1$) and increases with increasing n to be 18.9 for ethanol ($n = 2$), but, the value is kept unchanged with further increasing n, i.e., 19.3 for 1-propanol ($n = 3$) and 21.5 for 1-butanol ($n = 4$). These behaviors are similar to that obtained for $[C_nImH^+][TFSA^-]$ system in this work.

2.3.2 Relationship between pK_s and ΔpK_a

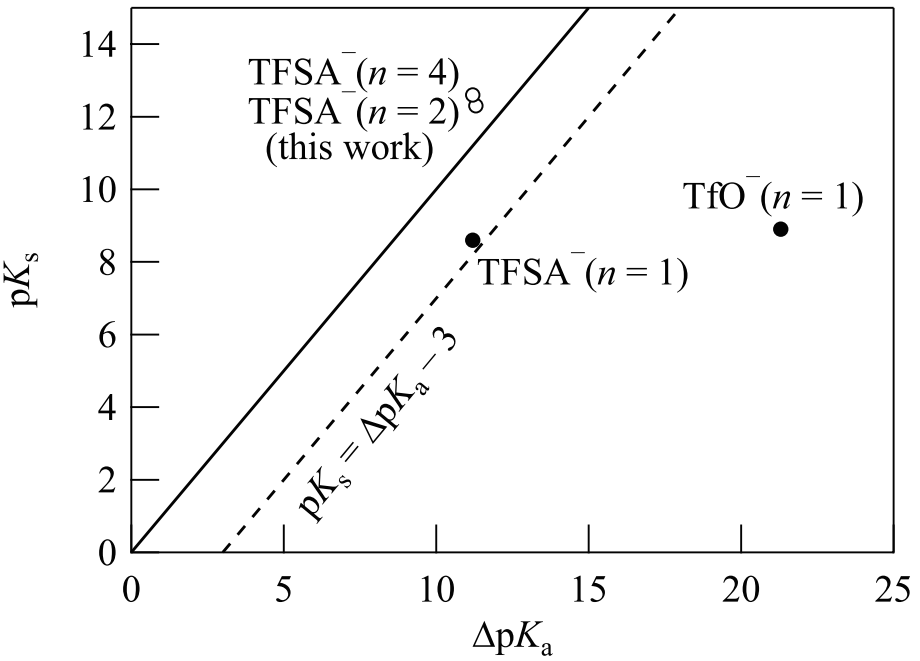

Figure 2.3. Relationship between pK_s and ΔpK_a in $[C_nImH^+][TFSA^-]$ with $n = 2$ and 4 (open circle), that with $n = 1$ and $[C_1ImH^+][TfO^-]$ (closed circle). The broken line with $pK_s = \Delta pK_a - 3$ corresponds to the result for some pILs.

Figure 2.3 shows the pK_s values obtained for the $[C_nImH^+][TFSA^-]$ ($n = 2$ and 4)

plotted against the corresponding ΔpK_a values, together with that for $[C_1ImH^+][TFSA^-]$ (325 K) and 1-methylimidazolium trifluoromethanesulfonate, $[C_1ImH^+][TfO^-]$(367 K) reported by Kanzaki et al. [34]. In addition, those for several pILs ($[C_1ImH^+][CF_3COO^-]$, $[C_1ImH^+][CH_3COO^-]$, $[C_1ImH^+][HCOO^-]$, $[C_2NH_3^+][NO_3^-]$ and a series of PILs composed of a ternary ammonium with 2-hydroxyethyl groups as a cation) already reported were also considered, which is shown as a broken line in this figure. In the several pILs, the pK_s vs ΔpK_a plots are represented by a straight line with $pK_s = \Delta pK_a - 3$ (broken line in Figure 2.3). As is well established, the ΔpK_a involves a hydration effect, and thus differs from the pK_s value determined by the experiments. Although temperature condition on the experiments is different from room temperature, the $[C_1ImH^+][TfO^-]$ (367 K) largely deviates from the straight line, which locates on the lower position from the line, i.e., $pK_s << \Delta pK_a$.

In the case of $[C_nImH^+][TFSA^-]$ system examined here, it was found that the pK_s values for $n = 2$ and 4 are appreciably larger than the corresponding values expected from the broken line. It seems that those are close to the relationship with $pK_s = \Delta pK_a$ (solid line in Figure 2.3), which is the first case among the pILs reported until now. Here, note that pK_s and ΔpK_a strongly depend on the solvation in pIL and water, respectively. The difference between them (that is, $pK_s - \Delta pK_a$) is related to the sum of each difference in the solvation free energies of cation, anion and their neutral species. The $pK_s - \Delta pK_a$ for $n = 2$ and 4 are 1.0 and 1.4, respectively, which is a positive value and significantly larger than those for another pILs [34], showing a negative value. To discuss this from thermodynamic aspect, I extended our study to temperature dependence of the pK_s to estimate the enthalpy and entropy of autoprotolysis reaction.

2.3.3 Thermodynamic parameters for autoprotolysis reaction in pILs

Table 2.1. pK_ss of $[C_2ImH^+][TFSA^-]$ in various temperature.

T / K	pK_s / mol^2 dm^{-6}
297.7	12.3(2)
300.5	12.2(1)
314.7	12.0(1)
333.2	11.6(2)

Potentiometric titration experiment as described above was carried out with varying various

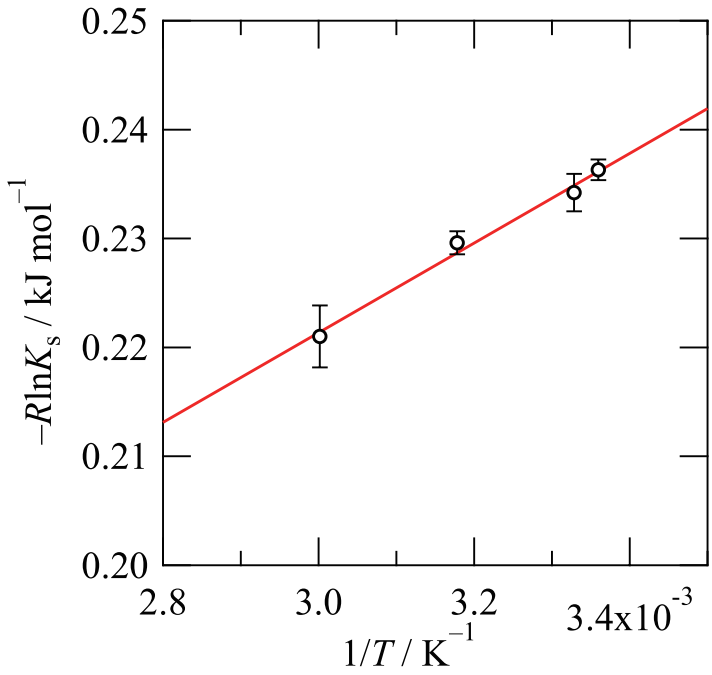

Figure 2.4. Van't Hoff plot obtained from temperature dependence of K_s for $[C_2ImH^+][TFSA^-]$.

temperatures as shown in Table 2.1. Figure 2.4 shows the pK_s values plotted against reciprocal temperature, i.e., van't Hoff plot, for the $[C_2ImH^+][TFSA^-]$. As can be seen in the figure, the plot showed a good linearity in the temperature range examined here, and then the enthalpy, $\Delta H°$ and entropy, $\Delta S°$ could be estimated from the slope and intercept in the straight line. The $\Delta H°$ and $\Delta S°$ values were estimated to be 41(3) kJ mol^{-1} and −0.10(1) kJ mol^{-1} K^{-1}, respectively, and the Gibbs energy, $\Delta G°$ at 298 K is 70.4 kJ mol^{-1}. The positive $\Delta H°$ suggests that the C_2ImH^+ is endothermically deprotonated in the pIL to from the neutral C_2Im. It has been established by calorimetric titration experiment that the $\Delta H°$ and $\Delta S°$ for the autoprotolysis reaction in $[C_2NH_3^+][NO_3^-]$ which is also a typical pIL are 83(2) and 0.09(1) kJ mol^{-1} K^{-1}, respectively, and the $\Delta G°$ is 54.9(3) (pK_a = 9.83 at 298 K).39 The $\Delta H°$ for $[C_2ImH^+][TFSA^-]$ is significantly smaller than that for $[C_2NH_3^+][NO_3^-]$, while the $\Delta S°$ is essentially the same in both pILs. I thus conclude that the smaller pK_a or $\Delta G°$ for $[C_2ImH^+][TFSA^-]$ than for $[C_2NH_3^+][NO_3^-]$ is mainly ascribed to the enthalpy term in the autoprotolysis reaction. The reaction enthalpy depends on the basicity of neutral specie in the solution, in this case, C_2Im and C_2NH_2. The basicity of C_2Im is appreciably smaller than that of C_2NH_2 according to the pK_a for both protonated species in aqueous system (pK_a = 7.2 and 10.6 for C_2ImH^+ and $C_2NH_3^+$, respectively). This leads to a weaker C_2Im–H^+ interaction relative to a C_2NH_2–H^+ one, resulting in a smaller reaction $\Delta H°$ in $[C_2ImH^+][TFSA^-]$ than that in $[C_2NH_3^+][NO_3^-]$.

2.4 Conclusion

The autoprotolysis reaction of $[C_nImH^+][TFSA^-]$ with $n = 2$ and 4 were investigated by potentiometric titration to directly and experimentally estimate the equilibrium constant, pK_s. The pK_s is appreciably larger than the corresponding ΔpK_a calculated by two pK_as for HA and HB^+ in aqueous system, which quite differs from the result for other pIL systems such as $[C_2NH_3{}^+][NO_3{}^-]$ etc. reported until now. From temperature dependence of the pK_s obtained by potentiometric titration, the ΔH° and ΔS° in the autoprotolysis reaction were determined in $[C_2ImH^+][TFSA^-]$. It was found that the reaction endothermerically undergoes and the ΔH° is smaller than that for $[C_2NH_3{}^+][NO_3{}^-]$. To obtain more insight into the acid-base properties of pILs, the pK_s data should be accumulated in various pILs and discussed from thermodynamic aspect.

Reference

[1] A. Noda, A. B. Susan, K. Kudo, S. Mitsushima, K. Hayamizu, and M. Watanabe. *J. Phys. Chem. B*, Vol. 107, pp. 4024–4033, 2003.

[2] R. Kawano, H. Matsui, C. Matsuyama, A. Sato, M. Susan, N. Tanabe, and M. Watanabe. *Journal of Photochemistry and Photobiology a-Chemistry*, Vol. 164, pp. 87–92, 2004.

[3] H. Shobukawa, H. Tokuda, S. Tabata, and M. Watanabe. *Electrochim. Acta*, Vol. 50, pp. 305–309, 2004.

[4] H. Tokuda, S. I. Tabata, M. Susan, K. Hayamizu, and M. Watanabe. *J. Phys. Chem. B*, Vol. 108, pp. 11995–12002, 2004.

[5] M. Halder, L. S. Headley, P. Mukherjee, X. Song, and J. W. Petrich. *J. Phys. Chem. A*, Vol. 110, pp. 8623–8626, 2006.

[6] P. Wasserscheid and K. Keim. *Angew. Chem. Int. Ed. Engl.*, Vol. 39, pp. 3772–3789, 2000.

[7] T. Welton. *Chem. Rev.*, Vol. 99, pp. 2071–2083, 1999.

[8] Z. Y. Duan, Y. L. Gu, J. Zhang, L. Y. Zhu, and Y. Q. Deng. *J. Mol. Catal. A: Chem.*, Vol. 250, pp. 163–168, 2006.

[9] K. E. Johnson, R. M. Pagni, and J. Bartmess. *Monatsh. Chem.*, Vol. 138, pp. 1077–1101, 2007.

[10] M. Feroci, I. Chiarotto, M. Orsini, G. Sotgiu, and A. Inesi. *Electrochim. Acta*, Vol. 56, pp. 5823–5827, 2011.

[11] M. J. Earle, J. Esperanca, M. A. Gilea, J. N. C. Lopes, L. P. N. Rebelo, J. W. Magee, K. R. Seddon, and J. A. Widegren. *Nature*, Vol. 439, pp. 831–834, 2006.

[12] H. Weingartner, A. Knocks, W. Schrader, and U. Kaatze. *J. Phys. Chem. A*, Vol. 105, pp. 8646–8650, 2001.

[13] H. Tokuda, K. Hayamizu, K. Ishii, M. Abu Bin Hasan Susan, and M. Watanabe. *J. Phys. Chem. B*, Vol. 108, pp. 16593–16600, 2004.

[14] C. A. Angell, N. Byrne, and J. P. Belieres. *Acc. Chem. Res.*, Vol. 40, pp. 1228–1236, 2007.

[15] A. Noda, K. Hayamizu, and M. Watanabe. *J. Phys. Chem. B*, Vol. 105, p. 4603, 2001.

[16] H. Shobukawa, H. Tokuda, M. a. B. H. Susan, and M. Watanabe. *Electrochim. Acta*, Vol. 50, pp. 3872–3877, 2005.

[17] P. Bonhote, A. P. Dias, N. Papageorgiou, K. Kalyanasundaram, and M. Gratzel. *Inorg. Chem.*, Vol. 35, pp. 1168–1178, 1996.

[18] J. Blath, N. Deubler, T. Hirth, and T. Schiestel. *Chem. Eng. J.*, Vol. 181, pp. 152–158, 2011.

[19] M. Besnard, M. I. Cabaco, F. V. Chavez, N. Pinaud, P. J. Sebastiao, J. a. P. Coutinho, J. Mascetti, and Y. Danten. *J. Phys. Chem. A*, Vol. 116, pp. 4890–4901, 2012.

[20] M. I. Cabaco, M. Besnard, Y. Danten, and J. a. P. Coutinho. *J. Phys. Chem. A*, Vol. 116, pp. 1605–1620, 2012.

[21] L. A. Blanchard, D. Hancu, E. J. Beckman, and J. F. Brennecke. *Nature*, Vol. 399, pp. 28–29, 1999.

[22] C. Cadena, J. L. Anthony, J. K. Shah, T. I. Morrow, J. F. Brennecke, and E. J. Maginn. *J. Am. Chem. Soc.*, Vol. 126, pp. 5300–5308, 2004.

[23] Y. Gu and T. P. Lodge. *Macromolecules*, Vol. 44, pp. 1732–1736, 2011.

[24] A. B. H. Susan, M. Y. Yoo, H. Nakamoto, and M. Watanabe. *Chem. Lett.*, Vol. 32, pp. 836–837, 2003.

[25] M. Hirao, H. Sugimoto, and H. Ohno. *J. Electrochem. Soc.*, Vol. 147, pp. 4168–4172, 2000.

[26] M. Picquet, I. Tkatchenko, I. Tommasi, P. Wasserscheid, and J. Zimmermann. *Adv. Synth. Catal.*, Vol. 345, pp. 959–962, 2003.

[27] H. Matsuoka, H. Nakamoto, M. Susan, and M. Watanabe. *Electrochim. Acta*, Vol. 50, pp. 4015–4021, 2005.

[28] S. Y. Lee, A. Ogawa, M. Kanno, H. Nakamoto, T. Yasuda, and M. Watanabe. *J. Am. Chem. Soc.*, Vol. 132, pp. 9764–9773, 2010.

[29] J. L. E. Campbell and K. E. Johnson. *J. Am. Chem. Soc.*, Vol. 117, pp. 7791–7800, 1995.

[30] C. Thornazeau, H. Olivier-Bourbigou, L. Magna, S. Luts, and B. Gilbert. *J. Am. Chem. Soc.*, Vol. 125, pp. 5264–5265, 2003.

[31] D. R. Macfarlane, J. M. Pringle, K. M. Johansson, S. A. Forsyth, and M. Forsyth. *Chem. Commun.*, pp. 1905–1917, 2006.

[32] L. M. Mihichuk, G. W. Driver, and K. E. Johnson. *Chemphyschem*, Vol. 12, pp. 1622–1632, 2011.

[33] Y. L. Yang and Y. Kou. *Chem. Commun.*, pp. 226–227, 2004.

[34] R. Kanzaki, H. Doi, X. Song, S. Hara, S. Ishiguro, and Y. Umebayashi. *J. Phys. Chem. B*, Vol. 116, pp. 14146–14152, 2012.

[35] M. Yoshizawa, W. Xu, and C. A. Angell. *J. Am. Chem. Soc.*, Vol. 125, pp. 15411–15419, 2003.

[36] R. Kanzaki, K. Uchida, X. Song, Y. Umebayashi, and S. Ishiguro. *Anal. Sci.*, Vol. 24,

pp. 1347–1349, 2008.

[37] R. Kanzaki, K. Uchida, S. Hara, Y. Umebayashi, S. Ishiguro, and S. Nomura. *Chem. Lett.*, Vol. 36, pp. 684–685, 2007.

[38] S. Ishiguro, Y. Umebayashi, R. Kanzaki, and K. Fujii. *Pure Appl. Chem.*, Vol. 82, pp. 1927–1941, 2010.

[39] R. Kanzaki, X. D. Song, Y. Umebayashi, and S. Ishiguro. *Chem. Lett.*, Vol. 39, pp. 578–579, 2010.

[40] B. Lenarcik and P. Ojczenasz. *J. Heterocycl. Chem.*, Vol. 39, pp. 287–290, 2002.

[41] S. Rondinini, P. Longhi, P. R. Mussini, and T. Mussini. *Pure Appl. Chem.*, Vol. 59, pp. 1693–1702, 1987.

Chapter 3

Brønsted Basicity of Solute Butylamine in an Aprotic Ionic Liquid Investigated by Potentiometric Titration

3.1 Introduction

In aqueous systems, acid-base properties, i.e., Brønsted acidity and basicity, are well established and understood, and it is thus known that they play a key role in chemical reactions in solution. As the indicative parameter of the acidity and basicity of solutes, the acid dissociation constants (pK_as) are well known and pK_as of numerous solutes have been reported in aqueous systems. These values can be determined by simple titration experiment by detecting pH, which can be measured using a popular glass electrode. However, in non-aqueous media such as ionic liquids (ILs), it is difficult to determine the absolute pK_as, because a glass electrode hardly work in the non-aqueous system. Instead of direct measurement, other techniques, such as ultraviolet-visible (UV-vis) and infrared (IR)/Raman spectroscopy have been applied to investigate the pK_as in non-aqueous solutions [1–5].

Recently, ILs have attracted attention as new solvents, and thus have been widely investigated for application (e.g. catalysys, separation and electrochemical devices) as mentioned in Chapter 1. However, the knowledge of acid-base reactions in ILs still remains limited, although they are one of the most fundamental and essential reactions in solution. ILs are classified into two categories (similar to non-aqueous molecular solvents), i.e., protic ILs (pILs) and aprotic ILs (aILs). pILs, $[HB^+][A^-]$, can be readily prepared by simply mixing

Brønsted acids (HA) and bases (B) [6–9]. Angell et al. proposed that the pK_a for $[HB^+][A^-]$ is defined by the deference between two acid dissociation constants, K_as, for HA and HB^+ in water, i.e., $\Delta pK_a = pK_a(HB^+) - pK_a(HA)$ [9]. The ΔpK_a is a good indicator of the acidity/basicity of a pIL, however it has limit because it does not take account for the hydration effect to the solute. Kanzaki and Umebayashi et al. firstly reported the directly measured pH in pILs using an ion-selective field effect transistor (IS-FET) or $Pt(H_2)$ electrode to evaluate the autoprotolysis constant, K_s, using potentiometric titration experiments [6, 8]. In the case of aILs, UV-visible spectroscopic investigations have been applied to aIL solutions containing a neutral solute as an indicator, with the protonation extent of the solute evaluated on the basis of the wavelength of the absorption band [3, 5]. It should be noted that, the directly measured pH (or $-\log[H^+]$) is one of the best indicators to determine the acid-base properties in solution [10, 11]. However, these direct investigations have rarely been performed on acids and bases in aILs, because a glass electrode does not show response to the $[H^+]$ in ILs, as mentioned above. In this study, the direct measurement of the pH was performed on an aIL 1-ethyl-3-methylimidazolium bis(trifluoromethanesulfonyl)amide ($[C_2mIm^+][TFSA^-]$) solution containing butylamine ($BuNH_2$) as a typical neutral solute molecule with strong basicity, and the acid dissociation constant of $BuNH_3^+$ in the $[C_2mIm^+][TFSA^-]$ aIL was estimated.

3.2 Experiment

3.2.1 Sample preparation

$[C_2mIm^+][TFSA^-]$ was prepared from 1-methylimidazole and 1-bromoethane according to the previously described procedure [12]. The water content was determined by using Karl Fisher titration to be less than 50 ppm. The $BuNH_2$ was dried with molecular sieves (4-A). The bis(trifluoromethanesulfonyl)amide acid (HTFSA, crystals) was used without further purification.

3.2.2 Potentiometric titration

An HTFSA solution (4.0×10^{-2} mol dm^{-3}, 4.0 cm^3) in a thermostated vessel at 298 K was titrated with the $BuNH_2$ solution (8.0×10^{-2} mol dm^{-3}) by using an auto-burette. The electromotive force (emf) was measured using an IS-FET electrode (HORIBA 0040-10D) [13], which is well established as showing an good Nernstian response to $[H^+]$ in ILs and non-aqueous solvents [7, 13]. The titration experiments were performed 3 times and

averaged. The data were analyzed according to Gran's method [14]. The details of the theory and analysis are described as follows.

3.2.3 Theory and Analysis

The acid-base reaction of $BuNH_2$ in $[C_2mIm^+][TFSA^-]$ aIL is described as

$$BuNH_2{}^+ \rightleftarrows BuNH_2 + H^+(\text{ or } [HTFSA]), \tag{3.1}$$

where K_a is the equilibrium constant for acid-base reaction. Here, It should be noted that the solvent $[C_2mIm^+][TFSA^-]$ undergoes autoprotolysis reaction to give the proton-dissociated specie (eq. 3.2) in the solution.

$$\begin{aligned} C_2mIm(H^+) + TFSA^- &\rightleftarrows C_2mIm + HTFSA, \\ K_s &= [C_2mIm][HTFSA](\text{ or } [C_2mIm][H^+]), \end{aligned} \tag{3.2}$$

where K_s is the autoprotolysis constant. In this section, 1-ethyl-3-methylimidazolium cation and its proton-dissociated one are described as $C_2mIm(H^+)$ and C_2mIm, respectively. The autoprotolysis reaction for solvent coexists with the above acid-base reaction in equilibrium, and then it is expected that the neutral C_2mIm acts as conjugated base for $BuNH_2$ in the solution. Total concentrations of HTFSA and base ($BuNH_2$), $C_{H,i}$ and $C_{B,i}$ at each titration point, i are

$$\begin{aligned} C_{H,i} = \frac{V_0[HTFSA]_0}{V_0 + V_i} &= [BuNH_3{}^+]_i + [HTFSA]_i - [C_2mIm] \\ &= [BuNH_3{}^+]_i + [HTFSA]_i - K_s/[HTFSA] \text{ and} \end{aligned} \tag{3.3}$$

$$C_{B,i} = [BuNH_3{}^+]_i + [BuNH_2]_i, \tag{3.4}$$

where V_0, V_i, $[HTFSA]_0$ and $[BuNH_2]_0$ are the initial volume for acid solution, the volume at titration point i, the initial concentrations of acid and base (titrant) solutions, respectively. In $C_H - C_B > 0$ region, namely, acid region in the solution, it is plausible that all BtNH2 molecules exist as protonated BuNH3+. Therefore, the eq. 3.4 can be approximated as $C_{B,i} = [BuNH_3{}^+]$ to lead to $[HTFSA] = C_{H,i} - C_{B,i} + K_s/[HTFSA]$. Here, I note that it is very difficult to determine the Ks value experimentally, because the C_2mIm is dissociated proton at C2 position within the $C_2mIm(H^+)$ cation and unstable in the solution. We thus assume here that the Ks is very small and is negligible in this system. Indeed, the potentiometric titration curve can be represented by concerning the acid-base reaction for $BuNH_2$ (eq. 3.1) only (see Figure 3.1). On the basis of this assumption, we obtain the simple equation, [HTFSA] =

$C_{\mathrm{H},i} - C_{\mathrm{B},i}$, if ${K_\mathrm{s}}^{1/2} << C_H - C_B$. From a Nernstain equation, the observed E_i at the titration point i is represented as

$$E_i = E^{\circ\prime} + (2.303RT/F)\log[\mathrm{HTFSA}]_i = E^{\circ\prime} + (2.303RT/F)\log(C_{\mathrm{H},i} - C_{\mathrm{B},i}), \quad (3.5)$$

where $E^{\circ\prime}$, R, T and F denote the standard electrode potential, the gas constant, temperature and Faraday constant. The observed E_is were analyzed according to Gran's method, which is well known in the analysis for an acid-base reaction by titration potentiometry. The $(V_0 + V_i)10^{E_i/(2.303RT/F)}$ is plotted against V_i on the basis of the following equation to give a straight line, and the slop and intercept essentially correspond to the $[\mathrm{BuNH_2}]_0$ and $E^{\circ\prime}$, respectively.

$$(V_0 + V_i)10^{E_i/(2.303RT/F)} = 10^{E^{\circ\prime}/(2.303RT/F)}(V_0[\mathrm{HTFSA}]_0 - V_i[\mathrm{BuNH_2}]_0) \quad (3.6)$$

In $C_\mathrm{H} - C_\mathrm{B} < 0$ (base region), all protons are distributed to base $\mathrm{BuNH_2}$ to form $\mathrm{BuNH_3}^+$. Therefore, eq. 3.3 is simplified as $C_\mathrm{H} = [\mathrm{BuNH_3}^+]$, and we thus obtained the following equation.

$$[\mathrm{H}^+] = \frac{K_\mathrm{a}C_\mathrm{H}}{C_\mathrm{B} - C_\mathrm{H}}. \quad (3.7)$$

From a Nernstain equation, the following equation including the E_i is obtained, and

$$\begin{aligned} &V_0[\mathrm{HTFSA}]_0 10^{-E_i/(2.303RT/F)} \\ &\qquad = 10^{-[\log K_\mathrm{a} + E^{\circ\prime}/(2.303RT/F)]}(V_i[\mathrm{BuNH_2}]_0 - V_0[\mathrm{HTFSA}]_0) \end{aligned} \quad (3.8)$$

If $[\mathrm{HTFSA}]_0$ is known, $[\mathrm{BuNH_2}]_0$ can be estimated from the intercept and slope in the left-hand side vs. V_i plot. Furthermore, from the intercepts in eq. 3.6 and 3.8, we can estimate the acid dissociation constant $\mathrm{p}K_\mathrm{a}$.

3.3 Results and discussion

Figure 3.1 shows a typical potentiometric titration curve obtained for the $\mathrm{BuNH_2}$ dissolved in $[\mathrm{C_2mIm}^+][\mathrm{TFSA}^-]$ solution. The value of E_i observed in the vessel (HTFSA solution) slightly and gradually decreased with adding the titrant ($\mathrm{BuNH_2}$ solution) and then fell rapidly at the equivalent neutral point, i.e., $[\mathrm{HTFSA}] = [\mathrm{BuNH_2}]$. Subsequently, the E_i decreased slightly under excess base conditions. The large emf jump up to approximately 850 mV indicates that $\mathrm{BuNH_2}$ has a large $\mathrm{p}K_\mathrm{a}$ value in $[\mathrm{C_2mIm}^+][\mathrm{TFSA}^-]$ aIL. For estimation of the apparent $\mathrm{p}K_\mathrm{a}$ value, the observed titration data were analyzed using Gran's method.

Figure 3.2 shows the Gran's plot for the obtained data. The experimental data fell on a straight lines in both the acidic and basic regions. According to Gran's plot, the slope and

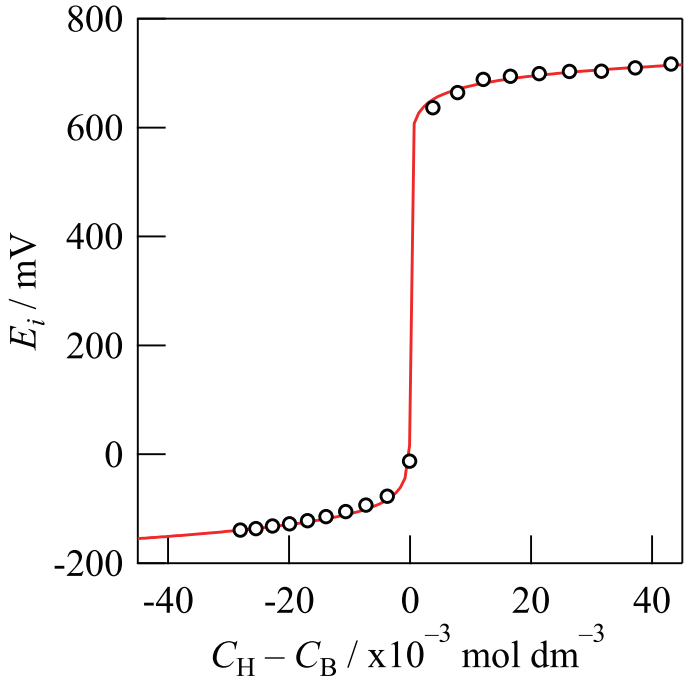

Figure 3.1. Potentiometric titration curve for the acid HTFSA with the base $BuNH_2$ in a $[C_2mIm^+][TFSA^-]$ solution. The solid line corresponds to the theoretical curve calculated with the experimentally determined pK_a.

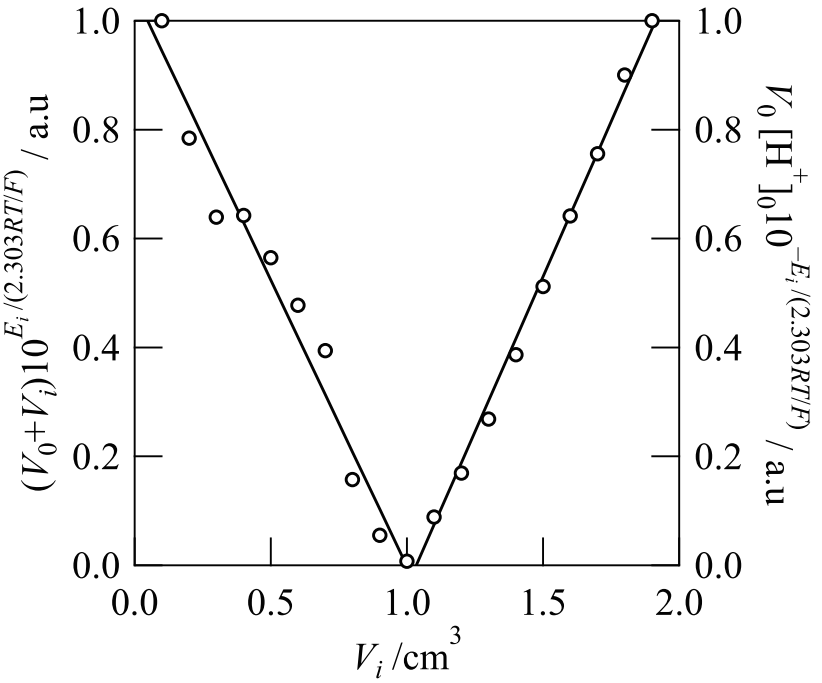

Figure 3.2. Gran's plot for the obtained E_is in $[C_2mIm^+][TFSA^-]$ solution. The straight lines (solid) show theoretical lines calculated with a linear squared fitting method. The data points on left and right lines are normalized by the value in $i = 1$, $i = 19$, respectively.

intercept of this plot leads to the quantitative evaluation of the apparent pK_a, which was estimated to be 16.6(1). The theoretical line calculated with this pK_a value is also shown in Figure 3.1 (the red solid line), which well reproduces the experimental titration curve.

From the estimated value, it was found that the pK_a of $BuNH_3^+$ in [C_2mIm$^+$][TFSA$^-$] is significantly larger than corresponding value in water (pK_a = 10.6 [15]). This indicates that $BuNH_2$ in the aIL acts as a stronger base than it does in water. Similar behavior has also been reported in other non-aqueous solutions [2, 11].

Recently, Barhdadi et al. reported the pK_a values of some neutral solutes in 1-butyl-3-methylimidazolium bis(trifluoromethanesulfonyl)amide ([C_4mIm$^+$][TFSA$^-$]) determined by potentiometric and cyclic voltammetric measurements using a platinized Pt(H_2) electrode [16]. They estimated the pK_a values of pyridine, 3-picoline, 2,6-lutidine, and 2,4,6-collidine to be 11.5, 11.2, 13.2, and 15.2, respectively, which are higher than the corresponding values in water (5.2, 5.68, 6.75, and 7.43, respectively). The differences in the pK_a values for these commonly used bases containing a nitrogen atom in [C_4mIm$^+$][TFSA$^-$] and water for these solutes, i.e., pK_a(IL) − pK_a(water), are 6.3, 5.5, 6.4, and 7.8, respectively. In the present study, $BuNH_2$ is also a base with a nitrogen atom, and the difference in the pK_a values is 6.0, which shows similar behavior to the values mentioned above. This similarity implies that the ΔpK_a value is related to the solvation in aIL, i.e., the difference in the solvation free energy of the solute in the IL and that in water.

Figure 3.3 shows the distribution of neutral RNH_2 (R = butyl or propyl) calculated with the pK_a values in [C_2mIm$^+$][TFSA$^-$] (this work), water, and the non-aqueous solvents tetrahydrofuran (THF) and acetonitrile (AN) [1]. The pK_a values in the water ($BuNH_2$), THF (propylamine, $PrNH_2$) and acetonitrile ($PrNH_2$) systems are 10.6 [15], 13.8 [1] and 18.2 [17], respectively. As can be clearly seen in Figure 3.3, the order of the basicity for $BuNH_2$ is water < THF < [C_2mIm$^+$][TFSA$^-$] < AN. This behavior can be ascribed to the solvation of the each species, particularly the protons in the solutions. Solvent parameters such as the dielectric constant, donor and acceptor numbers, E_T(30) are useful parameters for initially understanding the solvation behaivor in a solution [18, 19]. For example, the donor number, which reflects the electron-pair donation, is in the order [C_2mIm$^+$][TFSA$^-$] (11.2) < AN (14.1) < water (18.0) < THF (20.0). It is reasonable to assume that protons should be stabilized by a strong electron-pair donating solvent. Therefore, $BuNH_3^+$ would be more dissociated in solvents with larger donor numbers, resulting in a smaller pK_a. However, this trend is not observed for the actual pK_a values. Similarly, no significant relation between the pK_a and other solvent parameters was observed. However, it should be emphasized that $BuNH_3^+$ behaves as a stronger acid in the IL than it does in AN, although the electron donating

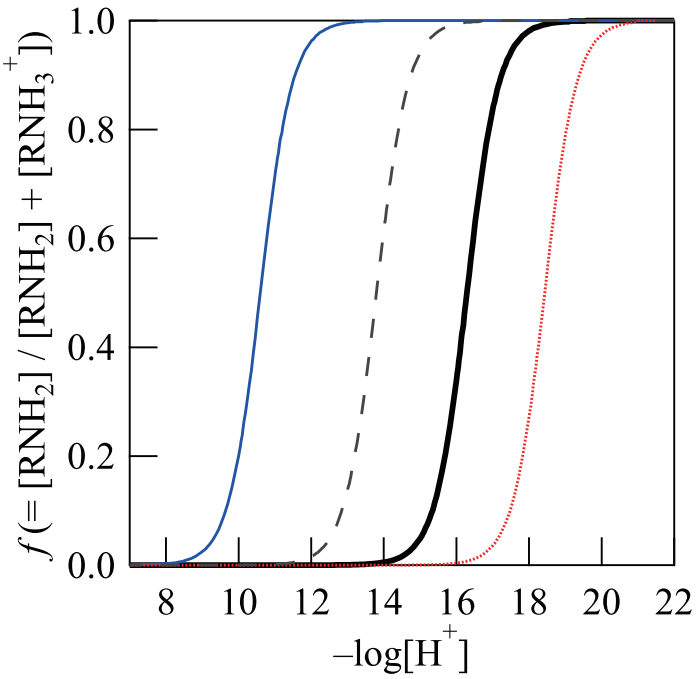

Figure 3.3. Distribution of amine species in $[C_2mIm^+][TFSA^-]$ (this work), water, THF, and acetonitrile calculated with the each pK_a values. The lines colored with blue, gray (broken), black (bold), and red (dotted) correspond to the water, THF, $[C_2mIm^+][TFSA^-]$ and acetonitrile systems, respectively.

ability for IL is weaker than that for AN.

3.4 Conclusion

The acid-dissociation constant, pK_a for $BuNH_3^+$ in $[C_2mIm^+][TFSA^-]$ aIL was successfully determined directly by using IS-FET electrode to be 16.6(1). This value is significantly larger than corresponding value for water (10.6), indicating that the $BuNH_2$ in aILs acts as a stronger Brønsted base than that in water. The value was compared with pK_a values in other non-aqueous solvents, however, there is no obvious relation between pK_a and conventional solvent parameters. To obtain more insight into the acid-base properties of solutes in IL systems, further knowledge of the thermodynamic and structural aspects of solvation in ILs are thus required.

Reference

[1] E. I. Rõõm, A. Kütt, I. Kaljurand, I. Koppel, I. Leito, I. A. Koppel, M. Mishima, K. Goto, and Y. Miyahara. *Chem. Eur. J.*, Vol. 13, pp. 7631–7643, 2007.

[2] L. Sooväli, I. Kaljurand, A. Kütt, and I. Leito. *Anal. Chim. Acta*, Vol. 566, pp. 290–303, 2006.

[3] D. R. Macfarlane, J. M. Pringle, K. M. Johansson, S. A. Forsyth, and M. Forsyth. *Chem. Commun.*, pp. 1905–1917, 2006.

[4] J. Stoimenovski, E. I. Izgorodina, and D. R. Macfarlane. *PCCP*, Vol. 12, pp. 10341–10347, 2010.

[5] C. Thomazeau, H. Olivier-Bourbigou, L. Magna, S. Luts, and B. Gilbert. *J. Am. Chem. Soc.*, Vol. 125, pp. 5264–5265, 2003.

[6] R. Kanzaki, K. Uchida, S. Hara, Y. Umebayashi, S. Ishiguro, and S. Nomura. *Chem. Lett.*, Vol. 36, pp. 684–685, 2007.

[7] R. Kanzaki, K. Uchida, X. Song, Y. Umebayashi, and S. Ishiguro. *Anal. Sci.*, Vol. 24, pp. 1347–1349, 2008.

[8] R. Kanzaki, H. Doi, X. Song, S. Hara, S. Ishiguro, and Y. Umebayashi. *J. Phys. Chem. B*, Vol. 116, pp. 14146–14152, 2012.

[9] M. Yoshizawa, W. Xu, and C. A. Angell. *J. Am. Chem. Soc.*, Vol. 125, pp. 15411–15419, 2003.

[10] I. Koppel, J. Koppel, P.-C. Maria, J.-F. Gal, R. Notario, V. M. Vlasov, and R. W. Taft. *Int. J. Mass Spectrom. Ion Processes*, Vol. 175, pp. 61–69, 1998.

[11] I. A. Koppel, J. Koppel, V. Pihl, I. Leito, M. Mishima, V. M. Vlasov, L. M. Yagupolskii, and R. W. Taft. *J. Chem. Soc., Perkin Trans. 2*, pp. 1125–1133, 2000.

[12] K. Fujii, T. Nonaka, Y. Akimoto, Y. Umebayashi, and S. Ishiguro. *Anal. Sci.*, Vol. 24, pp. 1377–1380, 2008.

[13] K. Izutsu and M. Ohmaki. *Talanta*, Vol. 43, pp. 643–648, 1996.

[14] G. Gran. *Analyst*, Vol. 77, pp. 661–671, 1952.

[15] *Tables of rate and equilibrium constants of heterolytic organic reactions*. VINITI, Moscow-Tartu, 1975-1985.

[16] R. Barhdadi, M. Troupel, C. Comminges, M. Laurent, and A. Doherty. *J. Phys. Chem. B*, Vol. 116, pp. 277–282, 2011.

[17] J. F. Coetzee and G. R. Padmanabhan. *J. Am. Chem. Soc.*, Vol. 87, pp. 5005–5010, 1965.

[18] Y. Marcus. *The properties of solvents*. Wiley series in solution chemistry. John Wiley

& Sons, New York, USA, 1998.

[19] M. Schmeisser, P. Illner, R. Puchta, A. Zahl, and R. Van Eldik. *Chem. Eur. J.*, Vol. 18, pp. 10969–10982, 2012.

Chapter 4

Effect of Protonation on the Solvation Structure of *N*-Butylamine in 1-Ethyl-3-methylimidazolium Bis(trifluoromethylsulfonyl)amide Studied by High-energy X-ray Total Scattering and Molecular Dynamics Simulations

4.1 Introduction

Room-temperature ionic liquids (ILs) composed of only ions show novel solvent properties, which quite differ from water or conventional organic solvents [1]. Due to their unique properties such as nonvolatility, nonflammability, thermal and electrochemical stability, ILs have attracted much attentions as promising solvents for many scientific fields such as organic synthetic chemistry [2, 3], electrochemistry [4–6], green chemistry [7, 8] and soft material science [9–12]. One of the most important characteristics of ILs is their designability, that is, one can bestow affinities on various molecules such as metal ions [6,13] organic molecules [3] and biopolymers [14–18] for dissolution them into ILs by designing structure of cation and anion. These dissolution properties are important for the application of ILs as a novel reaction field because many chemical reactions are performed in solution, where solute is dissolved.

Among the fundamental reactions, acid-base reaction is one of the most important reactions. In aqueous systems, acid-base properties, i.e., Brønsted acidity and basicity, are well established and understood to play a key role in chemical reactions in solution. However, in aprotic ILs (aILs), which have no dissociative protons in cation, knowledge of acid-base reactions is quite limited. Measurements of acid dissociation constant K_a, i.e. an indicative parameter of the acidity and basicity, are limited to indirect measurements such as ultraviolet-visible (UV-vis) and infrared (IR) spectroscopies [19–23] because a glass electrode is not available in typical ILs. McFarlane et al. investigated the position of the UV-vis absorption band in aILs containing a neutral solute as an indicator to point out that the acid-base properties in ILs essentially differ from that in water [21]. Barhdadi et al. directly performed cyclic voltammetry to estimate the pK_a values of some bases in 1-butyl-3-methylimidazolium bis(trifluoromethanesulfonyl)amide ($[C_4mIm^+][TFSA^-]$) [24]. The values are strongly dependent on the anion species of the IL and are significantly larger than the corresponding values in water. Krossing et al. calculated Gibbs solvation energies of the proton in ILs by quantum chemical calculations to report that ILs have novel acidity scale different from those of water or conventional solvents, which deeply depends on anion or cation species [25].

Recently, I directly determined the pK_a values of butylamine ($BuNH_2$) in the typical aIL, 1-ethyl-3-methylimidazolium bis(trifluoromethanesulfonyl)amide ($[C_2mIm^+][TFSA^-]$) by potentiometric titration using ion-sensitive field effect transistor (IS-FET) electrode [26]. The pK_a value was estimated to be 16.6(1) [26], which is significantly larger than that in water (pK_a = 10.6). This large difference in pK_a values is ascribed to the difference of Gibbs energy, which deeply depends on solvation by solvents. Thus, this result indicates that the solvation structure in ILs essentially differs from that in water.

In this work, I carried out high energy X-ray total scattering (HEXTS) measurements on $BuNH_2$ and $BuNH_3^+$ in $[C_2mIm^+][TFSA^-]$ solutions to elucidate the change of solvation structure after protonation. In order to show the solvation structure clearly, I performed MD simulation for this system. First, I discussed the solvation structure of $BuNH_2$ in $[C_2mIm^+][TFSA^-]$. On the basis of this result, I discussed the difference of solvation structure between $BuNH_2$ and $BuNH_3^+$.

4.2 Experiment

4.2.1 Materials

The IL, $[C_2mIm^+][TFSA^-]$ was synthesized according to conventional methods [27]. The water content in the IL was checked by Karl Fisher titration to be less than 50 ppm. *N*-butylamine ($BuNH_2$), purchased from Wako, was dried with molecular sieves (3A) and purified by filtering prior to use. The HTFSA was kept in a glovebox and used without further purification. By dissolving equimolar N-butylamine and HTFSA into $[C_2mIm^+][TFSA^-]$, 1-butylammonium $TFSA^-$ ($BuNH_3{}^+$) with $[C_2mIm^+][TFSA^-]$ solution was obtained.

4.2.2 HEXTS Experiments

HEXTS measurements were performed by using the HEXTS apparatus at the BL04B2 beamline of SPring-8 (Japan Synchrotron Radiation Research Institute, JASRI, Japan) [28, 29]). All of the measurements were performed at room temperature. The monochromatized X-ray of 61.4 keV was obtained using a Si(220) monochromator. The observed scattering intensity of the X-ray was corrected for absorption [30], polarization and incoherent scatterings [31, 32] to obtain coherent scattering intensities, $I_{\mathrm{coh}}(q)$. The experimental X-ray structure factor, $S^{\mathrm{exp}}(q)$, and the radial distribution function, $G^{\mathrm{exp}}(r)$, per stoichiometric volume were obtained as follows;

$$S^{\mathrm{exp}}(q) = \frac{I_{\mathrm{coh}}(q) - \sum n_i f_i(q)^2}{[\sum n_i f_i(q)]^2} + 1 \text{ and} \tag{4.1}$$

$$G^{\mathrm{exp}}(r) - 1 = \frac{1}{2\pi^2 r \rho_0} \int_0^{q_{\mathrm{max}}} q[S^{\mathrm{exp}} - 1] \sin(qr) \times \exp(-Bq^2) dq, \tag{4.2}$$

where n_i and $f_i(q)$ correspond to the number and atomic scattering factor of atom i, respectively, ρ_0 is the number density, and B is the damping factor [33].

4.2.3 MD Simulations

An MD simulation for an *NTP* ensemble (298 K and 1 atm) in a cubic cell was performed using Materials Explorer 4.0 program (Fujitsu), and the composition (number of ion pairs and solutes) in a given system is listed in Table 4.1. The simulation time was 2.0 ns for all

of the systems. The system was equilibrated for the first 50 ps with an interval of 0.2 fs, and the data collected at every 0.1 ps during 2.0 ns were analyzed to obtain the X-ray weighted structure factors and radial distribution functions, $S^{\mathrm{MD}}(q)$ and $G^{\mathrm{MD}}(r)$, respectively. CLaP and OPLS-AA force fields were used for IL ions and solutes ($BuNH_2$ and $BuNH_3^+$), respectively [34–38], including intermolecular Lennard-Jones and Coulombic interactions and intramolecular interactions with bond stretching, angle bending, and torsion of dihedral angles. The detailed procedure of MD simulations was described elsewhere [27, 39–47]. The density values obtained by the MD simulations showed good agreement with the corresponding experimental ones, which are also listed in Table 4.1. The $S^{\mathrm{MD}}(q)$ and $G^{\mathrm{MD}}(r)$ were calculated from the trajectory obtained by MD simulations to directly compare the MD result with HEXTS experiments, as follows,

$$S^{\mathrm{MD}}(q) = \begin{cases} \frac{\sum_i \sum_j [n_i(n_i-1)f_i(q)f_j(q)/N(N-1)]}{[\sum_k (n_k f_k(q)/N)]^2} \int_0^r 4\pi\rho_0 (g_{ij}^{\mathrm{MD}}(r) - 1)\frac{\sin qr}{qr} dr + 1 & (i = j) \\ \frac{\sum_i \sum_j [2n_i n_j f_i(q)f_j(q)/N^2]}{[\sum_k (n_k f_k(q)/N)]^2} \int_0^r 4\pi\rho_0 (g_{ij}^{\mathrm{MD}}(r) - 1)\frac{\sin qr}{qr} dr + 1 & (i \neq j) \end{cases} \tag{4.3}$$

,where the total number of atoms in the simulation box, N is given by $N = \Sigma_k n_{\mathrm{k}}$. The X-ray radial distribution function $G^{\mathrm{MD}}(r)$ was obtained from $S^{\mathrm{MD}}(q)$ by a Fourier transform procedure similar to that of $G^{\mathrm{exp}}(r)$.

Table 4.1. Compositions and densities of the systems for the MD simulations.

Solute species (concentration)[a]	Density / g cm^{-3} MD[b]	Exp[c]	Solute	Cation	Anion
$BuNH_2$ (15 mol%)	1.537	1.475	45	256	256
$BuNH_2$ (30 mol%)	1.496	1.414	110	256	256
$BuNH_3^+$ (30 mol%)	1.607	1.501	110	256	256

[a]Mol fraction of solute in IL, [C_2mIm$^+$][TFSA$^-$].

[b]Densities obtained from MD simulations.

[c]Densities obtained from experiments.

4.3 Results and discussion

4.3.1 HEXTS Experiment

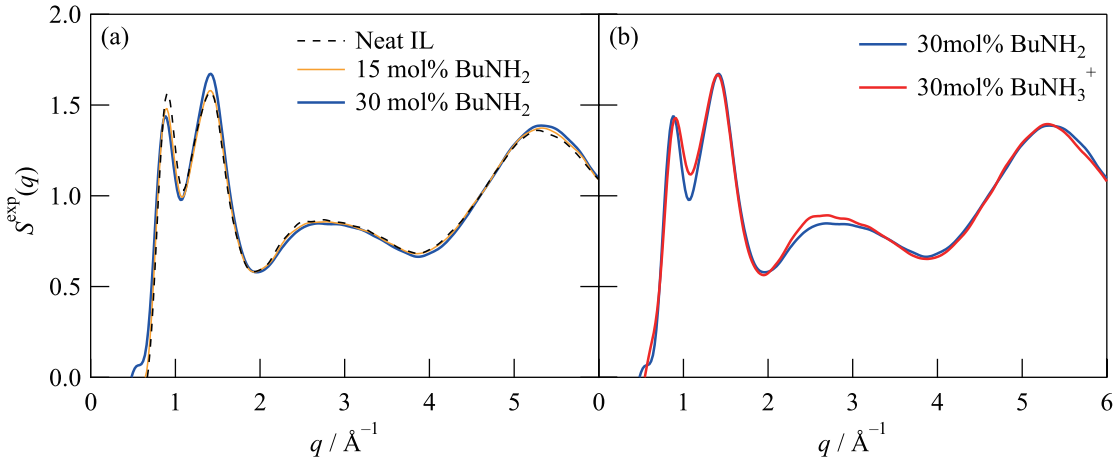

Figure 4.1. (a) $BuNH_2$ concentration dependence of X-ray structure factors, $S^{exp}(q)$'s, and (b) protonation effect to $S^{exp}(q)$ for $BuNH_2$ in $[C_2mIm^+][TFSA^-]$ solution.

Figure 4.1 (a) shows the observed $S^{exp}(q)$ for $BuNH_2$ in $[C_2mIm^+][TFSA^-]$ solutions in the q range of 0.2–6.0 $Å^{-1}$, together with the corresponding neat $[C_2mIm^+][TFSA^-]$. The first peak at 0.9 $Å^{-1}$ decreased in the intensity with increasing $BuNH_2$ concentration and the reverse was observed in the second one at 1.5 $Å^{-1}$. This indicates that intermolecular interaction between $BuNH_2$ and IL ions (anion and cation) is formed instead of ion–ion interaction of $[C_2mIm^+][TFSA^-]$ to form a new solvation structure surrounding $BuNH_2$. Figure 4.1 (b) shows the observed $S^{exp}(q)$ for $BuNH_3^+$ in $[C_2mIm^+][TFSA^-]$ solution together with the corresponding $BuNH_2$ data. As can be clearly seen, the shape of the first peak at 0.9 $Å^{-1}$ obviously became broader. This implies that solvation structure significantly changed by protonation.

Figure 4.2 shows the experimental radial distribution function, $G^{exp}(r)$, as a form of $r^2[G(r)-1]$ for 0–30 mol% $BuNH_2$ and 30 mol% protonated $BuNH_3^+$ in $[C_2mIm^+][TFSA^-]$ solutions in the r range of 0–10 Å. It has been established in our previous works that the peaks at $r < 3$ Å is mainly assigned to the intramolecular interactions for solute and solvent. In the r-range of 3–6 Å, the component for intermolecular interaction is seriously overlapped with that for the intramolecular interaction. Therefore, we tried to extract a partial radial distribution function for intermolecular component, particularly, $BuNH_2$–IL and $BuNH_3^+$–IL interaction, from the total $G^{MD}(r)$ to discuss solvation of $BuNH_2$ in IL solution.

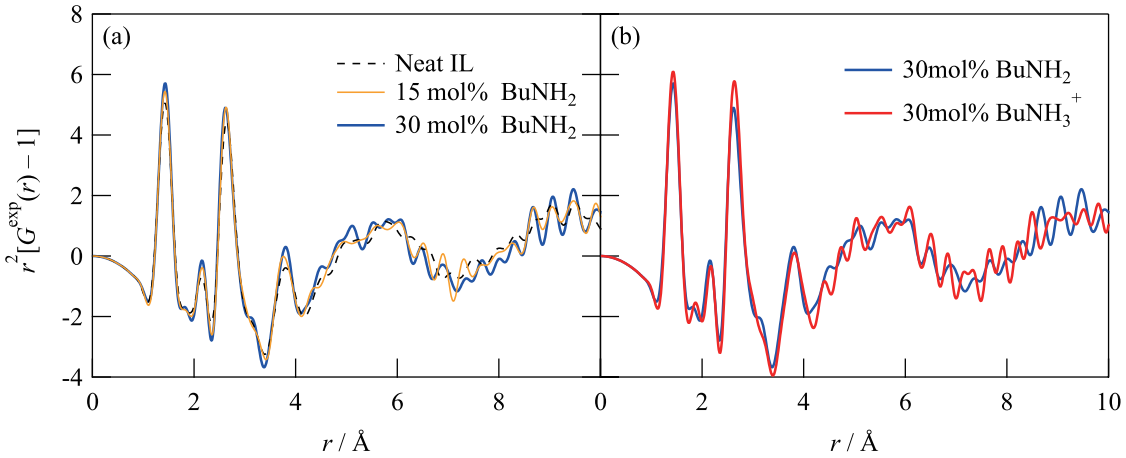

Figure 4.2. (a) $BuNH_2$ concentration dependence of radial distribution functions, $r^2[G(r) - 1]$'s, and (b) protonation effect to $r^2[G(r) - 1]$ for $BuNH_2$ in $[C_2mIm^+][TFSA^-]$ solution.

4.3.2 MD Simulations

Figure 4.3 shows X-ray weighted radial distribution functions, $r^2[G^{MD}(r) - 1]$'s, for (a) 15, (b) 30 mol% $BuNH_2$ and (c) 30 mol% $BuNH_3^+$ in $[C_2mIm^+][TFSA^-]$ solutions, together with the corresponding $r^2[G^{exp}(r) - 1]$'s obtained by HEXTS experiments. It was clearly found that the MD results well reproduce the HEXTS ones for all of the experiments examined here. The MD-derived total $G^{MD}(r)$ can be divided into intra- and intermolecular components, $G^{MD}{}_{intra}(r)$ and $G^{MD}{}_{inter}(r)$. We thus extracted the partial $G^{MD}{}_{intra}(r)$'s and $G^{MD}{}_{inter}(r)$'s to discuss the solvation structure of $BuNH_2$ and $BuNH_3^+$ in $[C_2mIm^+][TFSA^-]$. By separating two type of the $G(r)$, the peaks observed in Figure 4.3 can be assigned. The peaks at 1.5, 2.1, and 2.7 Å in the $r^2[G(r) - 1]$ were mainly assigned to the intramolecular correlations within C_2mIm^+ and $TFSA^-$ components according to our previous report [27] and thus the other peaks might be assigned to the intermolecular correlations. To discuss the intermolecular correlation in detail, the $G^{MD}{}_{inter}(r)$ is separated to six intermolecular interactions, that is, solute–anion, solute–cation, solute–solute, cation–anion, anion–anion, and cation–cation components, which are discussed in detail in the following sections.

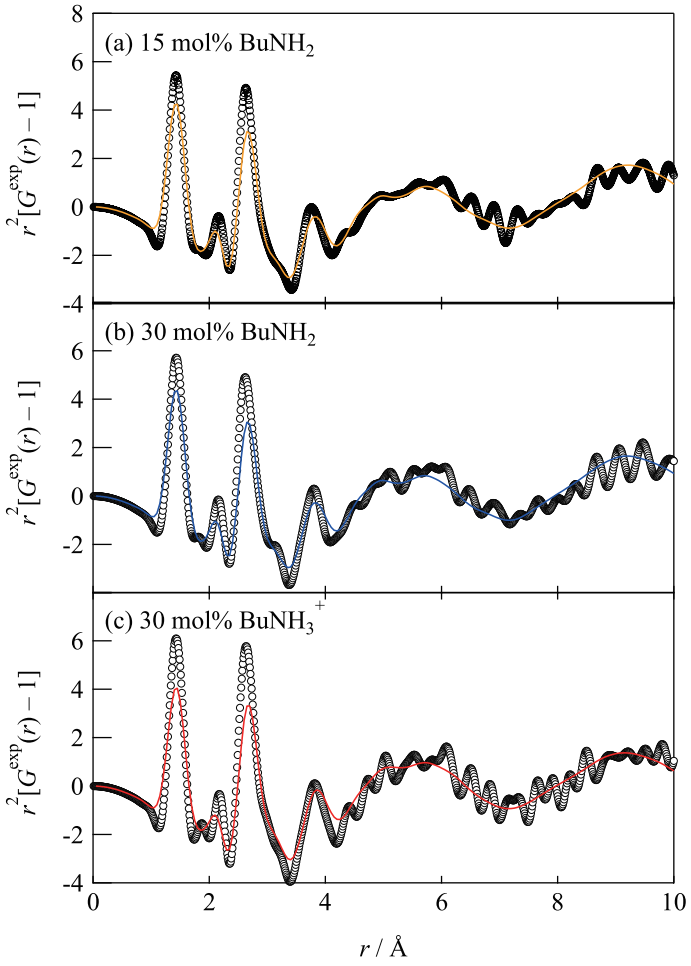

Figure 4.3. Radial distribution function, $r^2[G^{\mathrm{MD}}(r) - 1]$'s, for (a) 15, (b) 30 mol% $BuNH_2$ and (c) 30 mol% $BuNH_3^+$ in $[C_2mIm^+][TFSA^-]$ solutions. The open circles correspond to the experimental $r^2[G^{\mathrm{exp}}(r) - 1]$'s, and the solid lines correspond to the theoretical $r^2[G^{\mathrm{MD}}(r) - 1]$'s derived from MD simulations.

4.3.3 Solvation Structure of $BuNH_2$ in $[C_2mIm^+][TFSA^-]$

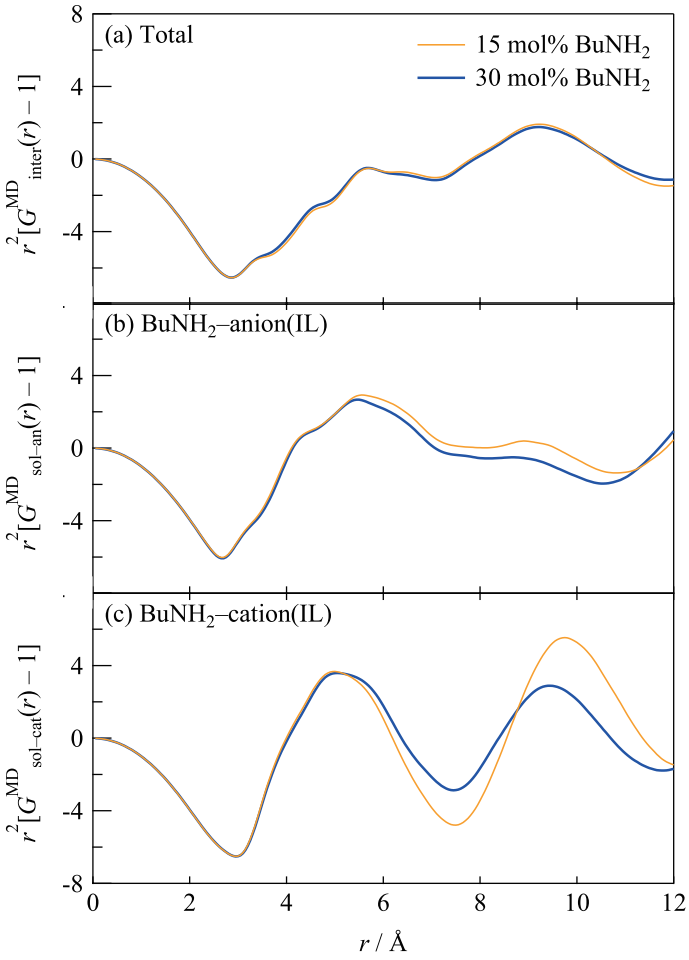

Figure 4.4. X-ray weighted (a)total $G^{MD}{}_{inter}(r)$, as a form of $r^2[G(r) - 1]$ obtained from MD simulations for 15–30 wt% $BuNH_2$ in $[C_2mIm^+][TFSA^-]$ solutions, together with the partial $G^{MD}{}_{inter}(r)$'s for (b) solute–cation(IL), $r^2[G^{MD}{}_{sol-cat}(r)-1]$, and (b) solute–anion(IL), $r^2[G^{MD}{}_{sol-an}(r) - 1]$, interactions.

Figure 4.4 shows total $G^{MD}{}_{inter}(r)$ as a form of $r^2[G(r) - 1]$ for 15–30 wt% $BuNH_2$ in $[C_2mIm^+][TFSA^-]$ solutions, together with the corresponding partial $G^{MD}{}_{inter}(r)$'s for solute–anion(IL) and solute–cation(IL) components ($r^2[G^{MD}{}_{sol-cat(r)} - 1]$ and $r^2[G^{MD}{}_{sol-an(r)} - 1]$, respectively). Here, the partial radial distribution functions, $r^2[G^{MD}{}_{i-j} - 1]$'s (i and j correspond to solute, cation or anion species), are normalized by the number of combinations of ion pairs at rmax (= 20 Å in this work) and their X-ray scattering abilities, i.e. $r2[G^{MD}{}_{i-j}(r)/G^{MD}{}_{i-j}(r_{max}) - 1]$. In Figure 4.4 (a), the total $r^2[G^{MD}{}_{inter}(r) - 1]$ exhibited a clear peak a at 4.6 Å, which corresponds to the nearest-neighbor interaction in this system.

It is clearly seen in Figure 4.4 (b) that the main peaks at 4.6 Å in the total $r^2[G^{\mathrm{MD}}{}_{\mathrm{inter}}(r) - 1]$ can be assigned to the $BuNH_2$–anion(IL) interactions. The peaks at 5.7 and 9.2 Å in total $r^2[G^{\mathrm{MD}}{}_{\mathrm{inter}}(r) - 1]$ also can be assigned to the $BuNH_2$–anion(IL) interactions. As can be seen from Figure 4.4 (c), $r^2[G^{\mathrm{MD}}{}_{\mathrm{sol-cat}}(r) - 1]$ showed a clear peak at 5.0 Å, indicating that the C_2mIm^+ cations are the second neighbor of $BuNH_2$. We thus concluded that the $BuNH_2$ molecules are preferentially solvated by the $TFSA^-$ anion in the $[C_2mIm^+][TFSA^-]$ and then, contributions of the C_2mIm^+ cation to the solvation are relatively small.

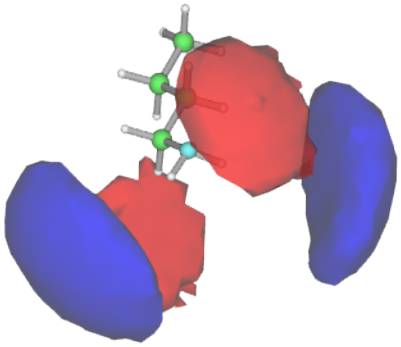

Figure 4.5. SDFs of the center of mass of $TFSA^-$ anion and C_2mIm^+ cation surrounding N atoms within $BuNH_2$, obtained for 30 mol% $BuNH_2$ in $[C_2mIm^+][TFSA^-]$. The blue and red clouds indicate the isoprobability surface of $TFSA^-$ anion and C_2mIm^+ cation, respectively.

Figure 4.5 shows typical spatial distribution functions (SDFs) calculated from center of mass of $TFSA^-$ anion (blue cloud) and C_2mIm^+ cation (red cloud) surrounding N atoms within $BuNH_2$, calculated from the MD trajectory. The clouds in the SDFs indicate the isoprobability surfaces of a given ion. It was found that the center of mass of the $TFSA^-$ anion is located around the H atoms within the NH_2 group and then C_2mIm^+ cation is located between anions. Here, we note the SDFs reported for typical imidazolium-based ILs with balky anions, $[C_nmIm^+][X^-]$ with X = $TFSA^-$ [40] and FSA^- [47]. These anions have low polarity and highly delocalized charge and the interaction between cation and anion is almost from an electrostatic contribution. However, the O atoms in $TFSA^-$ has still considerable polarity, thus hydrogen bond between H and O atom observed in this system. We concluded that $TFSA^-$ anion has the polarity and then forms a hydrogen bond with the $BuNH_2$ molecule.

4.3.4 Solvation Structure of $BuNH_3^+$ in $[C_2mIm^+][TFSA^-]$

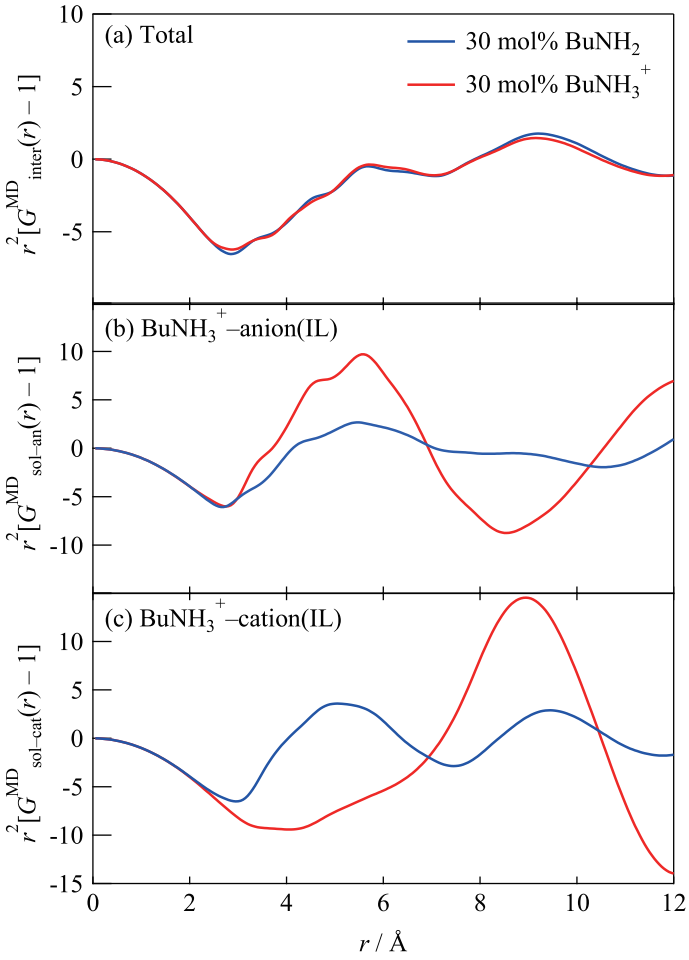

Figure 4.6. X-ray weighted (a)total $G^{MD}{}_{inter}(r)$, as a form of $r^2[G(r) - 1]$ obtained from MD simulations for 30 wt% $BuNH_2$ and $BuNH_3^+$ in $[C_2mIm^+][TFSA^-]$ solutions, together with the partial $G^{MD}{}_{inter}(r)$'s for (b) solute–cation(IL), $r^2[G^{MD}{}_{sol-cat}(r) - 1]$, and (b) solute–anion(IL), $r^2[G^{MD}{}_{sol-an}(r) - 1]$, interactions.

Figure 4.6 shows total $G^{MD}{}_{inter}(r)$ as a form of $r^2[G(r) - 1]$ for 30 wt% $BuNH_2$ and $BuNH_3^+$ in $[C_2mIm^+][TFSA^-]$ solutions, together with the corresponding partial $G^{MD}{}_{inter}(r)$'s for solute–anion(IL) and solute–cation(IL) components ($r^2[G^{MD}{}_{sol-cat(r)} - 1]$ and $r^2[G^{MD}{}_{sol-an(r)} - 1]$, respectively). In Figure 4.6 (a), the total $r^2[G_{inter}(r) - 1]$ exhibited a similar peak to the $BuNH_2$ system, however, the shape around 4.0 Å, which corresponds to the nearest-neighbor interaction, slightly changed. As can be seen from Figure 4.6 (b), a clear peak was observed at 4.2 Å. The peak position moves from 4.6 to 4.2 Å by protonation, indicating $TFSA^-$ anion shows stronger interaction with $BuNH_3^+$ than $BuNH_2$ system. On

the other hand, in Figure 4.6 (c), the second neighbor peak from C_2mIm^+ cation is observed at 9 Å. This indicates that the $BuNH_3^+$–cation(IL) interaction becomes significantly weaker than $BuNH_2$ system instead of the strong $BuNH_3^+$–anion(IL) interaction. We thus concluded that the $BuNH_3^+$ molecules are more preferentially solvated by the $TFSA^-$ anion in the $[C_2mIm^+][TFSA^-]$ than the $BuNH_2$ system.

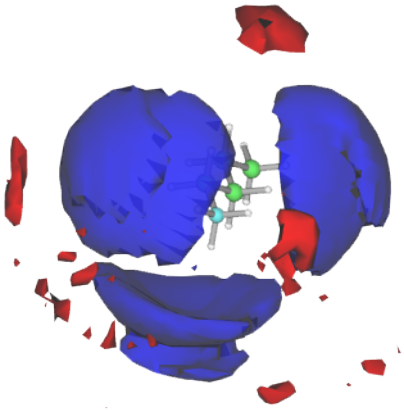

Figure 4.7. SDFs of the center of mass of $TFSA^-$ anion and C_2mIm^+ cation surrounding N atoms within $BuNH_3^+$, obtained for 30 mol% $BuNH_3^+$ in $[C_2mIm^+][TFSA^-]$. The blue and red clouds indicate the isoprobability surface of $TFSA^-$ anion and C_2mIm^+ cation, respectively.

Figure 4.7 shows typical SDFs calculated from center of mass of $TFSA^-$ anion (blue cloud) and C_2mIm^+ cation (red cloud) surrounding N atoms within $BuNH_3^+$, calculated from the MD trajectory. As with the $BuNH_2$ system, it was found that the center of mass of the $TFSA^-$ anion is located around the H atoms within the NH_3^+ group. However, note that, the coordination number of $TFSA^-$ anion increased from 2 to 3 by protonation. On the other hand, C_2mIm^+ cation is located outside anions, which indicates that the interaction with $BuNH_3^+$ for C_2mIm^+ cation is significantly weaker than that for $TFSA^-$ anion. This results indicate that the solvation structure of $TFSA^-$ anion plays a key role in the large stabilization energy by protonation of $BuNH_2$ in aprotic IL.

4.3.5 Atom-atom interaction between amine and $TFSA^-$ anion.

To discuss local interactions of solute and anion in detail, we further analyzed the MD results to evaluate the atom–atom pair correlation functions, $g^{MD}_{atom-atom}(r)$'s. Here, we focused on the atom–atom interactions for intermolecular solute–anion components.

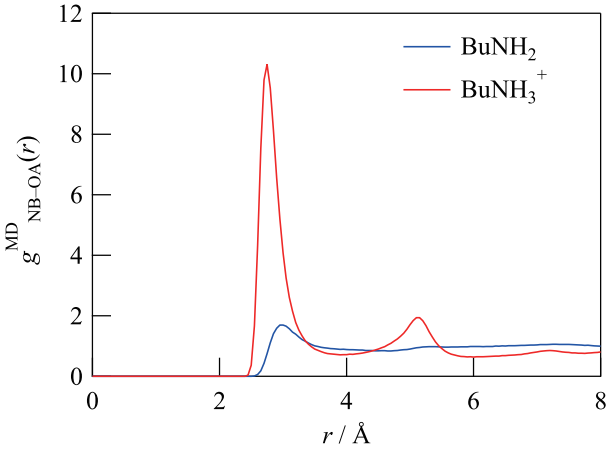

Figure 4.8. Atom–atom pair correlation functions, $g^{\mathrm{MD}}{}_{\mathrm{atom-atom}}(r)$'s for O atom within $TFSA^-$ anion around N atom for (a) $BuNH_2$ and (b) $BuNH_3{}^+$ systems.

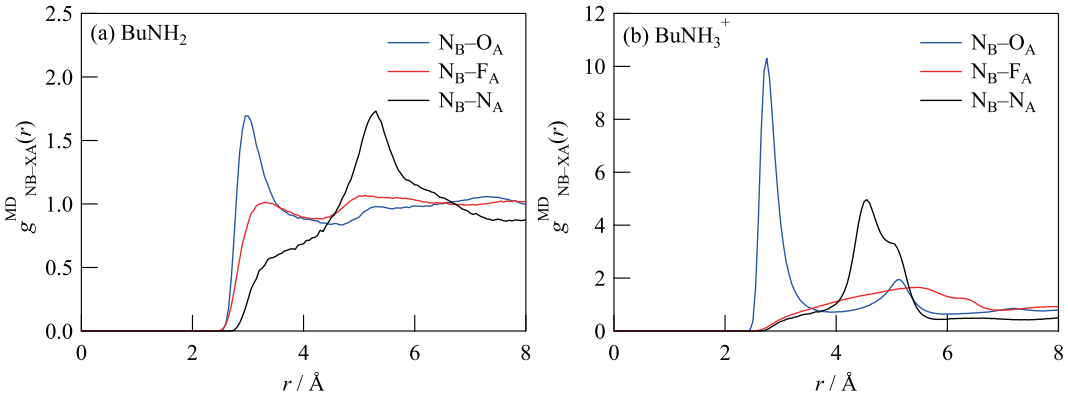

Figure 4.9. Atom–atom pair correlation functions, $g^{\mathrm{MD}}{}_{\mathrm{atom-atom}}(r)$'s for O, F and N atoms within $TFSA^-$ anion around N atom for (a) $BuNH_2$ and (b) $BuNH_3{}^+$ systems.

Figure 4.8 shows the $g^{\mathrm{MD}}{}_{\mathrm{NB-OA}}(r)$'s for the interaction between N atom within the $BuNH_2$ or $BuNH_3{}^+$ (N_B) and O atom within $TFSA^-$ anion (O_A). Other $g^{\mathrm{MD}}{}_{\mathrm{NB-XA}}$'s (X = N, O, F and S) were shown in Figure 4.9. The first peak position of $g^{\mathrm{MD}}{}_{\mathrm{NB-OA}}(r)$ for $BuNH_2$ system appeared at 3.0 Å, whereas corresponding peak position for other $g^{\mathrm{MD}}{}_{\mathrm{NB-XA}}$'s were longer than it (see figure 4.9). In $BuNH_3{}^+$ system, The first peak position of $g^{\mathrm{MD}}{}_{\mathrm{NB-OA}}(r)$ also appeared at 2.8 Å and similar behavior to $BuNH_2$ system was observed. The distance of the closest N-H (solute) · · · O (anion) correlation in both systems are consistent with the distance for the hydrogen bond (N-H · · · O, 2.8–3.1 Å). [48] We thus concluded that hydrogen bond mainly contributes to the the correlation between solute ($BuNH_2$ or $BuNH_3{}^+$) and anion ($TFSA^-$). Here, note that a significant difference is found in the first peak intensity between two systems. We thus estimated the coordination number of O atoms within $TFSA^-$ anion around N atom within $BuNH_2$ or $BuNH_3{}^+$ to discuss the difference in detail.

The coordination numbers of the O atom within $TFSA^-$ anion around N atom within

Table 4.2. Coordination number of atoms in the first and second solvation shell of N_B-O_A in $BuNH_2$ and $BuNH_3^+$.

	Coordination number (peak position / Å)	
Solute species	First peak	Second peak
$BuNH_2$ (30 mol%)	2.58 (3.0)	- (-)
$BuNH_3^+$ (30 mol%)	4.99 (2.8)	6.75 (5.1)

$BuNH_2$ or $BuNH_3^+$ were listed in Table 4.2. In the $BuNH_2$ system, the coordination number of nearest-neighbor O atom is approximately 2 due to two N-H bond within $BuNH_2$. On the other hand, in the $BuNH_3^+$ system, the coordination number increased to be approximately 5, which is more than 3, i.e., the number of N-H bond within $BuNH_3^+$. This indicates that the $BuNH_3^+$ was highly attracted by negative charge of O atom to form new solvation structure, that is, partially two O atom within one $TFSA^-$ anion were attracted to exist within first solvation shell around N atom. In addition, a second peak was clearly observed in the $BuNH_3^+$ system. The coordination number for the second peak was estimated to be 6.75, which is more than that for the first peak. This result indicates that all of the O atom within surrounding $TFSA^-$ anion were attracted by positive charge of $BuNH_3^+$, resulting in more ordered orientation of $TFSA^-$ anion than $BuNH_2$ system, where the second peak was not observed. We thus concluded that the protonation strongly affects the solvation structure and coordination number of anion, resulting in large Gibbs energy of protonation.

4.4 Conclusion

The solvation structures of $BuNH_2$ and $BuNH_3^+$ in $[C_2mIm^+][TFSA^-]$ were investigated by HEXTS experiments and MD simulations and quantitatively discussed in terms of structural parameters such as distance, orientation, and coordination number for inter- and intramolecular interactions in the solutions to elucidate large pK_a value of $BuNH_3^+$. The experimental radial distribution functions, $r^2[G^{MD}(r) - 1]$, were well reproduced by theoretical ones derived from MD simulations for all of the systems examined here. It was found that the $BuNH_2$ and $BuNH_3^+$ molecules are preferentially solvated with the $TFSA^-$ anion rather than the C_2mIm^+ cation. We pointed out that the hydrogen bond between O_A (anion) and H_N ($BuNH_2$ or $BuNH_3^+$) is predominant in the solute–IL interaction due to a localized negative charge within four oxygen atoms of the anion. After protonation, the coordination number of $TFSA^-$ anion increased from 2 to 3, resulting in the large stabilization

energy. Eventually, we concluded that drastic change of solvation structure results in large pK_{a} value.

Reference

[1] T. Welton. *Chem. Rev.*, Vol. 99, pp. 2071–2083, 1999.

[2] A. J. Carmichael, M. J. Earle, J. D. Holbrey, P. B. Mccormac, and K. R. Seddon. *Org. Lett.*, Vol. 1, pp. 997–1000, 1999.

[3] C. Chiappe and D. Pieraccini. *J. Phys. Org. Chem.*, Vol. 18, pp. 275–297, 2005.

[4] M. C. Buzzeo, R. G. Evans, and R. G. Compton. *ChemPhysChem.*, Vol. 5, pp. 1106–1120, 2004.

[5] M. Galinski, A. Lewandowski, and I. Stepniak. *Electrochim. Acta*, Vol. 51, pp. 5567–5580, 2006.

[6] S. Seki, Y. Kobayashi, H. Miyashiro, Y. Ohno, A. Usami, Y. Mita, N. Kihira, M. Watanabe, and S. Terada. *J. Phys. Chem. B*, Vol. 110, pp. 10228–10230, 2006.

[7] A. Farran, C. Cai, M. Sandoval, Y. Xu, J. Liu, M. J. Hernaiz, and R. J. Linhardt. *Chem. Rev.*, Vol. 115, pp. 6811–6853, 2015.

[8] M. C. Bubalo, S. Vidovic, I. R. Redovnikovic, and S. Jokic. *J. Chem. Technol. Biotechnol.*, Vol. 90, pp. 1631–1639, 2015.

[9] T. Ueki and M. Watanabe. *Chem. Lett.*, Vol. 35, pp. 964–965, 2006.

[10] T. Ueki and M. Watanabe. *Langmuir*, Vol. 23, pp. 988–990, 2007.

[11] T. Kato. *Angew. Chem. Int. Ed.*, Vol. 49, pp. 7847–7848, 2010.

[12] K. Fujii, H. Asai, T. Ueki, T. Sakai, S. Imaizumi, U. Chung, M. Watanabe, and M. Shibayama. *Soft Matter*, Vol. 8, pp. 1756–1759, 2012.

[13] S. Dai, Y. H. Ju, and C. E. Barnes. *J. Chem. Soc., Dalton Trans.*, Vol. 8, pp. 1201–1202, 1999.

[14] R. Madeira Lau, F. Van Rantwijk, K. R. Seddon, and R. A. Sheldon. *Org. Lett.*, Vol. 2, pp. 4189–4191, 2000.

[15] F. Rantwijk and R. A. Sheldon. *Chem. Rev.*, Vol. 107, pp. 2757–2785, 2007.

[16] M. Moniruzzaman, N. Kamiya, K. Nakashima, and M. Goto. *Green Chem.*, Vol. 10, pp. 497–500, 2008.

[17] R. P. Swatloski, S. K. Spear, J. D. Holbrey, and R. D. Rogers. *J. Am. Chem. Soc.*, Vol. 124, pp. 4974–4975, 2002.

[18] Y. Fukaya, K. Hayashi, M. Wada, and H. Ohno. *Green Chem.*, Vol. 10, pp. 44–46, 2008.

[19] E. I. Rõõm, A. Kütt, I. Kaljurand, I. Koppel, I. Leito, I. A. Koppel, M. Mishima, K. Goto, and Y. Miyahara. *Chem. Eur. J.*, Vol. 13, pp. 7631–7643, 2007.

[20] L. Sooväli, I. Kaljurand, A. Kütt, and I. Leito. *Anal. Chim. Acta*, Vol. 566, pp. 290–303,

2006.

[21] D. R. Macfarlane, J. M. Pringle, K. M. Johansson, S. A. Forsyth, and M. Forsyth. *Chem. Commun.*, pp. 1905–1917, 2006.

[22] J. Stoimenovski, E. I. Izgorodina, and D. R. Macfarlane. *PCCP*, Vol. 12, pp. 10341–10347, 2010.

[23] C. Thomazeau, H. Olivier-Bourbigou, L. Magna, S. Luts, and B. Gilbert. *J. Am. Chem. Soc.*, Vol. 125, pp. 5264–5265, 2003.

[24] R. Barhdadi, M. Troupel, C. Comminges, M. Laurent, and A. Doherty. *J. Phys. Chem. B*, Vol. 116, pp. 277–282, 2011.

[25] D. Himmel, S. K. Goll, F. Scholz, V. Radtke, I. Leito, and I. Krossing. *Chemphyschem*, Vol. 16, pp. 1428–1439, 2015.

[26] K. Fujii, K. Hashimoto, T. Sakai, Y. Umebayashi, and M. Shibayama. *Chem. Lett.*, Vol. 42, pp. 1250–1251, 2013.

[27] K. Fujii, R. Kanzaki, T. Takamuku, Y. Kameda, S. Kohara, M. Kanakubo, M. Shibayama, S. Ishiguro, and Y. Umebayashi. *J. Chem. Phys.*, Vol. 135, p. 244502, 2011.

[28] S. Kohara, K. Suzuya, Y. Kashihara, N. Matsumoto, N. Umesaki, and I. Sakai. *Nucl. Instrum. Meth. A*, Vol. 467-468, pp. 1030–1033, 2001.

[29] M. Isshiki, Y. Ohishi, S. Goto, K. Takeshita, and T. Oshikawa. *Nucl. Instrum. Meth. A*, Vol. 467-468, pp. 663–666, 2001.

[30] S. Sakai. *Kek report*, Vol. 90-16. National Laboratory for High Energy Physics, Tsukuba, Japan, 1990.

[31] D. T. Cromer. *J. Chem. Phys.*, Vol. 50, pp. 4857–4859, 1969.

[32] D. T. Cromer and R. J. Howerton. *J. Phys. Chem. Ref. Data*, Vol. 4, pp. 471–538, 1975.

[33] E. N. Maslen, A. G. Fox, M. A.O' keefe. *International tables for crystallography*, 第 C 巻. Kluwer, Dorfrecht, The Netherlands, 1999.

[34] W. D. Cornell, P. Cieplak, C. I. Bayly, I. R. Gould, K. M. Merz, D. M. Ferguson, D. C. Spellmeyer, T. Fox, J. W. Caldwell, and P. A. Kollman. *J. Am. Chem. Soc.*, Vol. 117, pp. 5179–5197, 1995.

[35] W. Damm, A. Frontera, J. Tirado-Rives, and W. L. Jorgensen. *J. Org. Chem.*, Vol. 18, pp. 1955–1970, 1997.

[36] J. N. a. C. Lopes and A. a. H. Pádua. *J. Phys. Chem. B*, Vol. 108, pp. 2038–2047, 2004.

[37] J. N. a. C. Lopes, M. F. C. Gomes, and A. a. H. Pádua. *J. Phys. Chem. B*, Vol. 110, pp. 16816–16818, 2006.

[38] K. Murzyn, M. Bratek, and M. Pasenkiewicz-Gierula. *J. Phys. Chem. B*, Vol. 117, pp.

16388–16396, 2013.

[39] S. Fukuda, M. Takeuchi, K. Fujii, R. Kanzaki, T. Takamuku, K. Chiba, H. Yamamoto, Y. Umebayashi, and S. Ishiguro. *J. Mol. Liquids*, Vol. 143, pp. 2–7, 2008.

[40] K. Fujii, Y. Soejima, Y. Kyoshoin, S. Fukuda, R. Kanzaki, Y. Umebayashi, T. Yamaguchi, S. Ishiguro, and T. Takamuku. *J. Phys. Chem. B*, Vol. 112, pp. 4329–4336, 2008.

[41] K. Fujii, S. Seki, S. Fukuda, T. Takamuku, S. Kohara, Y. Kameda, Y. Umebayashi, and S. Ishiguro. *J. Mol. Liquids*, Vol. 143, pp. 64–69, 2008.

[42] Y. Umebayashi, W.-L. Chung, T. Mitsugi, S. Fukuda, M. Takeuchi, K. Fujii, T. Takamuku, R. Kanzaki, and S. Ishiguro. *J. Comput. Chem. Jpn.*, Vol. 7, pp. 125–134, 2008.

[43] K. Fujii, T. Mitsugi, T. Takamuku, T. Yamaguchi, Y. Umebayashi, and S. Ishiguro. *Chem. Lett.*, Vol. 38, pp. 340–341, 2009.

[44] R. Kanzaki, T. Mitsugi, S. Fukuda, K. Fujii, M. Takeuchi, Y. Soejima, T. Takamuku, T. Yamaguchi, Y. Umebayashi, and S. Ishiguro. *J. Mol. Liquids,*, Vol. 147, pp. 77–82, 2009.

[45] Y. Umebayashi, H. Hamano, S. Tsuzuki, J. N. a. C. Lopes, A. a. H. Pádua, Y. Kameda, S. Kohara, T. Yamaguchi, K. Fujii, and S. Ishiguro. *J. Phys. Chem. B*, Vol. 114, pp. 11715–11724, 2010.

[46] H. Asai, K. Fujii, K. Nishi, T. Sakai, K. Ohara, Y. Umebayashi, and M. Shibayama. *Macromolecules*, Vol. 46, pp. 2369–2375, 2013.

[47] K. Fujii, S. Seki, K. Ohara, Y. Kameda, H. Doi, S. Saito, and Y. Umebayashi. *J. Solution Chem.*, Vol. 43, pp. 1655–1668, 2014.

[48] K. Nakamoto, M. Margoshes, and R. E. Rundle. *J. Am. Chem. Soc.*, Vol. 77, pp. 6480–6486, 1955.

Chapter 5

Gelation Mechanism of Tetra-armed Poly(ethylene glycol) in Aprotic Ionic Liquid Containing Non-volatile Proton Source, Protic Ionic Liquid

5.1 Introduction

3D Polymer networks combined with ionic liquids (ILs), i.e., iongels are investigated and applied as polymer electrolytes for electrochemical devises [1–6], polymer actuators [7–11], and membranes for gas separations [12–17]. Iongels are well known as environmentally green materials [18, 19] because ILs have negligible volatility, non-flammability, thermal and chemical stabilities [20–22]. Physicochemical and electrochemical properties of iongels strongly depend on solubility of polymers in ILs, and these properties can be controlled by combination of polymers and ILs. That is, the iongels composed of polymers which have good compatibility with ILs can contain a large amount of solvent IL, resulting in high ion conductivity and gas absorption selectivity. Ueki and Watanabe reviewed the solubility of several polymers in typical aprotic ILs (aILs) [23]. They pointed out that certain combinations of polymers and ILs show temperature-induced phase separations. Both lower and upper critical solution temperature (LCST and UCST, respectively) type phase separations occur in the ILs, and their phase separation temperatures can be easily changed by the polymer-IL combinations. Furthermore, the cross linked iongels obtained by their combinations show

reversible swelling/shrinking behavior, that is, a volume phase transition [24].

In the development of iongels as polymer electrolytes and gas separation membranes, one of the requirements for the applications is establishment of iongel with high mechanical toughness at low polymer and high solvent IL contents. Lodge et al. reported high toughness iongels composed of ABA-type triblock copolymers in conventional aILs with relatively low polymer concentrations (10–20 wt%), which show high ionic conductivity and high performance as CO_2 separation membranes [25, 26]. Recently, they have also reported high toughness iongel with 10 wt% triblock copolymer based on poly(styrene-*b*-ethylene oxide-*b*-styrene), which is prepared by chemical cross-linking in IL [27, 28]. Kamio et al. proposed the thin membranes for CO_2 separations using poly(vinyl pyrrolidone)-based iongels containing 50–70 wt% amino acid-based IL [29–31]. The free-standing iongel containing 70 wt% amino acid-based IL exhibits the compression breaking stress of 1 MPa for 60% strain, resulting in good CO_2 permeability and separation performance. We also proposed high toughness iongel using tetra-armed poly(ethylene glycol) (TetraPEG) as a network polymer [32, 33]. The TetraPEG iongel can be prepared by cross-end coupling reaction of two different amine- and *N*-hydroxysuccinimide-terminated TetraPEGs (TetraPEG-NH_2 and TetraPEG-NHS, respectively) in aILs to give a free-standing iongel even with low polymer content (3–6 wt%). The mechanical properties of the TetraPEG iongel, for example, the maximum breaking compression modulus reaches 18 MPa (83.5% strain) at 6 wt% polymer content. The excellent mechanical toughness is ascribed to a homogeneous polymer network structure according to our structural study [34–37].

According to our systematic study on TetraPEG hydrogel system, the gelation reaction of TetraPEGs strongly depends on the pH in solution. It has been established in our previous work that TetraPEG gelation undergoes as a simple second-order reaction kinetics, $-d[\text{-NH}_2]/dt = k_{\text{gel}}[\text{-NH}_2][\text{-NHS}]$ in aqueous system, where k_{gel} is the reaction rate constant [38–40]. Furthermore, I have pointed out that the gelation time is directly related to the acid-base reaction of the terminal NH_2 group within TetraPEG-NH_2 (TetraPEG-NH_2 + $H^+ \rightleftarrows$ TetraPEG-NH_3^+). The concentration of NH_2 group decreases in a lower pH (or higher $[H^+]$), resulting in a longer gelation time. It is thus expected in an aIL system that has no dissociative H^+ within either the cation or the anion, the addition of H^+ sources is thus required for gelation control. I recently proposed the addition of protic IL (pIL) as a non-volatile H^+ source into solvent aIL [41]. The gelation time of TetraPEG in $[C_2mIm^+][TFSA^-]$ is evidently prolonged in the presence of 1-ethyllimidazolium $TFSA^-$, $[C_2ImH^+][TFSA^-]$ (pIL). This implies that the acid-base properties of TetraPEG-NH_2 in $[C_2mIm^+][TFSA^-]$ play a key role on the gelation process as well as the hydrogel system.

However, knowledge of acid-base properties of solutes in solvent aILs is still limited at the present stage [42, 43]. Particularly, those in polymer/aIL systems have never been reported yet.

In this work, I report the pIL effects on the gelation mechanism of TetraPEG in aIL systems. I mainly focus on the acid-base equilibrium of the terminal NH_2 groups within TetraPEG, and discuss the relationship between gelation mechanism and mechanical properties of TetraPEG iongel.

5.2 Experiment

5.2.1 Materials

NH_2-terminated and NHS-terminated TetraPEGs (TetraPEG-NH_2 and TetraPEG-NHS, respectively) were prepared from tetrahydroxyl-terminated PEG, which is described in elsewhere in detail [32]. The molecular weight (M_w) of TetraPEG-NH_2 and TetraPEG-NHS were 20 kg mol^{-1}. The aIL, 1-ethyl-3-methylimidazolium bis(trifluoromethanesulfonyl)amide ($[C_2mIm^+][TFSA^-]$) and 1-ethyl-3-methylimidazolium tetrafluoroborate ($[C_2mIm^+][BF_4^-]$) were synthesized according to conventional methods [44]. Water contents in the aILs were checked by Karl Fisher titration to be less than 50 ppm.

The pILs used in this work are 1-ethylimidazolium bis(trifluoromethanesulfonyl)amide ($[C_2ImH^+][TFSA^-]$) and 1-ethylimidazolium tetrafluoroborate ($[C_2ImH^+][BF_4^-]$). Equimolar amounts of HTFSA and 1-ethylimidazole (C_2Im) as a base are mixed in acetonitrile. The acetonitrile solution was dried in a vacuum at room-temperature during 1 day to obtain $[C_2ImH^+][TFSA^-]$. The C_2Im was dried with molecular sieves (3A), and purified by distillation. The HTFSA was kept in a glove box and used without further purification. Similarly, equimolar amounts of HBF_4 and C_2Im were mixed in water, and then the aqueous solution was dried in a vacuum at room-temperature for 1 day to obtain $[C_2ImH^+][BF_4^-]$. Water contents in the pILs was also checked by Karl Fisher titration to be less than 100 ppm for both $[C_2ImH^+][TFSA^-]$ and $[C_2ImH^+][BF_4^-]$. Density measurements were performed for the $[C_2ImH^+][TFSA^-]$ and $[C_2ImH^+][BF_4^-]$. The values were 1.577 g cm^{-3} and 1.343 g cm^{-3}, respectively.

5.2.2 Rheological measurement

Rheological measurements were performed using a stress control rheometer (MCR-501, Anton Paar, Austria) with a cone plate geometry to estimate the gelation time. Iongel samples

were prepared as follows: First, mixed IL solvent were prepared by adding a small amount of pIL to aIL in both $TFSA^-$ and BF_4^- system. The pIL concentrations ranged from 1.2 to 4.3×10^{-3} mol dm^{-3}. Second, TetraPEG-NH_2 and TetraPEG-NHS macromer solutions (cocentration, c = 50 mg/mL = 3 wt%, M_w = 20 kg mol^{-1}) were prepared by dissolving TetraPEG macromer in mixed IL solvent. Finally, the mixture of equivalent amounts of macromer solutions was stirred for 1 minute and set on thermostatic plate (25.0°C). The sample (570 μL) was held between two plates and the time dependences of the storage modulus (G') and loss modulus (G'') for the gelation process were monitored under shearing by plates. The strain and angular frequency were set to 2% and 1 Hz, respectively.

5.2.3 Potentiometric titration

HTFSA (acid) and TetraPEG-NH_2 (base) in [C_2mIm$^+$][$TFSA^-$] were prepared in a glove box. The TetraPEG-NH_2 solution (concentration of terminal NH_2 group, c_{NH2} = 9.4×10^{-3} mol dm^{-3}, 2.8 cm^3) was titrated with the HTFSA solution ($c_H = 3.1\times10^{-2}$ mol dm^{-3}) in a vessel with a water jacket at 298 K. The electromotive force (emf), E_i at each titration point, i was measured by using an ion-selective field effect transistor (IS-FET) electrode (HORIBA 0040-10D) coupled with an Ag/AgCl reference electrode that was separated from the sample by a porous ceramic separator with a double-junction (HORIBA 2565A-10T). This electrode system is well established to show an excellent Nernstian response to [H^+] and quick response with 3 min in ILs and non-aqueous solvents [45–47]. The titration experiments were performed three times and the observed data were analyzed according to Gran's method to determine an equilibrium constant, $K_{a(NH3)}$ given by the following acid-base reaction (eq. 5.1 and 5.2)

$$\text{TetraPEG-NH}_3^+ \rightleftarrows \text{TetraPEG-NH}_2 + \text{H}^+ \text{ (or HTFSA) and} \tag{5.1}$$

$$K_{a(NH3)} = \frac{[\text{-NH}_2][\text{H}^+]}{[\text{-NH}_3^+]}. \tag{5.2}$$

From a Nernstian equation, the observed E_i at the titration point is represented as

$$E_i = E^{\circ\prime} + (2.303RT/F)\log[\text{H}^+]_i, \tag{5.3}$$

where $E^{\circ\prime}$, R, T, F denote the standard electrode potential, the gas constant, temperature and Faraday constant, respectively. The observed E_is were analyzed on the basis of Gran's

method. Here, total concentrations of H^+ (HTFSA) and base (TetraPEG-NH_2), $C_{H,i}$ and $C_{B,i}$ at each titration point, i are

$$C_{H,i} = \frac{V_i[H^+]_0}{V_0 + V_i} = [\text{-}NH_3{}^+]_i + [H^+]_i \text{ and} \tag{5.4}$$

$$C_{B,i} = \frac{V_0[\text{-}NH_2]_0}{V_0 + V_i} = [\text{-}NH_2]_i + [\text{-}NH_3{}^+]_i, \tag{5.5}$$

where V_0, V_i, $[\text{-}NH_2]_0$ and $[H^+]_0$ are the initial volume for base solution, the titrated volume at titration point i, the initial concentrations of base and acid (titrant) solutions, respectively. According to Gran's method, the left-hand side of the following equation plotted against V_i to give a straight line in $C_H > C_B$ region (acid region) and the slope and the intercept essentially correspond to the $[H^+]_0$ and $E^{\circ\prime}$, respectively.

$$(V_0 + V_i)10^{E_i/(2.303RT/F)} = 10^{E^{\circ\prime}/(2.303RT/F)}(V_i[H^+]_0 - V_0[\text{-}NH_2]_0). \tag{5.6}$$

In $C_H < C_B$ region (base region), the following equation including the E_i is obtained,

$$V_i[H^+]_0 10^{-E_i/(2.303RT/F)} = 10^{-[\log K_{a(NH3)} + E^{\circ\prime}/(2.303RT/F)]}(V_0[\text{-}NH_2]_0 - V_i[H^+]_0). \tag{5.7}$$

From the slope and the intercept in the left-hand side vs. V_i plot of the eq. 5.7, the $pK_{a(NH3)}$ can be obtained. The details of the theory and analysis are described in our previous work [43, 48] or Chapter 2 and 3. The acid-base reaction of neutral C_2Im in $[C_2mIm^+]$ $[TFSA^-]$ was also investigated by similar potentiometric titration, i.e., the HTFSA in $[C_2mIm^+][TFSA^-]$ solution ($c_H = 8.6 \times 10^{-2}$ mol dm^{-3}, 3.5 cm^3) was titrated with the C_2Im in $[C_2mIm^+][TFSA^-]$ solution (concentration of C_2Im, $c_{C2Im} = 6.6 \times 10^{-1}$ mol dm^{-3}), resulting in the determination of $pK_{a(C2ImH)}$ given by eq. 5.8 and 5.9 as follows.

$$C_2ImH^+ \rightleftarrows C_2Im + H^+ \text{ (or [HTFSA]) and} \tag{5.8}$$

$$K_{a(C2ImH)} = \frac{[C_2Im][H^+]}{[C_2ImH^+]}. \tag{5.9}$$

5.2.4 Stretching measurement

The rectangular $[C_2mIm^+][TFSA^-]$ iongel films (5.0×30.0×1.0 mm) were prepared under room-temperature in the same way described in the rheological measurement. Concentrations

of TetraPEG-NH_2 and TetraPEG-NHS were set to be 50 mg/mL (3 wt%). The pIL concentrations were 1.4 and 2.3×10^{-3}mol dm^{-3}, corresponding to be 29 and 48% of the -NH_2 group concentration (4.8×10^{-3} mol dm^{-3}), respectively. The stretching measurement was carried out using a mechanical testing apparatus (EZ-TEST, SHIMADZU, Japan) at a velocity of 10 mm min^{-1}.

5.3 Results and discussion

5.3.1 Protic IL effect on the gelation time

As mentioned in Introduction, reaction time on TetraPEG gelation strongly depends on the concentration of H^+, $[H^+]$ in IL. Therefore, I focused on pILs as non-volatile H^+ sources. In this work, $[C_2ImH^+][TFSA^-]$ and $[C_2ImH^+][BF_4^-]$ that are analogous pILs of $[C_2mIm^+][TFSA^-]$ and $[C_2mIm^+][BF_4^-]$ aILs, respectively, were added into the corresponding TetraPEG/aIL solutions, and I firstly confirmed experimentally the relationship between gelation time and pIL concentration using rheological measurements.

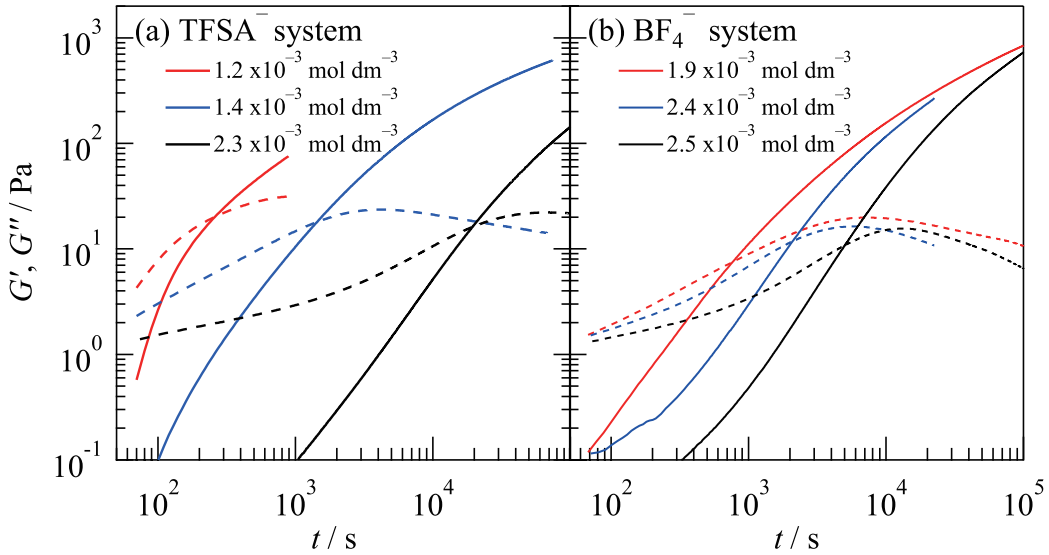

Figure 5.1. pIL concentration dependences of dynamic moduli, G' (solid line) and G'' (broken line) for the gelation of TetraPEG in C_2mIm^+-based ILs with (a) $TFSA^-$ and (b) BF_4^- anions plotted against the reaction time (t). The concentration of polymer was set to be 3 wt%.

Figure 5.1 (a) shows typical results of the storage (G') and loss (G'') moduli for the gelation of 3 wt% TetraPEG in $[C_2mIm^+][TFSA^-]$ aIL with varying $[C_2ImH^+][TFSA^-]$ pIL concentration, c_{pIL}. Both G' and G'' gradually increased with increasing the reaction

time, t. The intersection of the G' and G'' profiles were clearly observed for all the pIL concentrations, which corresponds to the gelation point [49, 50]. I also investigated the G' and G'' in $[C_2mIm^+][BF_4^-]$ aIL containing $[C_2ImH^+][BF_4^-]$ pIL, which is shown in Figure 5.1 (b). Similar to the $TFSA^-$ system, both G' and G'' increased with t, and then the gelation points were clearly observed for all the c_{pILs} examined here.

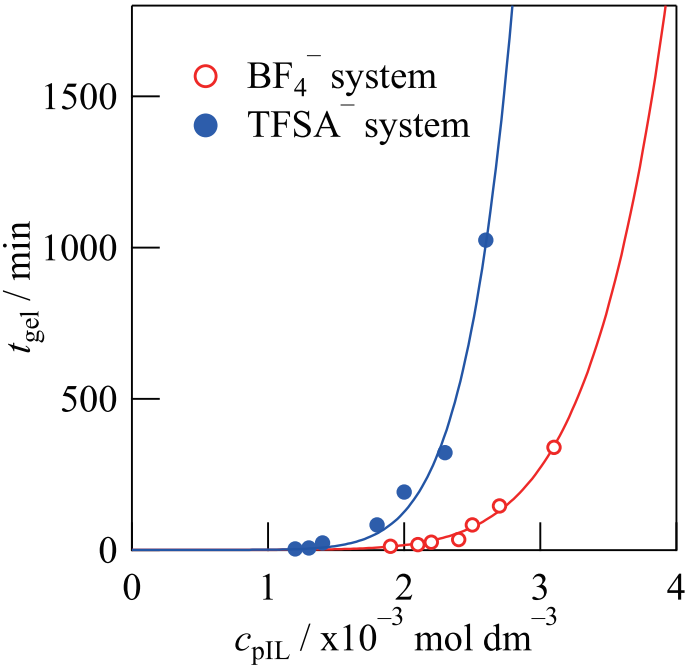

Figure 5.2. Gelation time corresponding to the intersection of G' and G'' (t_{gel}) plotted against the pIL concentrations (c_{pIL}).

Figure 5.2 shows the reaction time at each gelation point (here, I call gelation time, t_{gel}) plotted against c_{pIL}. It was found that the t_{gel} is gradually and systematically prolonged with increasing the c_{pIL} for both $TFSA^-$ and BF_4^- systems. The t_{gel} at a given c_{pIL} was appreciably longer in the $TFSA^-$ system than in the BF_4^- one. At the present stage, it is difficult to clearly interpret the anion effect on the t_{gel}. However, at least, I can propose that the t_{gel} can be successfully controlled from seconds to hours by the addition of pIL (proton source) into aIL (solvent). To understand the effect of c_{pIL} or H^+ concentration on the t_{gel} in detail, I investigated the acid-base reaction of terminal NH_2 group within TetraPEG-NH_2 in aIL. It might be expected that the acid-base equilibrium of pIL adding as a proton source in solvent aIL plays an essential role in the t_{gel}. In this work, the acid-base properties of TetraPEG-NH_2 and conjugate base of pIL cation, C_2Im, were quantitatively evaluated by a direct pH measurement in solvent aIL to determine their acid dissociation constants, pK_a values.

5.3.2 Acid-base Reaction of Prepolymer in Aprotic IL

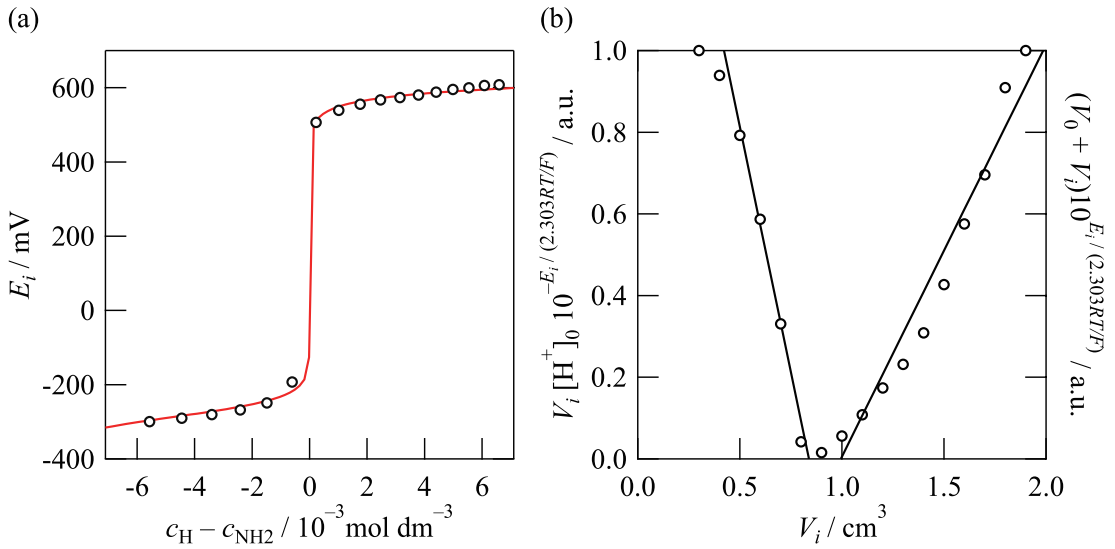

Figure 5.3. (a) Potentiometric titration curves for base TetraPEG-NH_2 titrated with acid HTFSA in a [C_2mIm$^+$][TFSA$^-$] solution. The solid line corresponds to the theoretical curve calculated by using the pK_a obtained from Gran's plot. (b) Gran's plot for the observed titration data. The straight line (solid) shows theoretical line calculated by a linear squared fitting method.

Figure 5.3 (a) shows a typical potentiometric titration curve observed for the TetraPEG-NH_2 in [C_2mIm$^+$][TFSA$^-$] solution. The value of E_i in the TetraPEG-NH_2 (base) solution slightly and gradually increased with the addition of the titrant HTFSA (acid) solution. The value sharply increased at the equivalent neutral point, indicating concentration of TetraPEG-NH_2, [-NH_2] is equal to [HTFSA] at the point. The large E_i jump (approximately 800 mV) was observed in the TetraPEG-NH_2/[C_2mIm$^+$][TFSA$^-$] system. This suggests that the protonated TetraPEG-NH_2 (i.e., TetraPEG-NH_3^+) has a large acid dissociation constant, p$K_{a(NH3)}$ value in [C_2mIm$^+$][TFSA$^-$]. To estimate the apparent p$K_{a(NH3)}$ value, the observed titration data were analyzed using Gran's method, which is shown in Figure 5.3 (b). The experimental data fell on a straight line in both the acidic and basic regions to result in the quantitative evaluation of the apparent p$K_{a(NH3)}$ value. The p$K_{a(NH3)}$ value was estimated to be 16.4(5) mol dm^{-3}. The calculated curve using the p$K_{a(NH3)}$ value is shown by the solid line colored with red in Figure 5.3 (a). As can be seen in Figure 5.3 (a), the calculated curve successfully reproduced the experimental titration points. Here, I note that the p$K_{a(NH3)}$ value of the TetraPEG-NH_2 obtained here is almost similar to the corresponding value of analogous

model molecule, butylamine ($BuNH_2$) in [C_2mIm^+][$TFSA^-$] [43]. This suggests that there are essentially no molecular-weight dependence on the acid-base property of NH_2 group in aILs.

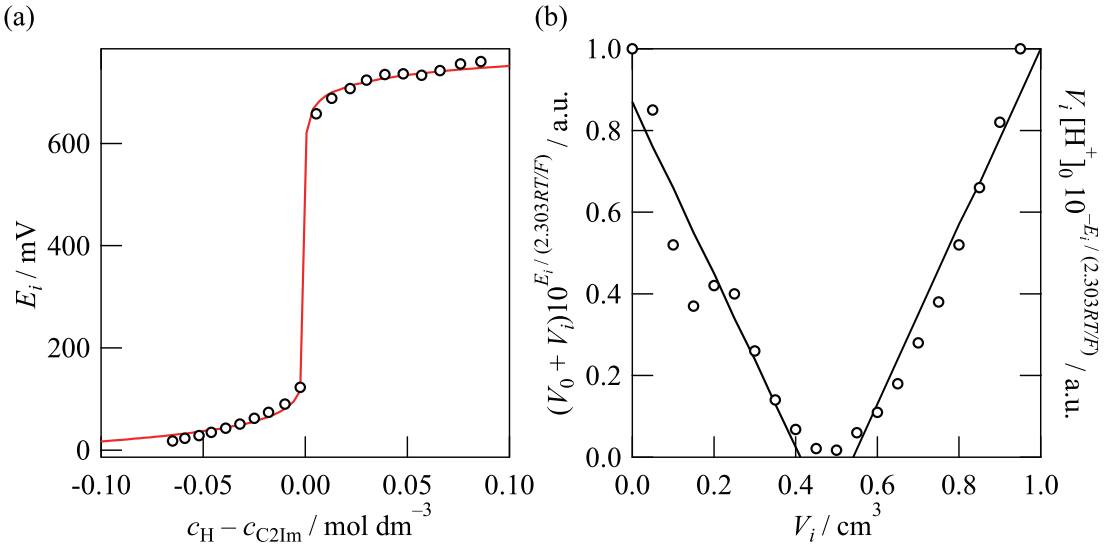

Figure 5.4. (a) Potentiometric titration curves for acid HTFSA titrated with base C_2Im in [C_2mIm^+][$TFSA^-$] solution. The solid line corresponds to the theoretical curve calculated by using the pK_a value obtained from Gran's plot. (b) Gran's plot for the observed titration data. The straight line (solid) shows theoretical line calculated by a linear squared fitting method.

Figure 5.4 (a) shows a typical potentiometric titration curve observed for the C_2Im in [C_2mIm^+][$TFSA^-$] solution. Similar to the TetraPEG-NH_2 system, the E_i in the HTFSA (acid) gradually decreased with the addition of the C_2Im (base) titrant solution, followed by the sharp increase in the E_i at the neutralization point, $c_H - c_{C2Im} = 0$. It was found that the extent of E_i jump (approximately 600 mV) is appreciably small relative to that for the TetraPEG-NH_2 system. This is because apparent pK_a is lower for the C_2Im system than for the TetraPEG-NH_2 one. By applying Gran's plot analysis to the observed data, the apparent p$K_{a(C2ImH)}$ for the protonated C_2Im was successfully estimated to be 13.7(9) mol dm^{-3}. The result of the Gran's plot is shown in Figure 5.4 (b). The calculated potentiometric curve using the p$K_{a(C2ImH)}$ value is shown as solid red line in Figure 5.4 (b). It seems that the calculated curves slightly deviated from the experimental data relative to the TetraPEG-NH_2 system, particularly, in the range of $c_H - c_{C2Im} < 0$. However, I finally concluded that p$K_{a(C2ImH)}$ value obtained here is reasonable, because a pK_a value is directly related to the extent of E_i jump. In [C_2mIm^+][$TFSA^-$] (aIL), The pK_a value for the acid-base reaction of C_2Im is two-order smaller than that of TetraPEG-NH_2. This means that the Brønsted basicity of TetraPEG-NH_2 is significantly stronger than that of C_2Im in the [C_2mIm^+][$TFSA^-$] aIL. That

is, most of H^+ in the aIL solution preferentially protonated the TetraPEG-NH_2 to form the TetraPEG-$NH_3{}^+$, whereas cation of pIL exists as neutral C_2Im.

In the present TetraPEG iongel system, a small amount of pIL with a dissociative H^+ is added into the TetraPEG in aIL solution to control the gelation time. Based on the facts obtained here, the gelation mechanism may be proposed as follows; (1) when pIL ($[C_2ImH^+][TFSA^-]$ in this work) is added into TetraPEG/aIL solution, the H^+ dissociated from the C_2ImH^{++} cation binds to the TetraPEG-NH_2 to form the TetraPEG-$NH_3{}^+$. (2) The concentration of the TetraPEG-$NH_3{}^+$ in the aIL is much larger than that of the C_2ImH^{++} because of the 2-order larger $pK_{a(NH3)}$ relative to the $pK_{a(C2ImH)}$. (3) The TetraPEG-$NH_3{}^+$ cannot react with TetraPEG-NHS. Hence, the concentration of reactive NH_2 group decreases with increasing c_{pIL} (or $[H^+]$) to lead to a long gelation time.

Finally, I note the acid-base properties of TetraPEG-NH_2 and C_2Im in aqueous solutions. The pK_a values of TetraPEG-NH_2 and C_2Im in water were reported to be 9.2 and 7.2, respectively. Both pK_as in $[C_2mIm^+][TFSA^-]$ (aIL) were around 7-order larger than the corresponding values in water. This indicates the solutes in aIL act as a much stronger Brønsted base than those in water. The large difference of pK_a between aIL and aqueous solutions are originated from the solvation of solutes (both neutral and protonated species), which should be investigated in terms of thermodynamic and structural aspects as described in Chapter 4.

5.3.3 Reaction Efficiency

Figure 5.5 (a) shows stretching stress-elongation curves obtained for TetraPEG iongel prepared in $[C_2mIm^+][TFSA^-]$ containing $[C_2ImH^+][TFSA^-]$ (c_{pIL} = 0, 1.4 and 2.3×10^{-3} mol dm^{-3}). The stretching stress (σ) gradually increased by elongation (λ) and reached to the breaking stress at λ_{max} = 4.8, 3.0 and 2.5 for c_{pIL} = 0, 1.4 and 2.3×10^{-3} mol dm^{-3}, respectively. The breaking stress decreased with increasing c_{pIL}. From the initial slop of the observed stress-strain curve, I can estimate the elastic modulus G for TetraPEG iongel. The Gs were estimated to be 2.8, 1.7 and 0.9 kPa for the iongels with c_{pIL} = 0, 1.4 and 2.3×10^{-3} mol dm^{-3}, respectively.

The linear relationship between G and c_{pIL} was found in Figure 5.5 (b), which implies that the mechanical strength of TetraPEG iongel can be controlled by adding pIL, in other words, acid-base reaction of TetraPEG-NH_2. According to our systematic study for TetraPEG hydrogel system, the decrease in the G value is directly related to incompleteness of gelation reaction or reaction efficiency of amide bond (cross linking point). The same might be applied

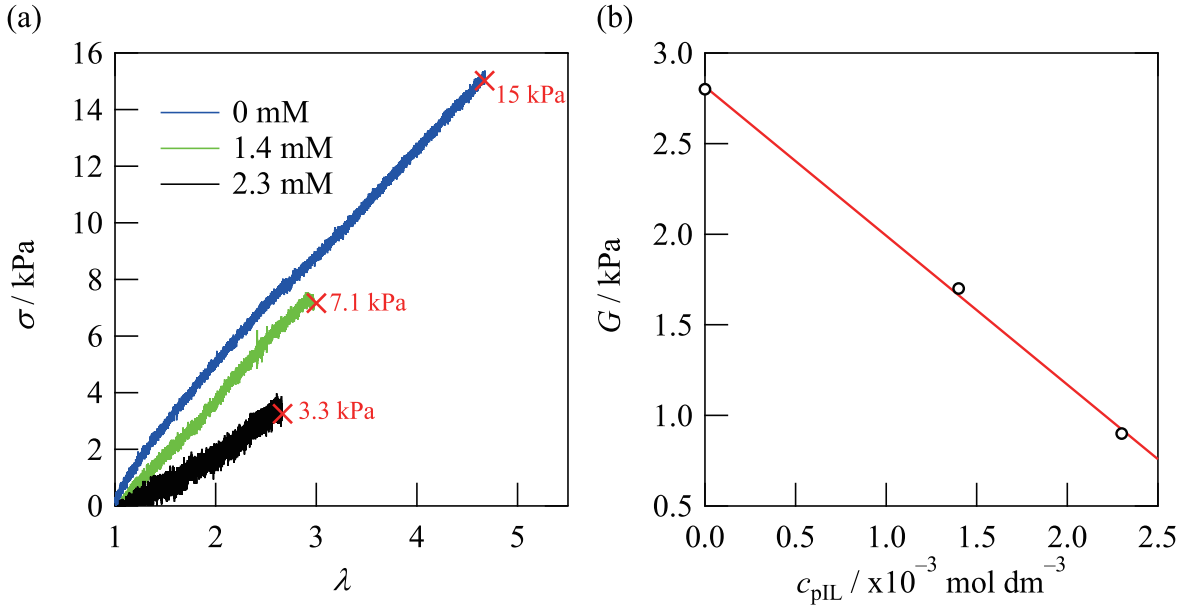

Figure 5.5. (a) Stress-elongation curve for 3 wt% TetraPEG iongels with varying pIL concentration, c_{pIL}. The cross marker (×) shows the breaking point. (b) Elastic modulus, G plotted against c_{pIL}.

to the present iongel system, i.e., c_{pIL} or $[H^+]$ in solvent aIL affects the reaction efficiency of TetraPEG iongel. I thus examined to evaluate reaction efficiency, p in this system based on a tree-like theory and phantom network model [51–55]. The relationship between G and p is described as

$$G = c({}_4C_3P(F^{\mathrm{out}})[1 - P(F^{\mathrm{out}})]/2 + [1 - P(F^{\mathrm{out}})]^4)RT \text{ and} \tag{5.10}$$

$$P(F^{\mathrm{out}}) = (1/p - 3/4)^{1/2} - 1/2, \tag{5.11}$$

where c, R, T and $P(F^{\mathrm{out}})$ correspond to the preparation concentration of bonds, gas constant, temperature and probability that one of 4 arms leads out to polymer network, respectively.

Figure 5.6 shows the ps obtained for c_{pIL} = 0, 1.4 and 2.3×10^{-3} mol dm^{-3}. The p was 72% for $c_{\mathrm{pIL}} = 0 \times 10^{-3}$ mol dm^{-3} (neat aIL), and the value was linearly decreased with increased c_{pIL}. This suggests that cross-end coupling reaction (formation of amide bond) is appreciably suppressed by a little amount of H^+ in the solution. I can propose that the acid-base reaction of TetraPEG-NH_2 in aIL is predominant in this gelation system.

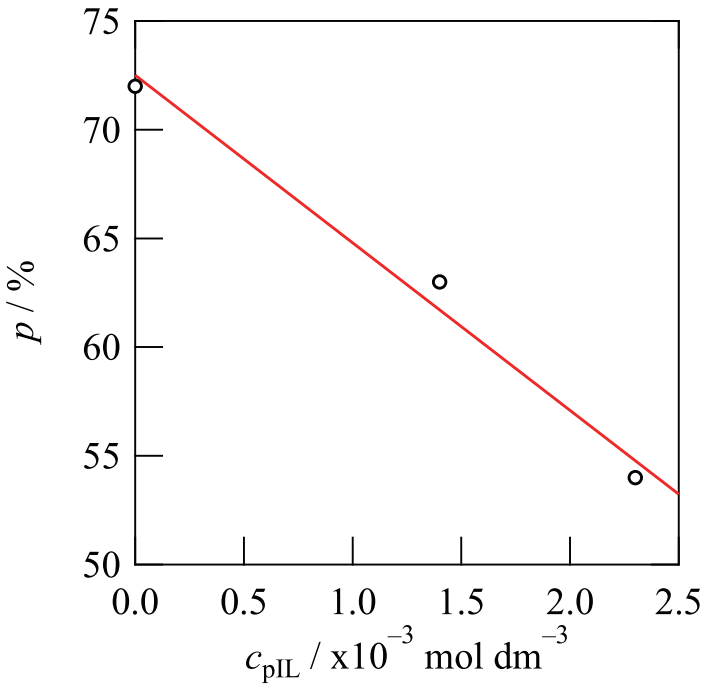

Figure 5.6. pIL concentration dependence on reaction efficiency, p.

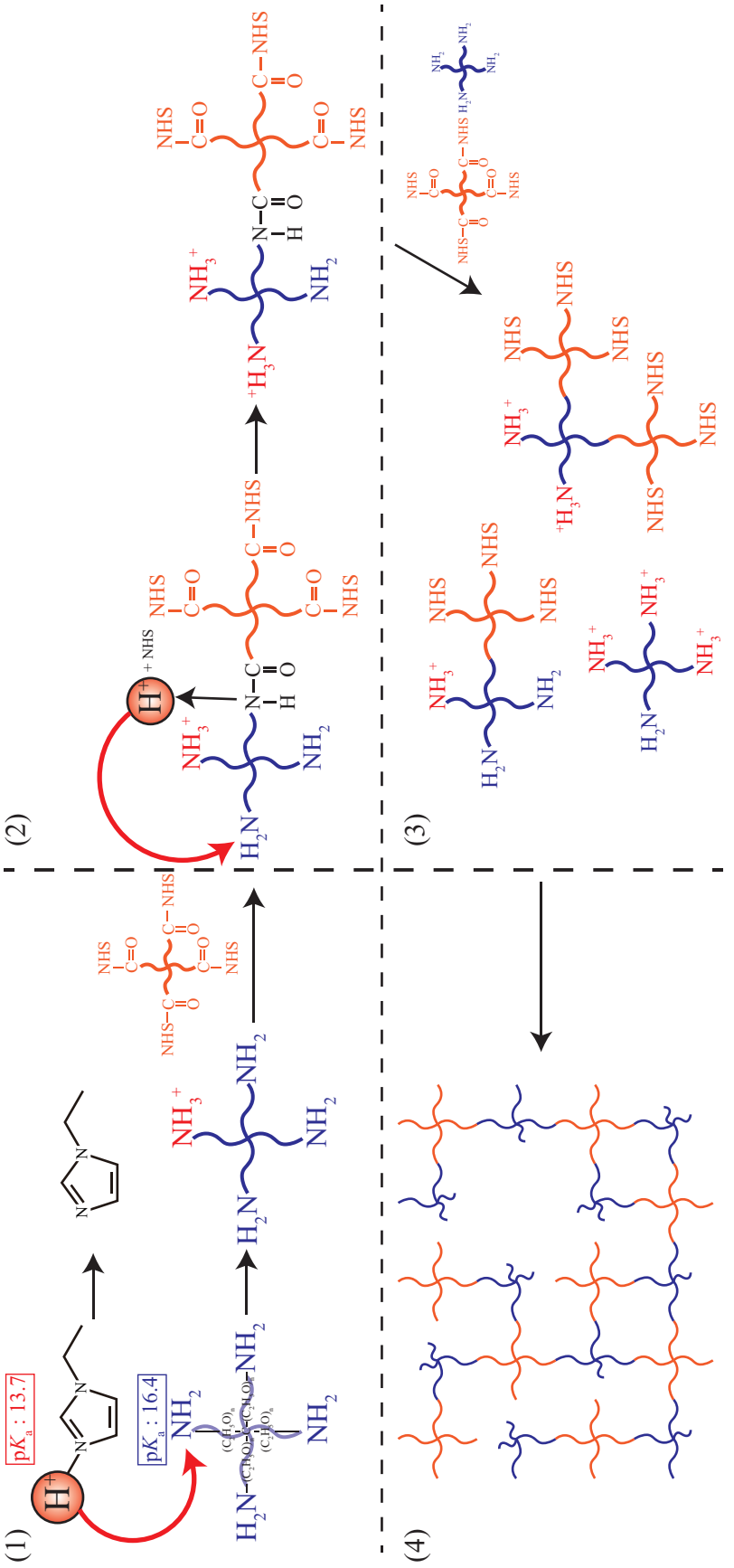

Figure 5.7. Possible gelation mechanism in TetraPEG iongel system

Finally, I conclude TetraPEG gelation mechanism in ILs (Figure. 5.7). In TetraPEG-NH_2/[C_2mIm$^+$][TFSA$^-$] (aIL) solutions containing [C_2ImH$^+$][TFSA$^-$] (pIL), most of H^+ ions within the C_2ImH^{++} cation of pIL are dissociated and then binds to TetraPEG-NH_2 to from TetraPEG-$NH_3{}^+$ (step 1). This is because the p$K_{a(NH3)}$ is 2-order larger than the p$K_{a(C2Im)}$. The TetraPEG coexists as protonated TetraPEG-$NH_3{}^+$ and neutral TetraPEG-NH_2 in the solution, and then the latter only reacts with TetraPEG-NHS to form the amide bond (HN–CO). The TetraPEG-$NH_3{}^+$ cannot form the amide bond, resulting in a residual unreactive group. The gelation time, tg thus depend on the distribution ratio of TetraPEG-$NH_3{}^+$: TetraPEG-NH_2, which is controlled by [H^+] or c_{pIL}. After amide bond formation, the H^+ and NHS^- are dissociated from NH_2- and NHS-terminated polymers, respectively. The dissociated H^+ preferentially binds to the reactive NH_2 group due to its strong Brønsted basicity (large pK_a) (step 2). Thus, the reactive NH_2 group within TetraPEG gradually decreases with proceeding the gelation reaction (step 3). When all the reactive NH_2 groups are protonated completely by the dissociated H^+, the gelation reaction is stopped to give defects in polymer network (step 4). The [H^+] in the solution (aIL, in this work) thus predominates the reaction efficiency, p of TetraPEG iongel, which can be quantitatively controlled by initial pIL concentration and its acid-base property (p$K_{a(C2Im)}$).

5.4 Conclusion

The gelation reaction of TetraPEG in [C_2mIm$^+$][TFSA$^-$] aIL was investigated in terms of gelation time, acid-base reaction and reaction efficiency. The gelation behavior of TetraPEG strongly depends on the [H^+] in the solution. I thus control the gelation reaction by adding [C_2ImH$^+$][TFSA$^-$] pIL as a proton source, in this work. The gelation time of TetraPEG in [C_2mIm$^+$][TFSA$^-$] aIL can be successfully controlled by the pIL concentration, c_{pIL}, suggesting that the acid-base properties of terminal group of TetraPEG and pIL play a key role on the gelation reaction. The acid dissociation constant, pK_a of protonated TetraPEG-$NH_3{}^+$ and C_2ImH^{++} (pIL cation) are quantitatively determined in [C_2mIm$^+$][TFSA$^-$] aIL. The pK_a value for the TetraPEG-$NH_3{}^+$ (16.4) is significantly larger than that of the C_2ImH^{++}, which indicates that most of H^+ in the system preferentially binds to the NH_2 group within TetraPEG. The TetraPEG-$NH_3{}^+$ cannot react with TetraPEG-NHS to give the unreactive terminal groups. I thus conclude that reaction efficiency or extent of defect polymer network in TetraPEG iongel is essentially dominated by the concentration of TetraPEG-$NH_3{}^+$ depending on [H^+] (or c_{pIL}) in the solvent [C_2mIm$^+$][TFSA$^-$].

Reference

[1] S. a. M. Noor, P. M. Bayley, M. Forsyth, and D. R. Macfarlane. *Electrochim. Acta*, Vol. 91, pp. 219–226, 2013.

[2] M. Diaz, A. Ortiz, and I. Ortiz. *J. Memb. Sci.*, Vol. 469, pp. 379–396, 2014.

[3] H. Z. Song, N. N. Zhao, W. C. Qin, B. Duan, X. Y. Ding, X. Wen, P. Qiu, and X. W. Ba. *J. Mater. Chem. A*, Vol. 3, pp. 2128–2134, 2015.

[4] M. Galinski, A. Lewandowski, and I. Stepniak. *Electrochim. Acta*, Vol. 51, pp. 5567–5580, 2006.

[5] M. Armand, F. Endres, D. R. Macfarlane, H. Ohno, and B. Scrosati. *Nat. Mater.*, Vol. 8, pp. 621–629, 2009.

[6] J. M. Lu, F. Yan, and J. Texter. *Prog. Polym. Sci.*, Vol. 34, pp. 431–448, 2009.

[7] I. Must, V. Vunder, F. Kaasik, I. Poldsalu, U. Johanson, A. Punning, and A. Aabloo. *Sens. Actuators B Chem.*, Vol. 202, pp. 114–122, 2014.

[8] N. Terasawa and K. Asaka. *Sens. Actuators B Chem.*, Vol. 193, pp. 851–856, 2014.

[9] S. Imaizumi, H. Kokubo, and M. Watanabe. *Macromolecules*, Vol. 45, pp. 401–409, 2012.

[10] J. Ding, D. Z. Zhou, G. Spinks, G. Wallace, S. Forsyth, M. Forsyth, and D. R. Macfarlane. *Chem. Mater.*, Vol. 15, pp. 2392–2398, 2003.

[11] T. Fukushima, K. Asaka, A. Kosaka, and T. Aida. *Angew. Chem. Int. Ed. Engl.*, Vol. 44, pp. 2410–2413, 2005.

[12] W. M. Mcdanel, M. G. Cowan, T. K. Carlisle, A. K. Swanson, R. D. Noble, and D. L. Gin. *Polymer*, Vol. 55, pp. 3305–3313, 2014.

[13] M. Karaszova, M. Kacirkova, K. Friess, and P. Izak. *Sep. Purif. Technol.*, Vol. 132, pp. 93–101, 2014.

[14] L. A. Blanchard, D. Hancu, E. J. Beckman, and J. F. Brennecke. *Nature*, Vol. 399, pp. 28–29, 1999.

[15] J. E. Bara, D. E. Camper, D. L. Gin, and R. D. Noble. *Acc. Chem. Res.*, Vol. 43, pp. 152–159, 2010.

[16] M. Hasib-Ur-Rahman, M. Siaj, and F. Larachi. *Chem. Eng. Process.*, Vol. 49, pp. 313–322, 2010.

[17] J. E. Bara, T. K. Carlisle, C. J. Gabriel, D. Camper, A. A. Finotello, D. L. Gin, and R. D. Noble. *Ind. Eng. Chem. Res.*, Vol. 48, pp. 2739–2751, 2009.

[18] D. R. Macfarlane, N. Tachikawa, M. Forsyth, J. M. Pringle, P. C. Howlett, G. D. Elliott,

J. H. Davis, M. Watanabe, P. Simon, and C. A. Angell. *Energy. Environ. Sci.*, Vol. 7, pp. 232–250, 2014.

[19] H. Wang, G. Gurau, and R. D. Rogers. *Chem. Soc. Rev.*, Vol. 41, pp. 1519–1537, 2012.

[20] N. De Vos, C. Maton, and C. V. Stevens. *Chemelectrochem*, Vol. 1, pp. 1258–1270, 2014.

[21] P. Wasserscheid and K. Keim. *Angew. Chem. Int. Ed. Engl.*, Vol. 39, pp. 3772–3789, 2000.

[22] R. Sheldon. *Chem. Commun.*, pp. 2399–2407, 2001.

[23] M. J. Park, I. Choi, J. Hong, and O. Kim. *J. Appl. Polym. Sci.*, Vol. 129, pp. 2363–2376, 2013.

[24] T. Ueki and M. Watanabe. *Langmuir*, Vol. 23, pp. 988–990, 2007.

[25] Y. Gu and T. P. Lodge. *Macromolecules*, Vol. 44, pp. 1732–1736, 2011.

[26] Y. Y. Gu, E. L. Cussler, and T. P. Lodge. *J. Memb. Sci.*, Vol. 423, pp. 20–26, 2012.

[27] C. D.; Lodge T. P. S. L. Zhang, Keun H.; Frisbie. *Macromolecules*, Vol. 44, pp. 940–949, 2011.

[28] Y. Gu, S. Zhang, L. Martinetti, K. H. Lee, L. D. Mcintosh, C. D. Frisbie, and T. P. Lodge. *J. Am. Chem. Soc.*, Vol. 135, pp. 9652–9655, 2013.

[29] S. Kasahara, E. Kamio, T. Ishigami, and H. Matsuyama. *Chem. Commun.*, Vol. 48, pp. 6903–6905, 2012.

[30] S. Kasahara, E. Kamio, A. Yoshizumi, and H. Matsuyama. *Chem. Commun.*, Vol. 50, pp. 2996–2999, 2014.

[31] S. Kasahara, E. Kamio, A. Otani, and H. Matsuyama. *Ind. Eng. Chem. Res.*, Vol. 53, pp. 2422–2431, 2014.

[32] T. Sakai, T. Matsunaga, Y. Yamamoto, C. Ito, R. Yoshida, S. Suzuki, N. Sasaki, M. Shibayama, and U. Chung. *Macromolecules*, Vol. 41, pp. 5379–5384, 2008.

[33] K. Fujii, H. Asai, T. Ueki, T. Sakai, S. Imaizumi, U. Chung, M. Watanabe, and M. Shibayama. *Soft Matter*, Vol. 8, pp. 1756–1759, 2012.

[34] T. Matsunaga, T. Sakai, Y. Akagi, U. Chung, and M. Shibayama. *Macromolecules*, Vol. 42, pp. 6245–6252, 2009.

[35] T. Matsunaga, T. Sakai, Y. Akagi, U. Chung, and M. Shibayama. *Macromolecules*, Vol. 42, pp. 1344–1351, 2009.

[36] H. Asai, K. Fujii, T. Ueki, T. Sakai, U. Chung, M. Watanabe, Y. S. Han, T. H. Kim, and M. Shibayama. *Macromolecules*, Vol. 45, pp. 3902–3909, 2012.

[37] H. Asai, K. Nishi, T. Hiroi, K. Fujii, T. Sakai, and M. Shibayama. *Polymer*, Vol. 54, pp. 1160–1166, 2013.

[38] K. Nishi, K. Fujii, M. Chijiishi, Y. Katsumoto, U. Chung, T. Sakai, and M. Shibayama. *Macromolecules*, Vol. 45, pp. 1031–1036, 2012.

[39] K. Nishi, H. Asai, K. Fujii, Y.-S. Han, T.-H. Kim, T. Sakai, and M. Shibayama. *Macromolecules*, Vol. 47, pp. 1801–1809, 2014.

[40] K. Nishi, K. Fujii, Y. Katsumoto, T. Sakai, and M. Shibayama. *Macromolecules*, Vol. 47, pp. 3274–3281, 2014.

[41] K. Fujii, T. Makino, K. Hashimoto, T. Sakai, M. Kanakubo, and M. Shibayama. *Chem.Lett.*, Vol. 44, pp. 17–19, 2015.

[42] R. Barhdadi, M. Troupel, C. Comminges, M. Laurent, and A. Doherty. *J. Phys. Chem. B*, Vol. 116, pp. 277–282, 2011.

[43] K. Fujii, K. Hashimoto, T. Sakai, Y. Umebayashi, and M. Shibayama. *Chem. Lett.*, Vol. 42, pp. 1250–1251, 2013.

[44] K. Fujii, R. Kanzaki, T. Takamuku, Y. Kameda, S. Kohara, M. Kanakubo, M. Shibayama, S. Ishiguro, and Y. Umebayashi. *J. Chem. Phys.*, Vol. 135, p. 244502, 2011.

[45] R. Kanzaki, K. Uchida, S. Hara, Y. Umebayashi, S. Ishiguro, and S. Nomura. *Chem. Lett.*, Vol. 36, pp. 684–685, 2007.

[46] R. Kanzaki, K. Uchida, X. Song, Y. Umebayashi, and S. Ishiguro. *Anal. Sci.*, Vol. 24, pp. 1347–1349, 2008.

[47] R. Kanzaki, H. Doi, X. Song, S. Hara, S. Ishiguro, and Y. Umebayashi. *J. Phys. Chem. B*, Vol. 116, pp. 14146–14152, 2012.

[48] K. Hashimoto, K. Fujii, and M. Shibayama. *J. Mol. Liquids*, Vol. 188, pp. 143–147, 2013.

[49] C. Y. M. Tung and P. J. Dynes. *J. Appl. Polym. Sci.*, Vol. 27, pp. 569–574, 1982.

[50] M. Kurakazu, T. Katashima, M. Chijiishi, K. Nishi, Y. Akagi, T. Matsunaga, M. Shibayama, U. Chung, and T. Sakai. *Macromolecules*, Vol. 43, pp. 3935–3940, 2010.

[51] D. R. Miller and C. W. Macosko. *Macromolecules*, Vol. 9, pp. 206–211, 1976.

[52] H. M. James and E. Guth. *J. Chem. Phys.*, Vol. 10, pp. 455–481, 1943.

[53] Y. Akagi, T. Katashima, K. Fujii, T. Matsunaga, U. Chung, M. Shibayama, and T. Sakai. *Macromolecules*, Vol. 44, pp. 5817–5821, 2011.

[54] Y. Akagi, J. P. Gong, U. I. Chung, and T. Sakai. *Macromolecules*, Vol. 46, pp. 1035–1040, 2013.

[55] K. Nishi, M. Chijiishi, Y. Katsumoto, T. Nakao, K. Fujii, U. Chung, H. Noguchi, T. Sakai, and M. Shibayama. *J. Chem. Phys.*, Vol. 137, p. 224903, 2012.

Chapter 6

Defect-free Polymer Network Ion Gel Prepared in pH-buffering Ionic Liquid

6.1 Introduction

It is well established that room-temperature ionic liquids (ILs) consisting only of ions possess unique solvent properties such as nonvolatility, high thermal and electrochemical stabilities, and high designability; these are essentially different from the properties of conventional molecular solvents as mentioned in Chapter 1. More importantly, the high designability of ILs, i.e., the ease with which their cation/anion combinations and chemical structures can be designed, allows us to dissolve various compounds, such as inorganic electrolytes [1–4], organic molecules [5–8], and polymers [9–13], in IL media. One promising IL application is as a polymer gel electrolyte, or iongel, which is a three-dimensional polymer network swollen with ILs and used for electrochemical devices (e.g., batteries, capacitors, and actuators) [14–22] and gas-separation membranes [23–27]. However, such applications are still limited due to the low mechanical strength of iongels, which is ascribed to the inhomogeneity of the polymer network created in the cross-linking process [28]. Hence, a high polymer content (generally, 20–50 wt%) is required to yield a free-standing iongel with sufficient strength; however, this results in a low IL content. This leads to a decrease in the inherent IL properties, which is a serious problem in the development of iongels as new soft materials for application.

Recently, high-toughness iongels with low-polymer and high-IL (solvent) contents have been extensively explored and applied as gel electrolytes for Li ion batteries [29] and

gas-separation membranes [30–32]. Lodge et al. reported high-toughness iongels that showed high ionic conductivity and high CO_2 permselectibity [33, 34]. These were prepared using a chemically cross-linked ABA-type triblock copolymer, poly(styrene-*b*-ethylene oxide-*b*-styrene), with low polymer content (~10 wt%). Ito et al. reported an iongel composed of a slide-ring gel network (i.e., movable cross-links that disperse the tensile stress in the polymer network), which showed excellent maximum compression strain (up to 66%) and elastic modulus (~20 kPa) and had a low polymer content (~10 wt%) [35]. Kamio et al. reported a high-toughness iongel for use in a CO_2-separation membrane. It was produced by combining an amino acid IL and a double-network gel structure, and showed excellent CO_2-separation ability and a maximum breaking compression strength of more than 25 MPa. It also had a low polymer content (20 wt%) [36]. We focused on the relationship between the mechanical strength and polymer network homogeneity of iongels, and proposed a high-strength iongel produced using tetra-armed poly(ethylene glycol) (TetraPEG) as a network polymer. The TetraPEG iongel can be easily prepared by mixing two IL solutions containing amine- and *N*-hydroxysuccinimide-terminated TetraPEGs (TetraPEG-NH_2 and TetraPEG-NHS, respectively) to obtain a free-standing TetraPEG iongel with a polymer concentration of just 3–6 wt% [37, 38]. At 6 wt% polymer concentration, the TetraPEG iongel shows the high mechanical strength required in relevant applications: 18 MPa of maximum breaking compression modulus at 83.5% strain [37]. From a structural viewpoint, small-angle neutron scattering and dynamic light scattering experiments suggested that TetraPEG iongels prepared in aprotic ILs (aILs) have, relative to conventional iongels, a homogeneous polymer network structure [38]. However, in terms of mechanical properties, they are presently inferior to the corresponding hydrogels (TetraPEG hydrogels) [39]. This might be ascribed to connectivity defects caused during the gelation reaction in ILs.

In general, to achieve the production of homogeneous gels in A-B-type reactions, we need to control the reaction rate. If the reaction rate is too fast, the system becomes a gel state prior to the homogeneous mixing of prepolymers, thus preventing miscibility. We recently reported the gelation mechanism of TetraPEG prepolymers, i.e., the A-B-type cross-end coupling reaction of TetraPEG-NH_2 and TetraPEG-NHS, in a typical aprotic imidazolium-based IL, in terms of the gelation time and acid-base reaction of the TetraPEG [32,40,41]. I noted that the gelation reaction in this system strongly depends on the concentration of H^+ ($[H^+]$ or pH). That is, the acid-base reaction of the TetraPEG-NH_2 prepolymer, TetraPEG-NH_2 + H^+ $\rightleftarrows$ TetraPEG-$NH_3{}^+$, in the IL solution is important for understanding the gelation reaction because the protonated TetraPEG-$NH_3{}^+$ cannot react with TetraPEG-NHS. The gelation time can be freely controlled across a time range of several tens of seconds to hours depending

on [H^+]; however, the reaction efficiency at the cross-linking point decreases with increasing [H^+] [41]. We faced a dilemma: to control the reaction rate, we needed [H^+], but to increase the reaction efficiency, we needed to decrease [H^+]. Therefore, to achieve a less-defective, or near-ideal, polymer network iongel in the TetraPEG system, we need to prepare the iongel in an aIL medium with a pH-buffering capability. In fact, it has already been established that TetraPEG hydrogels with high toughness and a homogeneous polymer network can be prepared in aqueous solutions using a phosphate-type buffer giving constant pH (~7) during the gelation reaction [42, 43].

In the present work, to prepare a defect-free polymer network gel in an IL system, I established a pH-buffering IL solution system. I used a typical aIL, 1-ethyl-3-methylimidazolium bis(trifluoromethanesulfonyl)amide ([C_2mIm^+][$TFSA^-$]), as a solvent that has no dissociative proton within the C_2mIm^+ and $TFSA^-$] ions. I then added a mixture of protic IL (pIL) as a proton source and its conjugated base, i.e., 1-ethylimidazolium $TFSA^-$] ([C_2ImH^+][$TFSA^-$]) and 1-ethylimidazole (C_2Im), into the solvent aIL. I demonstrated the pH-buffering effect in this system by direct pH measurements using an IS-FET electrode. The gelation reaction of TetraPEGs was performed in the pH-buffering IL solution at a constant pH, and the obtained TetraPEG iongel was characterized in terms of its gelation kinetics and mechanical properties.

6.2 Experiment

6.2.1 Materials

TetraPEG-NH_2 and TetraPEG-NHS were purchased from Nippon Oil Fat and Co (Japan). The molecular weight (M_w) of both TetraPEGs was 20000 g mol^{-1}. The aIL, [C_2mIm^+][$TFSA^-$], was synthesized according to conventional methods [44, 45]. Water content in the aIL was checked by Karl Fisher titration to be less than 50 ppm. The pIL, [C_2ImH^+][$TFSA^-$], was prepared by mixing equimolar amounts of HTFSA and C_2Im in acetonitrile [46]. The acetonitrile solution was dried in vacuum at room temperature for 1 day to obtain [C_2ImH^+][$TFSA^-$]. The C_2Im was dried with molecular sieves (3A) and purified by distillation. The HTFSA was kept in a glovebox and used without further purification. Water content in the pIL was checked by Karl Fisher titration to be less than 100 ppm.

6.2.2 Potentiometric Titration

HTFSA, C_2Im, and TetraPEG-NH_2 in [C_2mIm^+][$TFSA^-$] solutions were prepared in a glovebox filled with N_2 gas. The HTFSA solution (3.3 cm^3, 3.1×10^{-1} mol dm^{-3}), in a vessel with a water jacket, was titrated with C_2Im solution (1.0 mol dm^{-3}) at 283, 293, 303, and 313 K. The electromotive force (E) was measured using an ion-selective field effect transistor (IS-FET) electrode (0040-10D, HORIBA, Japan) [47, 48] coupled with a Ag/AgCl reference electrode separated from the sample by a porous ceramic separator with a double junction [41, 46]. From the Nernstian equation, the observed E at each titration point i, E_i, is represented as

$$E_i = E^{\circ\prime} + \frac{2.303RT}{F} \log[H^+], \tag{6.1}$$

where $E^{\circ\prime}$, R, T, and F denote the standard electrode potential, gas constant, temperature, and Faraday constant, respectively. The E_i was analyzed based on Gran's method, as described elsewhere. [41, 49] In the acidic region, the Gran's plot, i.e., the left-hand side of the following equation plotted against titration volume at point i (V_i), gives a straight line and the slope and intercept correspond to $[C_2Im]_0$ and $E^{\circ\prime}$, respectively.

$$(V_0 + V_i)10^{E_i/(2.303RT/F)} = 10^{E^{\circ\prime}/(2.303RT/F)}(V_0[H^+]_0 - V_i[C_2Im]_0), \tag{6.2}$$

where V_0, $[C_2Im]_0$, and $[H^+]_0$ are the initial volume of acid solution and the initial solution concentrations of C_2Im and H^+, respectively. In the base region, the equation including E_i is obtained as follows

$$V_0[H^+]_0 10^{-E_i/(2.303RT/F)} = 10^{-[\log K_{a(C2ImH)} + E^{\circ\prime}/(2.303RT/F)]}(V_i[C_2Im]_0 - V_0[H^+]_0). \tag{6.3}$$

and the equilibrium constant for the acid-base reaction of C_2Im, $pK_{a(C2ImH)}$, is quantitatively estimated from the slope and intercept on the left-hand side of the plot against V_i. The same was applied to the determination of the acid-base equilibrium constant of TetraPEG-NH_2, $pK_{a(NH3)}$, in the IL solutions. The detail of the analysis is described in prevous Chapters.

6.2.3 Rheological Measurements

Rheological measurements were performed using a stress control rheometer (MCR-501, Anton Paar, Austria) with cone plate geometry, to obtain the gelation time. The pH

buffering [C_2mIm$^+$][TFSA$^-$] was prepared by adding 0.10 mol dm^{-3} [C_2ImH$^+$][TFSA$^-$] pIL and 1.0 mol dm^{-3} C_2Im to [C_2mIm$^+$][TFSA$^-$] aIL. TetraPEG-NH_2 and TetraPEG-NHS prepolymers were dissolved in the pH-buffering IL (100 mg/mL) in a glovebox to prepare 6 wt% TetraPEG-NH_2/IL and TetraPEG-NHS/IL solutions. The two TetraPEG solutions (1:1 by vol.) were mixed and stirred for 120 s. The mixed sample solution (570 μL) was held between two plates and the time dependences of the storage and loss moduli (G' and G'', respectively) for the gelation were monitored under shearing by the plates at 298 K. The strain and angular frequency were set to 2% and 1 Hz, respectively.

6.2.4 UV-vis spectroscopy

UV spectra were recorded using a UV-vis spectrophotometer (V-630, JASCO, Japan) to investigate degradation and gelation kinetics. In the degradation reaction of TetraPEG-NHS, the TetraPEG-NHS prepolymer was dissolved in IL and stirred for 600 s to prepare a 1.5 wt% TetraPEG-NHS/IL solution (the initial concentration of terminal NHS, $[\text{-NHS}]_0$, was 4.8×10^{-3} mol dm^{-3}), which was then poured into a 0.4-cm-thick quartz cell. The time dependences of the UV spectra were measured for the TetraPEG-NHS/IL solution at 283, 293, 303, and 313 K at a time interval of 600 s. In the gelation reaction, 3 wt% TetraPEG-NHS/IL and TetraPEG-NH_2/IL solutions ($[\text{-NH}_2]_0 = [\text{-NHS}]_0 = 4.8 \times 10^{-3}$ mol dm^{-3}) were mixed and stirred for 120 s, and then poured into the 0.4-cm-thick quartz cell. The detailed procedure for the UV measurements is the same as that for the degradation system described above.

6.2.5 Stretching Measurements

The dumbbell-shaped TetraPEG iongels (size for a portion of a rectangular shape: 2.0×12.0×2.0 mm^3) were prepared at room temperature by the procedure described above. The stretching measurement was carried out using a mechanical testing apparatus (Autograph AG-X plus; SHIMADZU, Japan) at a constant velocity of 60 mm min^{-1}. The measurement was performed three times and the observed moduli were averaged.

6.2.6 Gelation Kinetics

The gelation reaction of TetraPEG gel is an aminolysis reaction between the NH_2 and activated ester (NHS) groups, as shown in Figure 6.1. It has been established in our previous work that TetraPEG gelation proceeds as a simple second-order reaction [50–52]:

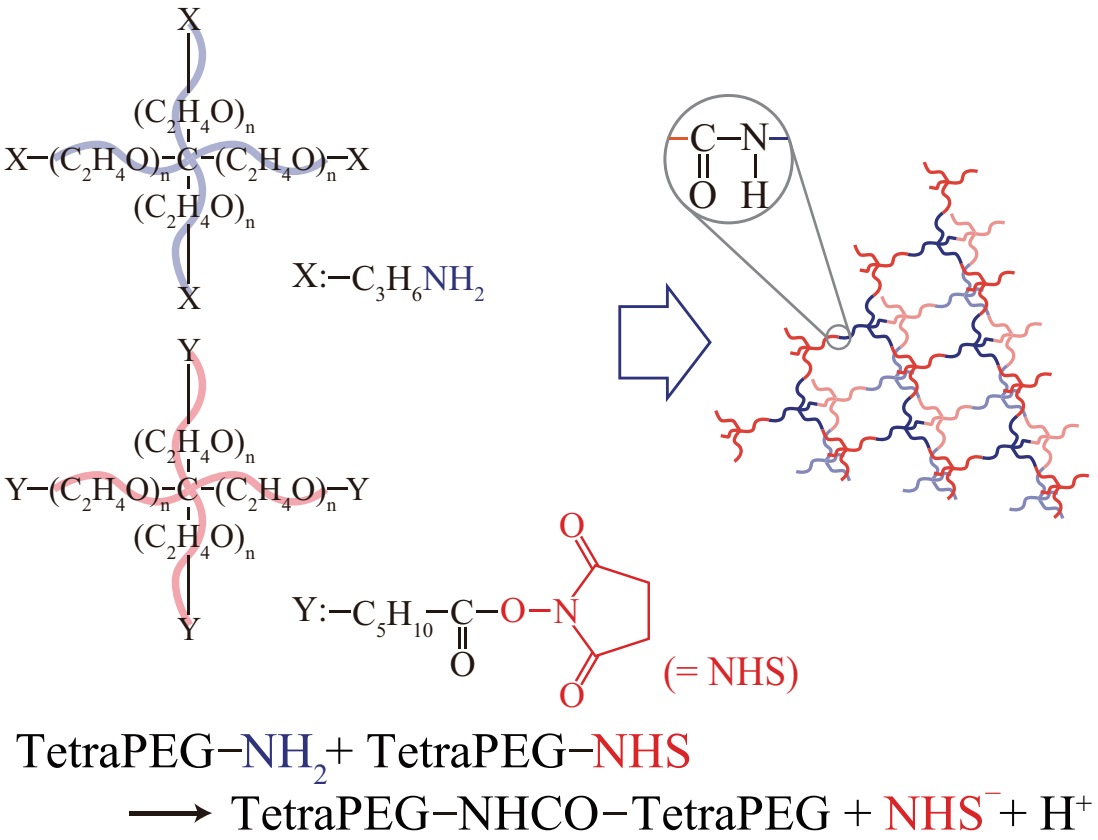

Figure 6.1. Schematic illustration of the gelation reaction of TetraPEGs.

$$d[\text{-NHCO-}]/dt = k_{\text{gel}}[\text{-NH}_2][\text{-NHS}], \tag{6.4}$$

where k_{gel}, [-NHCO-], [-NH_2], and [-NHS] correspond to the reaction rate constant for gelation, and the concentrations of amide bonds (cross-linking point), terminal -NH_2, and -NHS groups within the TetraPEG, respectively. Note that there are two reactions related to the gelation reaction: a degradation reaction of TetraPEG-NHS and an acid-base reaction of TetraPEG-NH_2. With regard to the former reaction, in an aqueous solution system, the TetraPEG-NHS gradually dissociates due to its hydrolysis reaction, which is given by the second-order reaction of [-NHS] and [OH^-] [51]. In the pH-buffering IL system, the degradation reaction of TetraPEG-NHS also occurs due to the C_2Im acting as a base. If I set an excess [C_2Im] condition relative to [-NHS], [C_2Im] can be assumed as a constant (=initial C_2Im concentration, $[C_2\text{Im}]_0$). Thus, the reaction rate for the degradation can be described as

$$-d[\text{-NHS}]/dt = k_{\text{deg}}[\text{-NHS}][C_2\text{Im}]_0 (= k_{\text{deg}}'[\text{-NHS}]), \tag{6.5}$$

where k_{deg} is the degradation rate constant and k_{deg}' is the apparent rate constant ($=k_{deg}[C_2Im]_0$). With the latter reaction, the -NH_2 group of TetraPEG coexists with the protonated -NH_3^+ group in equilibrium, according to the following acid-base reaction:

$$\text{TetraPEG-NH}_3^+ \rightleftarrows \text{TetraPEG-NH}_2 + \text{H}^+ \text{ (or HTFSA) and} \tag{6.6}$$

$$K_{a(NH3)} = \frac{[\text{-NH}_2][\text{H}^+]}{[\text{-NH}_3^+]}. \tag{6.7}$$

where $K_{a(NH3)}$ is the acid dissociation constant of the -NH_3^+ group. The NH_3^+ group does not react with the NHS group [51]; therefore, the reaction rate depends on the distribution of reactive -NH_2, f, as shown in the following equations:

$$d[\text{-NHCO-}]/dt = k_{gel}[\text{-NH}_2][\text{-NHS}] = k_{gel} f [\text{-NH}_2]_{total}[\text{-NHS}] \text{ and} \tag{6.8}$$

$$f = \frac{[\text{-NH}_2]}{[\text{-NH}_2]_{total}} = \frac{K_{a(NH3)}}{[\text{H}^+] + K_{a(NH3)}}, \tag{6.9}$$

where $[\text{-NH}_2]_{total}$ corresponds to the total concentration of amine groups (= [-NH_2] + [-NH_3^+]). Finally, the rate equation for the gelation reaction is given by

$$-d[\text{-NHS}]/dt = k_{gel} f [\text{-NH}_2]_{total}[\text{-NHS}] + k_{deg}[\text{-NHS}][C_2Im]_0. \tag{6.10}$$

6.3 Results and discussion

6.3.1 pH-Buffering Effect in Aprotic Ionic Liquid

In an aIL system ([C_2mIm^+][$TFSA^-$] in this work), the solvent aIL has no dissociative proton for both the cation and anion. On the other hand, a typical pIL, [C_2ImH^+][$TFSA^-$], has dissociative protons within the C_2ImH^+ cation and exhibits an acid-base equilibrium in solutions;

$$C_2ImH^+ \rightleftarrows C_2Im + H^+ \text{ (or HTFSA)}, \tag{6.11}$$

$$K_{a(C2ImH)} = [C_2Im][H^+]/[C_2ImH^+], \tag{6.12}$$

where C_2Im is the conjugated base in solution. It is thus plausible that $[C_2ImH^+][TFSA^-]$ acts as a nonvolatile proton source in the $[C_2mIm^+][TFSA^-]$ solution. Here, I note that the $[H^+]$, or pH, in the solution is given by

$$-\log[H^+] \text{ (or pH)} = pK_{a(C2ImH)} - \log \frac{[C_2ImH^+]}{[C_2Im]}, \tag{6.13}$$

suggesting that the solution pH can be determined from $pK_{a(C2ImH)}$ and the concentration ratio of protonated and neutral C_2Im species, $[C_2ImH^+]/[C_2Im]$. Thus, it is expected that a controlled pH condition can be achieved by adding both pIL ($[C_2ImH^+][TFSA^-]$) and its conjugated base (neutral C_2Im) into the solvent $[C_2mIm^+][TFSA^-]$ and determining the $pK_{a(C2ImH)}$ value. Initially, I determined the $pK_{a(C2ImH)}$ in $[C_2mIm^+][TFSA^-]$ by direct $[H^+]$ measurement using an IS-FET electrode (potentiometric titration).

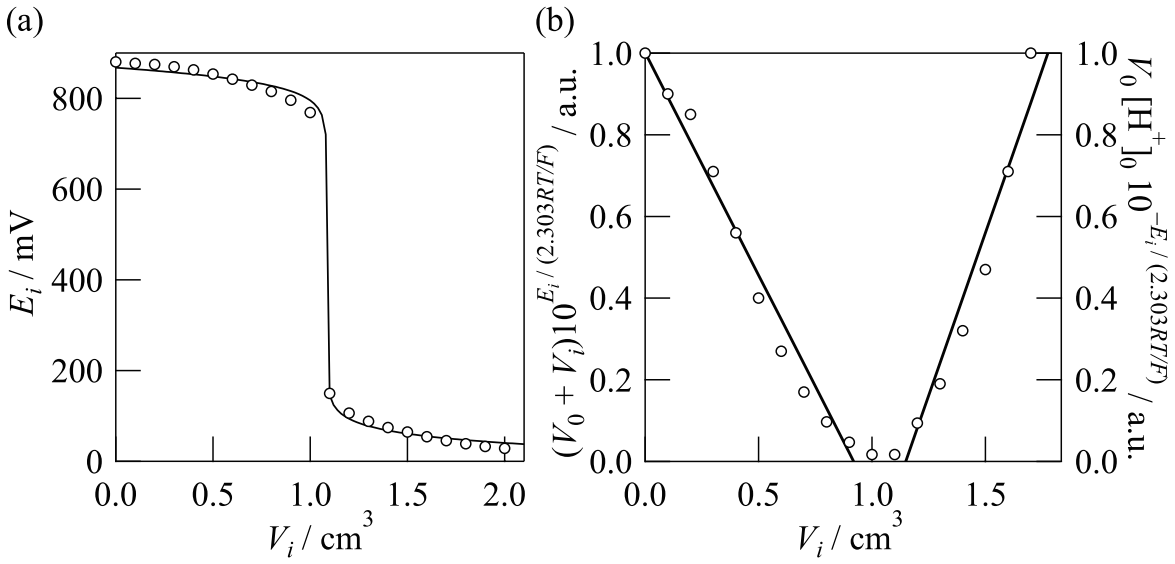

Figure 6.2. (a) Potentiometric titration curve for HTFSA solution titrated with C_2Im solution in $[C_2mIm^+][TFSA^-]$ at 293 K. The solid line corresponds to the theoretical curve calculated using the pK_a obtained from the Gran's plot. (b) Gran's plot obtained from the titration curve.

Figure 6.2 (a) shows a typical potentiometric titration curve observed for the HTFSA/$[C_2mIm^+][TFSA^-]$ solution (acid) titrated with the C_2Im/$[C_2mIm^+][TFSA^-]$ solution (base) at 293 K. Details of the potentiometry examined here are described in the Experimental section. The electromotive force, E, of the HTFSA solution slightly and gradually decreased with the addition of the titrant C_2Im solution. A large E jump (of approximately 600 mV) was observed at around the neutralization point (V_i = 1.0 cm^3),

indicating that C_2Im shows a larger pK_a value in [C_2mIm$^+$][TFSA$^-$] relative to that in aqueous solution (pK_a (aq.) = 7.3) [53]. To estimate the apparent p$K_{a(C2ImH)}$ value, the observed titration data were analyzed using Gran's method [49], and the typical result at 293 K is shown in Figure 6.2 (b). The experimental data fell on a straight line in both the acid ($0 < V_i/\mathrm{cm}^3 < 1$) and base ($V_i/\mathrm{cm}^3 > 1$) regions to give a quantitative evaluation of the apparent p$K_{a(C2ImH)}$. The p$K_{a(C2ImH)}$ value at 293 K was estimated to be 14.9(1), and its value at various other temperatures (283–313 K) is listed in Table 6.1.

Table 6.1. The p$K_{a(C2ImH)}$ and p$K_{a(NH3)}$ values determined by potentiometric titration at 283, 293, 303 and 313 K.

Temperature / K	p$K_{a(C2ImH)}$ / mol dm^{-3}	p$K_{a(NH3)}$ / mol dm^{-3}
283	14.6	16.1
293	14.9	16.4
303	15.2	16.9
313	15.5	17.3

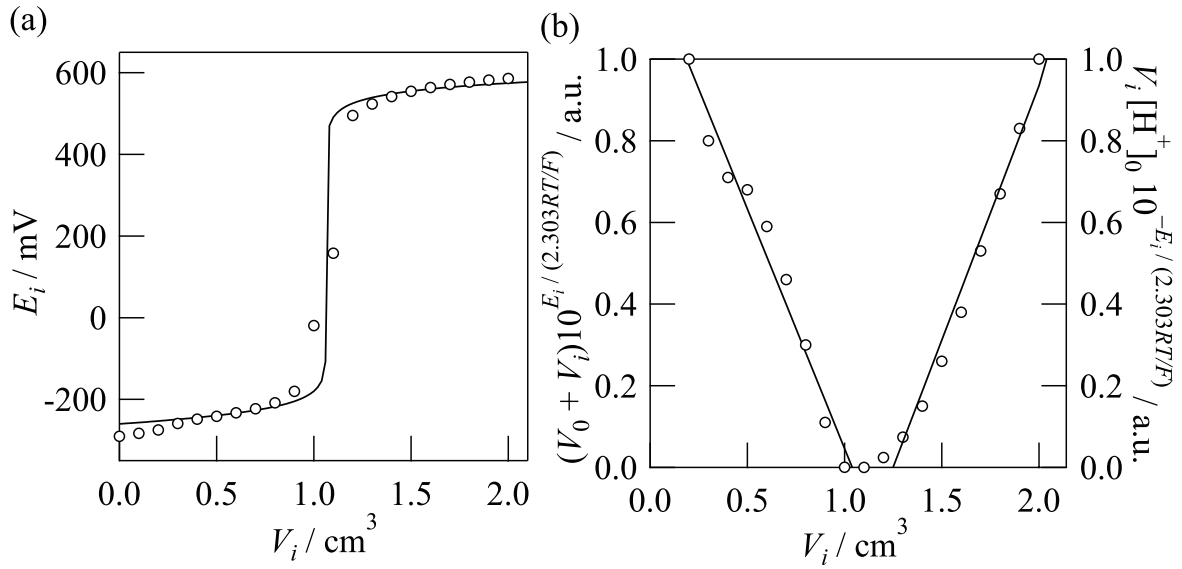

Figure 6.3. (a) Potentiometric titration curve for TetraPEG-NH_2 solution (2.7 cm^3, 8.2×10^{-3} mol dm^{-3}) titrated with HTFSA solution (2.0×10^{-2} mol dm^{-3}) at 293 K (solvent : in [C_2mIm$^+$][TFSA$^-$]). The solid line corresponds to the theoretical curve calculated by using the pK_a obtained from Gran's plot. (b) Gran's plot obtained from the titration curve.

As mentioned in the Introduction, TetraPEG gelation strongly depends on the concentration of reactive NH_2 groups within TetraPEG-NH_2 ([-NH_2]), which is calculated from $K_{a(NH3)}$,

$[H^+]$, and $[\text{-}NH_2]_{total}$ (see eq. 6.8). The $K_{a(NH3)}$ for the acid-base reaction, $\text{-}NH_3^+ \rightleftarrows \text{-}NH_2 + H^+$, in $[C_2mIm^+][TFSA^-]$ aIL was estimated using a potentiometric titration similar to that described above, and the experimental titration curve and Gran's plot are shown in Figures 6.3 (a) and (b), respectively. The $pK_{a(NH3)}$ value at 293 K was successfully determined to be 16.4(3), and its value at various other temperatures (283–313 K) is listed in Table 6.1.

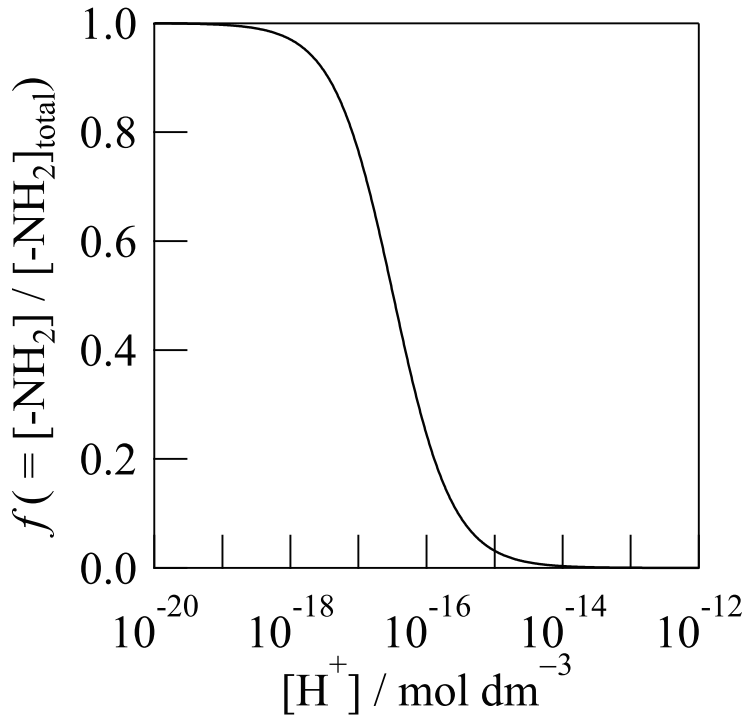

Figure 6.4. Distribution ratio of neutral amine group, *f*, plotted against $[H^+]$, calculated from the $pK_{a(NH3)}$ value in $[C_2mIm^+][TFSA^-]$ aIL at 293 K.

Figure 6.4 shows the fraction of $[\text{-}NH_2]$ to $[\text{-}NH_2]_{total}$, *f*, plotted against $[H^+]$, calculated using the obtained $pK_{a(NH3)}$ value (293 K). The *f* vs. $[H^+]$ line allows us to determine the concentration of reactive amine, $[\text{-}NH_2]$, at a given $[H^+]$. According to eq. 6.13, $[H^+]$ is directly related to the $[C_2ImH^+]/[C_2Im]$ ratio and $pK_{a(C2ImH)}$ (=14.9). Therefore, a constant *f* can be obtained during the gelation reaction by adjusting the amount of pIL and C_2Im added to the solvent aIL, i.e., the pH-buffering effect. To establish the dependence of the pH-buffering effect in $[C_2mIm^+][TFSA^-]$ aIL on the ratio of pIL and neutral C_2Im, I performed $[H^+]$ measurements at varying solution pIL and C_2Im concentration ratios during the gelation reaction of TetraPEGs, as follows.

6.3.2 Gelation Behavior in pH-Buffering IL

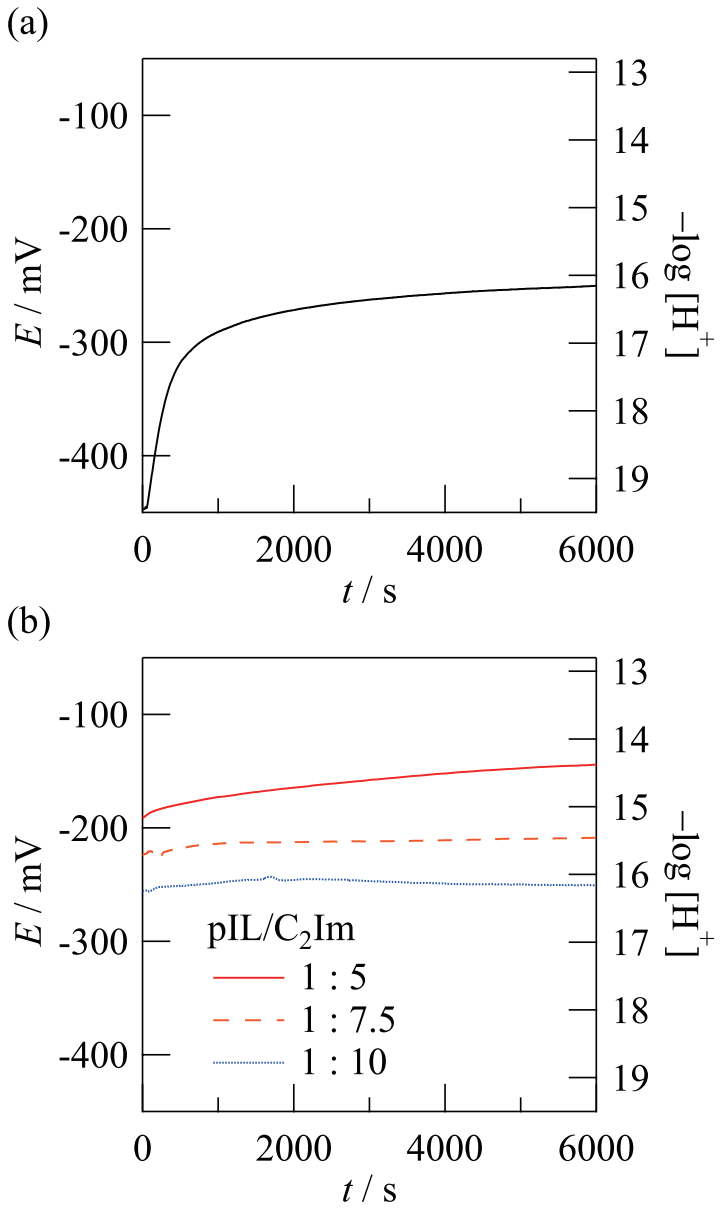

Figure 6.5. E variation observed in (a) $[C_2mIm^+][TFSA^-]$ with 6.0×10^{-3} mol dm^{-3} $[C_2ImH^+][TFSA^-]$ only, and with (b) 0.10 mol dm^{-3} $[C_2ImH^+][TFSA^-]$ + 0.5, 0.75, and 1.0 mol dm^{-3} C_2Im (solid red, broken orange, and dotted blue lines, respectively). The time interval is 10 s.

In Chapter 5, it was found that TetraPEG-NH_2 and TetraPEG-NHS prepolymers form the amide bond (-NHCO-) as a cross-linking point, resulting in the dissociation of H^+ from TetraPEG-NH_2 (Figure 6.1). Hence, the pH in the system gradually increases as the

gelation reaction proceeds. Dissociated H^+ preferentially binds to reactive NH_2 to give unreactive $NH_3{}^+$, and the gelation reaction is then terminated, leading to defects in the polymer network [41]. Figure 6.5 (a) shows the E variation (corresponding to $[H^+]$ variation) during the gelation reaction in $[C_2mIm^+][TFSA^-]$ (aIL) solution with 6.0×10^{-3} mol dm^{-3} $[C_2ImH^+][TFSA^-]$ (pIL) only. The E value appreciably increased (by approximately 200 mV) with passing reaction time t, indicating a significant pH increase in the gelation reaction. I found that the E increase is suppressed by adding neutral C_2Im as a conjugated base into the solution to reach a constant E at the concentration ratio pIL/C_2Im = 1:10 (dotted blue line in Figure 6.5 (b)). At pIL/C_2Im = 1:10, $[H^+]$ is maintained at around 7.1×10^{-17} mol dm^{-3} (pH = 16.2) during the gelation reaction at 298 K. This strongly suggests that the H^+ liberated to the bulk solution due to amide bond formation can be successfully buffered in an aIL solution containing both pIL and C_2Im (1:10). In the pIL/C_2Im = 1:5 and 1:7.5 systems, E slightly increased (by approximately 50 and 20 mV, respectively) as the gelation reaction proceeded, implying that the pH-buffering effect is not sufficient at these pIL/C_2Im compositions. I thus conclude that the $[C_2mIm^+][TFSA^-]$ solution with pIL/C_2Im = 1:10, which exhibits a successful pH-buffering effect, is more suitable for use as a reaction field for homogeneous TetraPEG network formation. By using the pH-buffering IL proposed here, we can set the parameters of $[H^+]$ and f (1.20×10^{-16} mol dm^{-3} and 0.213 at 293 K, respectively) related to the gelation reaction (eq 6.8 and 6.9), which are calculated by both $pK_{a(C2ImH)}$ and $pK_{a(NH3)}$ (=14.9 and 16.4, respectively), as determined above.

Figure 6.6 shows the storage (G') and loss (G'') moduli for the gelation of 100 mg/mL (= 6 wt%) TetraPEG in the pH-buffering IL, i.e., $[C_2mIm^+][TFSA^-]$ containing 0.10 mol dm^{-3} $[C_2ImH^+][TFSA^-]$ and 1.0 mol dm^{-3} C_2Im. The G'' gradually increased with increasing reaction time up to t = 3000 s, and subsequently decreased gradually. The G' rapidly increased at t = 2000 s and ultimately reached 10.8 kPa. The flat region of the G' curve at $t > 10^5$ s indicates that the gelation reaction is completed. Intersection of the G' and G'' profiles was seen at t = 2656 s, which corresponds to the gelation point, t_{gel} [54, 55]. According to previous theoretical studies [50, 56], t_{gel} is the point at which approximately one-third of the total terminal groups form cross-linking points (amide bonds).

I also carried out rheological measurements of the corresponding hydrogel system, 100 mg/mL (= 10 wt%) TetraPEG in aqueous solution with 0.20 mol dm^{-3} phosphate D-buffer (pH = 7.0), as shown in Figure 6.7. The G' and G'' profiles observed for the hydrogel system are almost the same as those for the pH-buffering IL system described above. This strongly suggests that the gelation reaction of TetraPEG prepolymers successfully proceeds in the pH-buffering IL, as well as in the hydrogel system, to form cross-linking points (amide bonds)

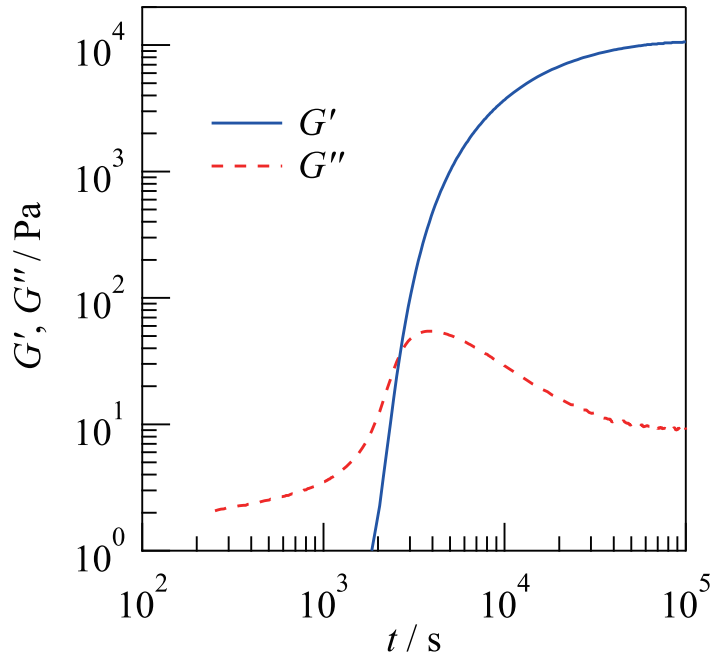

Figure 6.6. Time dependences of dynamic moduli, G' (solid line) and G'' (broken line) for the gelation of 6 wt% TetraPEG in the pH-buffering IL.

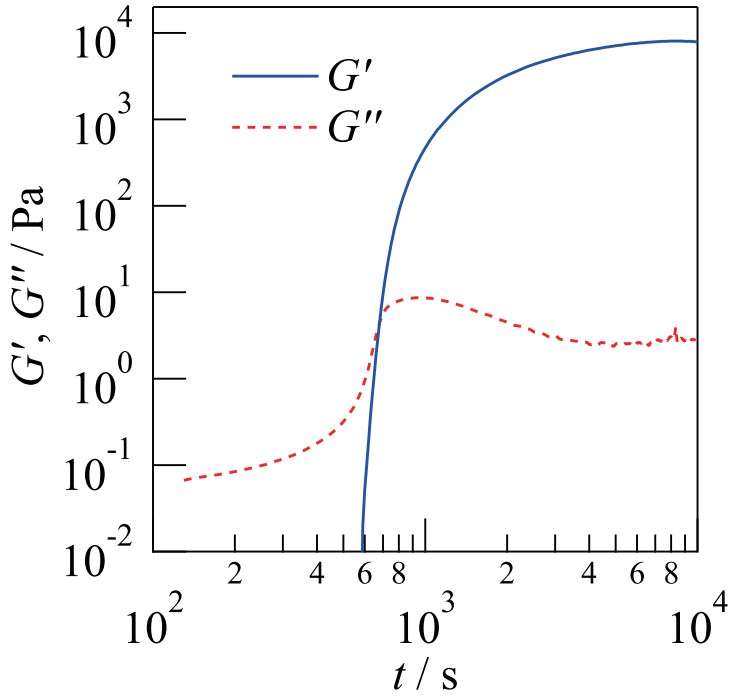

Figure 6.7. Time dependencies of dynamic moduli, G' (solid line) and G'' (broken line) for the gelation of 10 wt% TetraPEG in water with 0.2 mol dm^{-3} phosphate D-buffer (pH = 7.0) plotted against the reaction time (t).

with high reaction efficiency [43]. Here, I note that t_{gel} is markedly different between the hydrogel and iongel systems. The t_{gel} was estimated as 680 s for the hydrogel system, which is an order of magnitude smaller than that for the pH-buffering IL system (= 2656 s, this work). This difference may originate from the gelation reaction rates for both systems. I therefore investigated the gelation kinetics in the pH-buffering IL system and discuss the gelation mechanism in detail below.

6.3.3 Gelation Mechanism Based on Chemical Reaction Kinetics

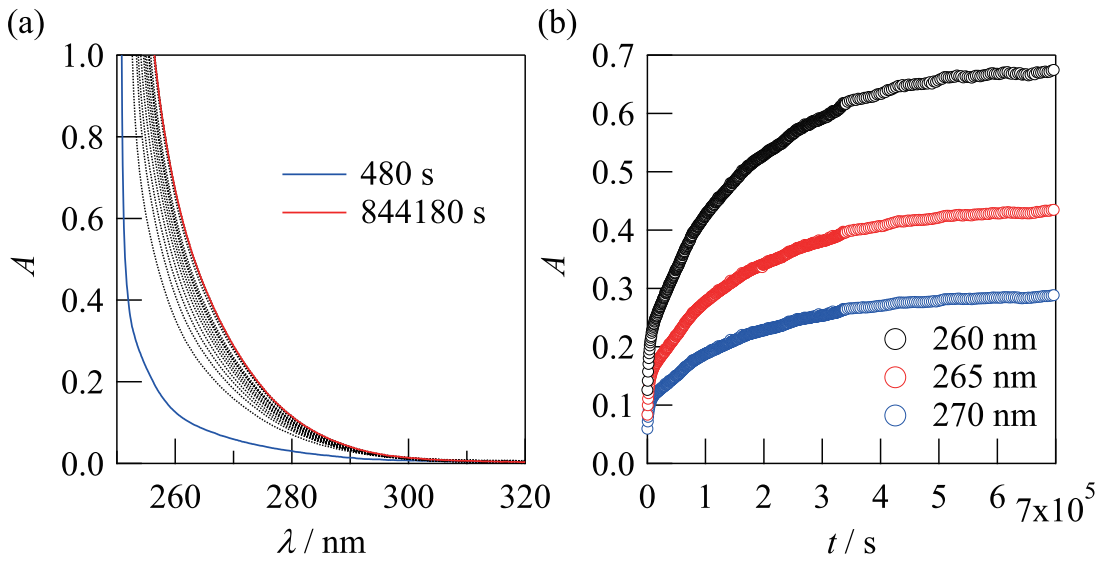

Figure 6.8. (a) Time dependence of UV spectra for the degradation of TetraPEG-NHS ([-NHS]$_0 = 4.8\times10^{-3}$ mol dm^{-3} in pH-buffering [C_2mIm$^+$][TFSA$^-$] at 293 K. The time interval of data shown in this figure is 36000 s. (b) As at 260, 265 and 270 nm plotted against reaction time, t.

From the viewpoint of chemical reaction kinetics, TetraPEG gelation is a competitive reaction with (1) amide bond formation (-NHCO-) between TetraPEG-NH_2 and TetraPEG-NHS, and (2) degradation of TetraPEG-NHS. First, I investigated the latter reaction in the pH-buffering IL to estimate the degradation rate constant, k_{deg}. In the previous work, I reported that the NHS^- ion degraded from TetraPEG-NHS exhibits UV absorption at around 260 nm, however, there are no spectra prior to degradation or gelation reaction [51, 52]. Figure 6.8 (a) shows the time dependence of UV spectra observed for the degradation reaction of 1.5 wt% TetraPEG-NHS in the pH-buffering IL (pIL/C_2Im = 1:10). In the present IL system, the observed spectra were saturated; therefore, there are no clear peaks around 260 nm. However, it can be seen that the absorbance, A, in the range 260–270 nm (shoulder)

systematically increases with increasing reaction time, t. Indeed, the time dependences of the shoulders at 260, 265, and 270 nm each gave a similar profile, as shown in Figure 6.8 (b).

I therefore used an A value of 260 nm as a probe for investigating the reaction kinetics. The A (260 nm) originating from the dissociated NHS^- at a given t is given by $A_{260}(t) = \varepsilon_{260} l[NHS^-](t)$, where ε is the molar absorption coefficient of NHS^- and l is the cell thickness (= 0.4 cm). When all the terminal -NHS is completely dissociated at $t = \infty$, due to degradation or gelation reactions, $A_{260}(\infty) = \varepsilon_{260} l[NHS^-](\infty)$ is obtained and $[NHS^-](\infty)$ equals the initial concentration of -NHS terminals within the TetraPEG prepolymer, $[\text{-NHS}]_0$. Thus, the NHS^- concentration at t can be described as $[NHS^-](t) = [\text{-NHS}]_0 A(t)/A(\infty)$.

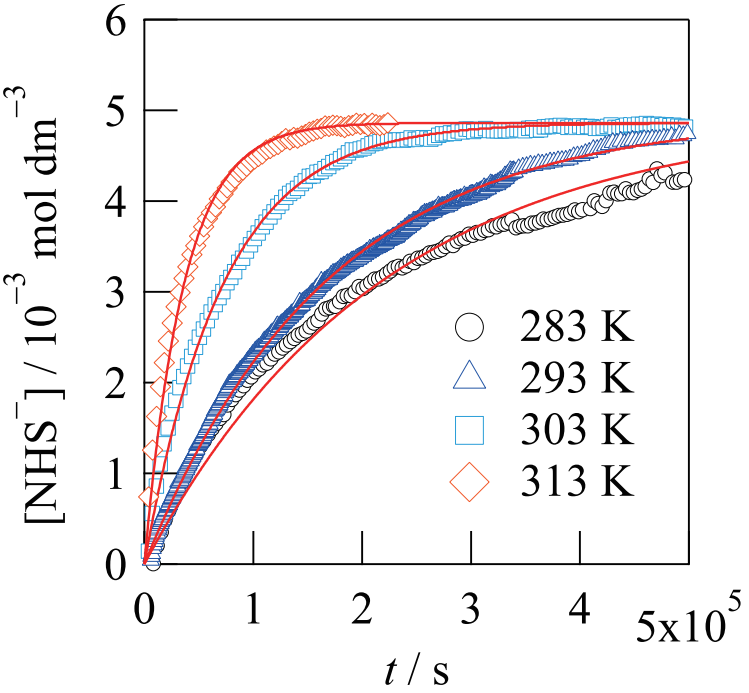

Figure 6.9. Kinetic traces obtained for the degradation reaction of TetraPEG-NHS at various temperatures. The solid line corresponds to the fitting result on the basis of eq. 6.5

Figure 6.9 shows kinetic traces for the degradation reaction in the pH-buffering IL at various temperatures. The $[NHS^-]$ dissociated from TetraPEG-NHS gradually increased with increasing t and the variations follow a simple exponential form for all temperatures. The kinetic traces were analyzed using least-square fitting based on eq. 6.5, to determine the k_{deg} values. The fitting results (solid red line) well represented the experimental data, and the determined k_{deg} at 293 K is 6.0×10^{-6} $(\text{mol dm}^{-3})^{-1}$ s^{-1}. The k_{deg} values at all temperatures examined here are listed in Table 6.2 and are used as fixed parameters in the data analysis for the gelation reaction kinetics.

Figure 6.10 shows the kinetic traces of $[NHS^-]$ for the gelation reaction of 3 wt%

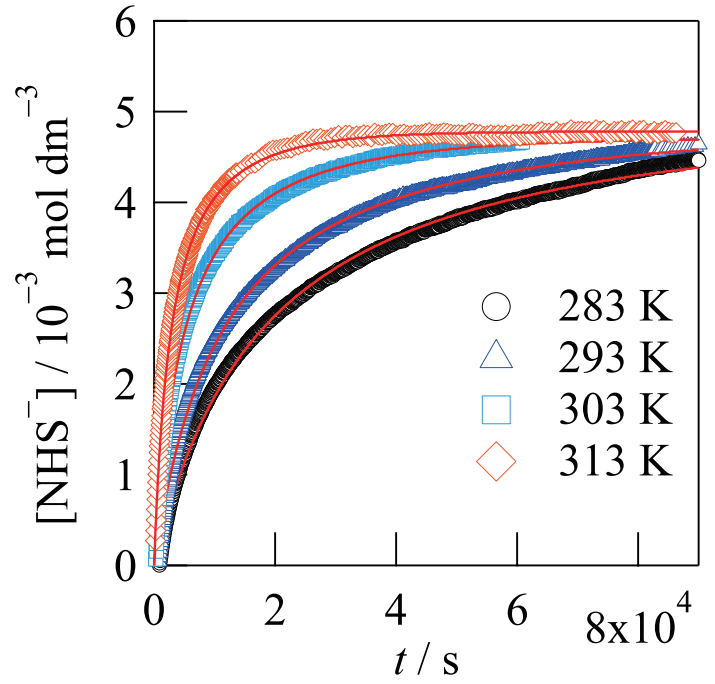

Figure 6.10. Kinetic trace obtained for the gelation reaction plotted against reaction time t at various temperatures. The solid line corresponds to the fitting result from eq. 6.10.

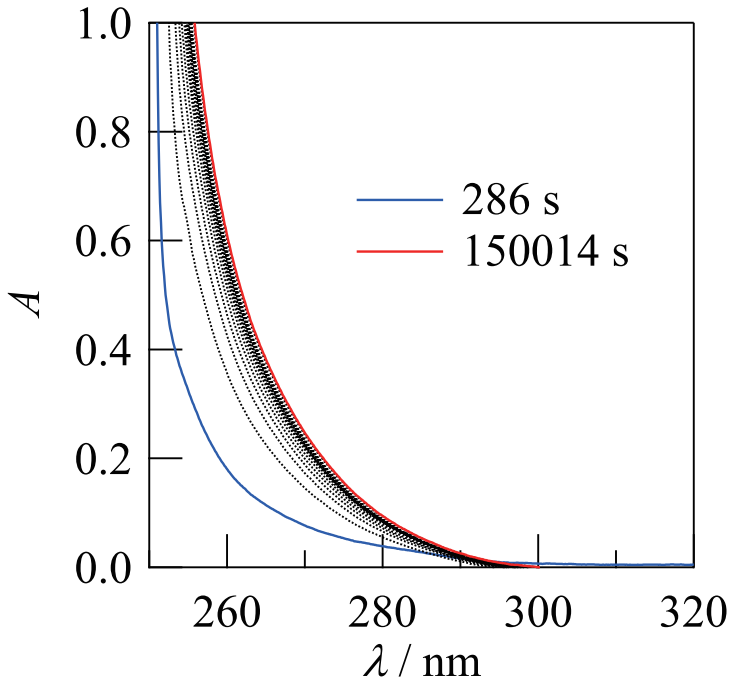

Figure 6.11. Time dependence of UV spectra for the gelation reaction of TetraPEGs ([-NH_2]$_{total}$ = [-NHS]$_0$ = 4.8×10^{-3} mol dm^{-3}) in pH-buffering [C_2mIm$^+$][TFSA$^-$] at 293 K. The time interval of data shown in this figure is 6000 s.

Table 6.2. The k_{deg} and k_{gel} values for the degradation and gelation reactions, respectively, at 283, 293, 303 and 313 K.

Temperature / K	k_{deg} / (mol dm^{-3})$^{-1}$ s^{-1}	k_{gel} / (mol dm^{-3})$^{-1}$ s^{-1}
283	4.6×10^{-6}	4.5×10^{-2}
293	6.0×10^{-6}	7.8×10^{-2}
303	1.4×10^{-5}	2.4×10^{-1}
313	2.8×10^{-5}	4.8×10^{-1}

TetraPEG-NH_2 and TetraPEG-NHS in the pH-buffering IL. The corresponding UV spectra are shown in Figure 6.11. The dissociated [NHS^-] gradually increases as the gelation reaction proceeds, and it was found that the time scale for the gelation reaction is an order of magnitude smaller than that for the degradation reaction (see x-axis in Figures 6.9 and 6.10). The kinetic traces were analyzed by least-square fitting on the basis of eq. 6.10, and k_{deg}, f, and [H^+] were fixed using the experimental values listed in Tables 6.2 and 6.3.

Table 6.3. The fixed parameters in the least-square fitting analysis for the gelation reaction, at 283, 293, 303 and 313 K.

Temperature / K	f	[H^+] / 10^{-16} mol dm^{-3}
283	0.253	2.34
293	0.213	1.20
303	0.179	0.65
313	0.151	0.36

The experimental data were in good agreement with the fitting results (solid red lines), indicating that TetraPEG gelation proceeds as a second-order reaction in the pH-buffering IL system and the aqueous TetraPEG solution system [50–52]. The k_{gel} value at 293 K was 7.8×10^{-2} (mol dm^{-3})$^{-1}$ s^{-1}, and its value at the other temperatures is listed in Table 6.2. Here, note that the k_{gel} in the TetraPEG hydrogel system is 70 (mol dm^{-3})$^{-1}$ s^{-1} at 293 K, which is 10^2–10^3 times larger than that in the present pH-buffering IL system [52]. I pointed out in the previous work that the k_{gel} for TetraPEG hydrogel is very small relative to other gelation systems such as cross-linking photopolymerization and diffusion-controlled reaction [52, 57–59]. Therefore, the gelation kinetics of TetraPEG hydrogel proceed according to a reaction-limited mechaniam, rather than diffusion-limited

mechanism. A reaction-limited mechanism with a slow reaction rate plays a key role in homogeneous polymer network formation from A-B-type cross-end coupling reactions [52]. In a reaction-limited reaction, the reaction rate of A and B prepolymers is much slower than their self-diffusion motions. Thus, A and B prepolymers can sufficiently diffuse and homogeneously mix with each other, before the cross-end coupling reaction occurs (in the case of TetraPEG gel, amide bond formation). I can thus propose that the gelation reaction of TetraPEG iongel is also based on a reaction-controlled mechanism, and that the slow gelation rate in the pH-buffering IL (such that TetraPEGs are mixed homogeneously) is essential for a defect-free polymer network. Indeed, the reaction efficiency of amide bond formation was indicated by both spectroscopic and mechanical stretching experiments to be near ideal (>90%); this is discussed in detail later.

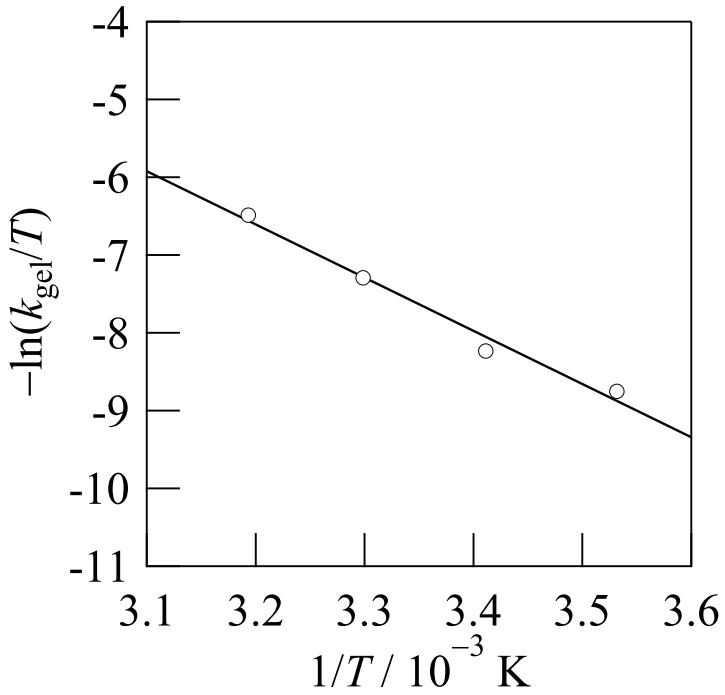

Figure 6.12. $\ln(k_{gel}/T)$ vs. $1/T$ as a form of Eyring plot.

Figure 6.12 shows k_{gel} plotted against reciprocal temperature, as a form of Eyring plot. Eyring plot gives a straight line even in the cross-linking reaction of polymers, which strongly suggests that k_{gel} values obtained here are thermodynamically meaningful. On the basis of the transition state theory, the activation enthalpy, $\Delta H^{\ddagger}$; entropy, $T\Delta S^{\ddagger}$; and Gibbs free energy, $\Delta G^{\ddagger}$, can be estimated from the slope and intercept of the following line: $\ln(k_{gel}/T) = -\Delta H^{\ddagger}/RT + \ln(k_B/h) + \Delta S^{\ddagger}/\mathrm{R}$, where R, k_B, and h correspond to gas constant, Boltzmann constant, and Planck's constant, respectively. $\Delta H^{\ddagger}$, $T\Delta S^{\ddagger}$, and $\Delta G^{\ddagger}$ were estimated to be 57(6) kJ mol^{-1}, −21(6) kJ mol^{-1}, and 78(8) kJ mol^{-1} (at 298 K), respectively. The

corresponding values for the aqueous solution system (TetraPEG hydrogel) are $\Delta H^{\ddagger}$ = 59 kJ mol^{-1}, $T\Delta S^{\ddagger}$ = −9 kJ mol^{-1}, and $\Delta G^{\ddagger}$ = 68 kJ mol^{-1} [51]. Comparing the IL and aqueous solution systems, $\Delta H^{\ddagger}$ is positive and almost the same for both systems; however, it is clear that $T\Delta S^{\ddagger}$ is appreciably different. The value is negatively larger in the IL system than in the aqueous solution system, which fully reflects the difference in $\Delta G^{\ddagger}$ between both systems. The negative entropy implies that the reaction process for the amide bond formation between TetraPEG-NH_2 and TetraPEG-NHS is associative at the transition state. Therefore, the positively larger $\Delta G^{\ddagger}$ in the IL implies that the intermediate chemical species in the amide bond formation is less stable in IL solution than in aqueous solution.

6.3.4 Reaction Efficiency and Mechanical Strength of TetraPEG Ion Gel

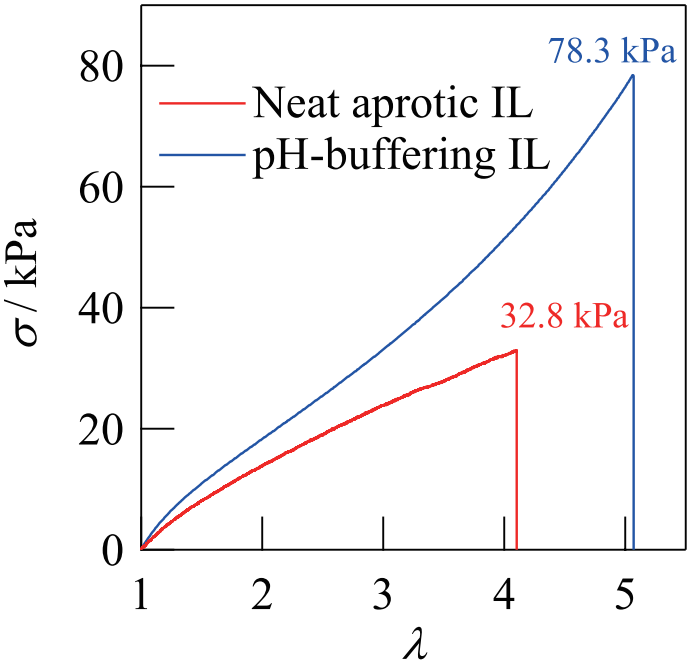

Figure 6.13. Stress-elongation curves for 6 wt% TetraPEG iongels prepared in pH-buffering and neat ILs.

Figure 6.13 shows the stretching stress-elongation curve for 6 wt% TetraPEG iongel prepared in the pH-buffering IL (pIL/C_2Im = 1:10), together with the corresponding curve in neat [C_2mIm$^+$][TFSA$^-$]. The stretching stress (σ) for the pH-buffering IL system increased by elongation (λ) and reached the breaking stress σ_{max} = 78.3 kPa at λ_{max} = 5.1, which was significantly higher than that for the neat IL system (σ_{max} = 32.8 kPa at λ_{max} = 4.1). From the initial slope of the observed stress-elongation curve, I can estimate the elastic modulus, G, for the TetraPEG iongels. The G values were estimated to be 10.9 and 7.7

kPa for the pH-buffering and neat IL systems, respectively. These results indicate that the mechanical strength and stiffness of the TetraPEG iongel is appreciably improved by applying the pH-buffering IL as a reaction field. The mechanical property of the TetraPEG iongel prepared in the pH-buffering IL is comparable to that of the corresponding TetraPEG hydrogel (G~11 kPa) in aqueous solution with a phosphate-type buffer (pH = 7) [39].

The G value is directly related to the reaction efficiency, p, of the cross-linking points, in this case, amide bonds formed in the gelation reaction. According to the tree-like theory and phantom network modeling, the relationship between G and p is described as

$$G = c({}_4C_3 P(F^{\text{out}})[1 - P(F^{\text{out}})]/2 + [1 - P(F^{\text{out}})]^4)RT \text{ and} \tag{6.14}$$

$$P(F^{\text{out}}) = (1/p - 3/4)^{1/2} - 1/2, \tag{6.15}$$

where c, R, T, and $P(F^{\text{out}})$ are the preparation concentration of bonds, gas constant, temperature, and the probability that one of the four arms does not lead to an infinite polymer network, respectively [56, 60]. Using the experimental G value, the p value of the TetraPEG iongel with pH-buffering IL was calculated to be 98%. The p value can also be evaluated from the reaction kinetics data (UV spectra) mentioned in the above section, and corresponds to the ratio of [-NHCO-]/[-NHS]$_0$ at reaction time $t = \infty$. By applying the experimental k_{gel}, k_{deg}, and f values to eq. 6.10, the concentrations of amide bonds ([-NHCO-]), degraded NHS ([NHS$^-$]), and residual NHS groups ([-NHS] = [-NHS]$_0$−[NHS$^-$]) are estimated at a given t. At $t = \infty$, where the gelation reaction is completed, [-NHCO-] and [NHS$^-$] were estimated to be 8.5×10^{-3} and 7.7×10^{-4} mol dm^{-3}, respectively; thus, p was obtained as 92% for the pH-buffering IL system. Although this p value is slightly smaller than the corresponding value obtained for the stretching measurement (98%), I can propose that the pH-buffering IL allows us to prepare a high-toughness iongel with a defect-free or less-defective polymer network.

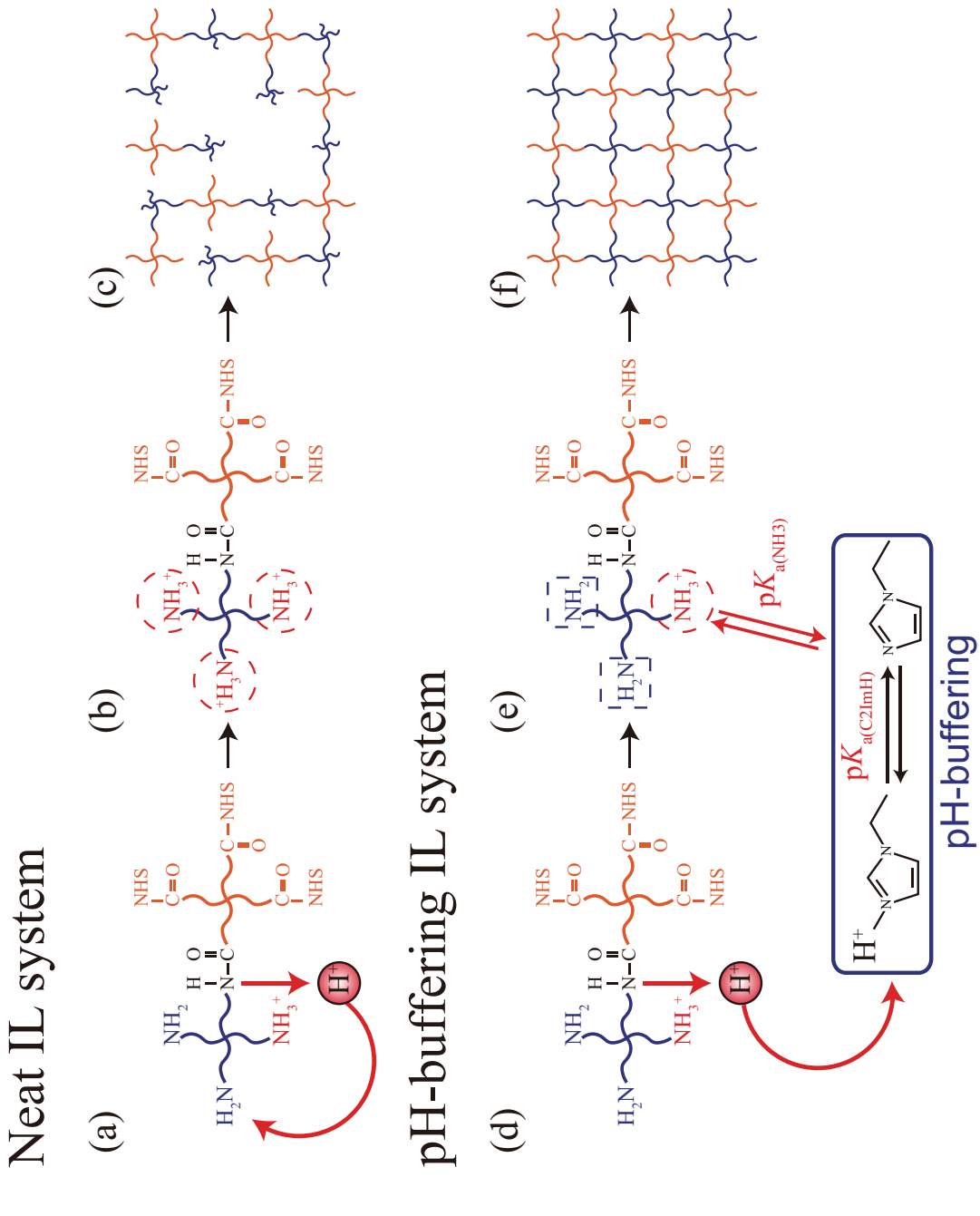

Figure 6.14. Possible gelation mechanism of TetraPEGs in neat IL (a–c) and pH-buffering IL systems (d–f).

Finally, I discuss the gelation mechanism of TetraPEG iongel, which is illustrated in Figure 6.14. In the neat IL system, the H^+, which is dissociated from TetraPEG-NH_2 when -NH_2 and -NHS groups form the amide bond, preferentially binds to the reactive -NH_2 due to its strong Brønsted basicity (pK_a = 16.4, this work) (Figure 6.14 (a)) [41]. The [H^+] increases as the gelation reaction proceeds, resulting in a decrease in reactive -NH_2 and an increase in protonated -$NH_3{}^+$ (Figure 6.14 (b)). The TetraPEG-$NH_3{}^+$ cannot form the amide bond, leading to an increase in residual unreactive groups. Hence, the gelation reaction is terminated in neat IL when all the reactive NH_2 groups are protonated by the dissociated H^+ to give a low reaction efficiency, p, or defects in the polymer network (Figure 6.14 (c)). In the pH-buffering IL proposed in this work, the H^+ dissociated from TetraPEG-NH_2 is absorbed by the pH-buffer, C_2Im, to give a constant [H^+] until the gelation reaction is completed (Figure 6.14 (d)). Therefore, the f value (the ratio of reactive -NH_2 to total -NH_2 concentrations) remains unchanged during gelation in the pH-buffering IL (Figure 6.14 (e)). The amide bond formation continuously proceeeds until all the TetraPEG-NHS or TetraPEG-NH_2 is completely reacted at $t \sim \infty$ (in this work, $t = 2.0 \times 10^5$ s for 6 wt% TetraPEG). This leads to a high reaction efficiency, p, of larger than 90% and gives a nearly ideal network with less network defects (Figure 6.14 (f)).

6.4 Conclusion

I proposed a "pH-buffering ionic liquid," i.e., a [C_2mIm$^+$][TFSA$^-$] aIL solution with [C_2ImH$^+$][TFSA$^-$] pIL (proton source) and its conjugated base, C_2Im, and applied it to the reaction field of homogeneous TetraPEG network formation. I demonstrated that the pH-buffering IL with [C_2ImH$^+$][TFSA$^-$]/C_2Im = 1:10 exhibits a successful pH-buffering effect during the gelation reaction to give a constant solution pH $\sim$ 16.2. From the kinetic aspect, the TetraPEG gelation reaction in the pH-buffering IL was characterized, and I found that (1) the gelation reaction proceeds as a second-order reaction, (2) the reaction rate constant (k_{gel} = 7.8 $\times$ 10^{-2} (mol dm^{-3})$^{-1}$ s^{-1}) is two orders of magnitude smaller than that in the corresponding hydrogel system, and (3) the gelation mechanism is likely a reaction-limited, rather than diffusion-limited, process because of the much smaller k_{gel} value in the IL system than in the water system. The reaction efficiencies, p values, corresponding to the extent of defects in the polymer network were estimated to be 98% and 92%, as obtained by mechanical stretching tests and UV-vis spectroscopy, respectively; these values are near ideal (i.e., 100%). I thus conclude that a pH-controlled reaction field, i.e., the pH-buffering IL proposed in this work, is essential to prepare a defect-free TetraPEG network iongel. This yields

a high-toughness iongel with a low polymer concentration, good handling properties, and high performance, for use in applications such as electrochemical devices and gas-separation membranes.

Reference

[1] H. Ohno. *Electrochemical aspects of ionic liquids*. Wiley-Interscience, Inc. Hoboken, New Jersey, 2005.

[2] H. Yoon, A. S. Best, M. Forsyth, D. R. Macfarlane, and P. C. Howlett. *PCCP*, Vol. 17, pp. 4656–4663, 2015.

[3] M. A. Navarra. *MRS Bull.*, Vol. 38, pp. 548–553, 2013.

[4] K. Fujii, H. Hamano, H. Doi, X. Song, S. Tsuzuki, H. Hayamizu, S. Seki, Y. Kameda, K. Dokko, M. Watanabe, and Y. Umebayashi. *J. Phys. Chem. C*, Vol. 117, pp. 19314–19324, 2013.

[5] J. N. a. C. Lopes, M. F. C. Gomes, and A. a. H. Pádua. *J. Phys. Chem. B*, Vol. 110, pp. 16816–16818, 2006.

[6] Z. S. Qureshi, K. M. Deshmukh, and B. M. Bhanage. *Clean Techn. Environ. Policy*, Vol. 16, pp. 1487–1513, 2014.

[7] T. Welton. *Chem. Rev.*, Vol. 99, pp. 2071–2083, 1999.

[8] H. Passos, M. G. Freire, and J. a. P. Coutinho. *Green Chem.*, Vol. 16, pp. 4786–4815, 2014.

[9] R. P. Swatloski, S. K. Spear, J. D. Holbrey, and R. D. Rogers. *J. Am. Chem. Soc.*, Vol. 124, pp. 4974–4975, 2002.

[10] R. Patel, M. Kumari, and A. B. Khan. *Appl. Biochem. Biotechnol.*, Vol. 172, pp. 3701–3720, 2014.

[11] T. Ueki and M. Watanabe. *Bull. Chem. Soc. Jpn.*, Vol. 85, pp. 35–50, 2012.

[12] H. Wang, G. Gurau, and R. D. Rogers. *Chem. Soc. Rev.*, Vol. 41, pp. 1519–1537, 2012.

[13] K. Fujii, T. Ueki, K. Niitsuma, T. Matsunaga, M. Watanabe, and M. Shibayama. *Polymer*, Vol. 52, pp. 1589–1595, 2011.

[14] M. Armand, F. Endres, D. R. Macfarlane, H. Ohno, and B. Scrosati. *Nat. Mater.*, Vol. 8, pp. 621–629, 2009.

[15] M. Diaz, A. Ortiz, and I. Ortiz. *J. Memb. Sci.*, Vol. 469, pp. 379–396, 2014.

[16] D. R. Macfarlane, N. Tachikawa, M. Forsyth, J. M. Pringle, P. C. Howlett, G. D. Elliott, J. H. Davis, M. Watanabe, P. Simon, and C. A. Angell. *Energy. Environ. Sci.*, Vol. 7, pp. 232–250, 2014.

[17] I. Must, V. Vunder, F. Kaasik, I. Poldsalu, U. Johanson, A. Punning, and A. Aabloo. *Sens. Actuators B Chem.*, Vol. 202, pp. 114–122, 2014.

[18] M. J. Park, I. Choi, J. Hong, and O. Kim. *J. Appl. Polym. Sci.*, Vol. 129, pp. 2363–2376, 2013.

[19] S. Y. Lee, A. Ogawa, M. Kanno, H. Nakamoto, T. Yasuda, and M. Watanabe. *J. Am. Chem. Soc.*, Vol. 132, pp. 9764–9773, 2010.

[20] N. Terasawa and K. Asaka. *Sens. Actuators B Chem.*, Vol. 193, pp. 851–856, 2014.

[21] S. Imaizumi, H. Kokubo, and M. Watanabe. *Macromolecules*, Vol. 45, pp. 401–409, 2012.

[22] J.-M. Tarascon and M. Armand. *Nature*, Vol. 414, pp. 359–367, 2001.

[23] L. C. Tome, C. Florindo, C. S. R. Freire, L. P. N. Rebelo, and I. M. Marrucho. *PCCP*, Vol. 16, pp. 17172–17182, 2014.

[24] M. Karaszova, M. Kacirkova, K. Friess, and P. Izak. *Sep. Purif. Technol.*, Vol. 132, pp. 93–101, 2014.

[25] J. E. Bara, D. E. Camper, D. L. Gin, and R. D. Noble. *Acc. Chem. Res.*, Vol. 43, pp. 152–159, 2010.

[26] J. E. Bara, T. K. Carlisle, C. J. Gabriel, D. Camper, A. A. Finotello, D. L. Gin, and R. D. Noble. *Ind. Eng. Chem. Res.*, Vol. 48, pp. 2739–2751, 2009.

[27] S. Kasahara, E. Kamio, T. Ishigami, and H. Matsuyama. *Chem. Commun.*, Vol. 48, pp. 6903–6905, 2012.

[28] T. Sakai. *Polym. J.*, Vol. 46, pp. 517–523, 2014.

[29] T. Hazama, K. Fujii, T. Sakai, M. Aoki, H. I. Mimura, H. Eguchi, Y. Todorov, N. Yoshimoto, and M. Morita. *J. Power Sources*, Vol. 286, pp. 470–474, 2015.

[30] S. Kasahara, E. Kamio, A. Otani, and H. Matsuyama. *Ind. Eng. Chem. Res.*, Vol. 53, pp. 2422–2431, 2014.

[31] S. Kasahara, E. Kamio, A. Yoshizumi, and H. Matsuyama. *Chem. Commun.*, Vol. 50, pp. 2996–2999, 2014.

[32] K. Fujii, T. Makino, K. Hashimoto, T. Sakai, M. Kanakubo, and M. Shibayama. *Chem.Lett.*, Vol. 44, pp. 17–19, 2015.

[33] Y. Y. Gu, E. L. Cussler, and T. P. Lodge. *J. Memb. Sci.*, Vol. 423, pp. 20–26, 2012.

[34] Y. Gu, S. Zhang, L. Martinetti, K. H. Lee, L. D. Mcintosh, C. D. Frisbie, and T. P. Lodge. *J. Am. Chem. Soc.*, Vol. 135, pp. 9652–9655, 2013.

[35] T. Moriyasu, T. Sakamoto, N. Sugihara, Y. Sasa, Y. Ota, T. Shimomura, Y. Sakai, and K. Ito. *Polymer*, Vol. 54, pp. 1490–1496, 2013.

[36] F. Moghadam, E. Kamio, A. Yoshizumi, and H. Matsuyama. *Chem. Commun.*, Vol. 51,

pp. 13658–13661, 2015.

[37] K. Fujii, H. Asai, T. Ueki, T. Sakai, S. Imaizumi, U. Chung, M. Watanabe, and M. Shibayama. *Soft Matter*, Vol. 8, pp. 1756–1759, 2012.

[38] H. Asai, K. Fujii, T. Ueki, T. Sakai, U. Chung, M. Watanabe, Y. S. Han, T. H. Kim, and M. Shibayama. *Macromolecules*, Vol. 45, pp. 3902–3909, 2012.

[39] Y. Akagi, T. Katashima, H. Sakurai, U. Chung, and T. Sakai. *RSC Advavces*, Vol. 3, pp. 13251–13258, 2013.

[40] K. Fujii, K. Hashimoto, T. Sakai, Y. Umebayashi, and M. Shibayama. *Chem. Lett.*, Vol. 42, pp. 1250–1251, 2013.

[41] K. Hashimoto, K. Fujii, K. Nishi, T. Sakai, N. Yoshimoto, M. Morita, and M. Shibayama. *J. Phys. Chem. B*, Vol. 119, pp. 4795–4801, 2015.

[42] T. Sakai, T. Matsunaga, Y. Yamamoto, C. Ito, R. Yoshida, S. Suzuki, N. Sasaki, M. Shibayama, and U. Chung. *Macromolecules*, Vol. 41, pp. 5379–5384, 2008.

[43] K. Nishi, H. Asai, K. Fujii, Y.-S. Han, T.-H. Kim, T. Sakai, and M. Shibayama. *Macromolecules*, Vol. 47, pp. 1801–1809, 2014.

[44] K. Fujii, R. Kanzaki, T. Takamuku, Y. Kameda, S. Kohara, M. Kanakubo, M. Shibayama, S. Ishiguro, and Y. Umebayashi. *J. Chem. Phys.*, Vol. 135, p. 244502, 2011.

[45] K. Fujii, T. Nonaka, Y. Akimoto, Y. Umebayashi, and S. Ishiguro. *Anal. Sci.*, Vol. 24, pp. 1377–1380, 2008.

[46] K. Hashimoto, K. Fujii, and M. Shibayama. *J. Mol. Liquids*, Vol. 188, pp. 143–147, 2013.

[47] K. Izutsu and M. Ohmaki. *Talanta*, Vol. 43, pp. 643–648, 1996.

[48] R. Kanzaki, K. Uchida, S. Hara, Y. Umebayashi, S. Ishiguro, and S. Nomura. *Chem. Lett.*, Vol. 36, pp. 684–685, 2007.

[49] G. Gran. *Analyst*, Vol. 77, pp. 661–671, 1952.

[50] M. Kurakazu, T. Katashima, M. Chijiishi, K. Nishi, Y. Akagi, T. Matsunaga, M. Shibayama, U. Chung, and T. Sakai. *Macromolecules*, Vol. 43, pp. 3935–3940, 2010.

[51] K. Nishi, K. Fujii, M. Chijiishi, Y. Katsumoto, U. Chung, T. Sakai, and M. Shibayama. *Macromolecules*, Vol. 45, pp. 1031–1036, 2012.

[52] K. Nishi, K. Fujii, Y. Katsumoto, T. Sakai, and M. Shibayama. *Macromolecules*, Vol. 47, pp. 3274–3281, 2014.

[53] B. Lenarcik and P. Ojczenasz. *J. Heterocycl. Chem.*, Vol. 39, pp. 287–290, 2002.

[54] M. J. Moura, M. M. Figueiredo, and M. H. Gil. *Biomacromolecules*, Vol. 8, pp. 3823–

3829, 2007.

[55] H. H. Winter and F. Chambon. *J. Rheology*, Vol. 30, p. 367, 1986.

[56] C. W. Macosko and D. R. Miller. *Macromolecules*, Vol. 9, pp. 199–206, 1976.

[57] K. Dusek. *Polym. Gels and Network*, Vol. 4, pp. 383–404, 1996.

[58] I. Mita, K. Horie, and M. Takeda. *Macromolecules*, Vol. 14, pp. 1428–1433, 1981.

[59] K. S. Anseth, L. M. Kline, T. A. Walker, K. J. Anderson, and C. N. Bowman. *Macromolecules*, Vol. 28, pp. 2491–2499, 1995.

[60] Y. Akagi, T. Katashima, K. Fujii, T. Matsunaga, U. Chung, M. Shibayama, and T. Sakai. *Macromolecules*, Vol. 44, pp. 5817–5821, 2011.

Chapter 7

Carbon Dioxide Separation Using High-toughness Iongel with Tetra-armed Polymer Network

7.1 Introduction

Room temperature ionic liquids (ILs) have been widely applied to electrochemical, synthetic and separation processes as green solvents due to their unique properties such as nonvolatility, nonflammability, good thermal stability, high ionic conductivity and so on. ILs are recognized as designable solvents, and their structural diversity enables us to control their solvent properties, for example, the miscibility with various chemicals such as metal ions, synthesized and biological polymers, and acidic gases. In the last decade, CO_2 absorption and separation technologies using ILs have attracted much attention, because CO_2 is highly soluble in ILs relative to other neutral gases like N_2, H_2, and CH_4. A large number of investigations have been performed until now to improve the CO_2 absorption properties since the first report on the high solubility of CO_2 in the dialkylimidazolium-based IL [1]. A membrane separation process generally requires smaller operational energy, lower running cost, and smaller equipment footprint compared with an absorption process. The supported IL membranes (SILMs), i.e., polymeric or inorganic porous materials filled with ILs, show comparable or higher permeabilities and selectivities of CO_2 than the conventional polymeric membranes [2, 3]. SILMs have a longer-term stability than the supported membranes with organic solvents, because of nonvolatility and high thermal stability of ILs. However, SILMs cannot hold ILs under pressurized conditions, which is a serious disadvantage for the gas separation membrane. Polymeric ILs, i.e., self cross-linking ILs were also applied as CO_2

separation membranes [4, 5]. However, it was pointed out that their separation performances are inferior to those of the SILMs due to the limited CO_2 diffusion in their rigid polymer matrix. Therefore, iongels with a low polymer content and/or a high fraction of "free" IL content are more favorable materials for the CO_2 separation membrane.

Recently, some research groups reported the CO_2 separation performances of the iongels with relatively low polymer contents [6–9]. Lodge et al. reported the iongel containing 15 wt% ABA-type triblock copolymer and 1-ethyl-3-methlimidazolium bis(trifluoromethanesulfonyl)amide, $[C_2mIm^+][TFSA^-]$ [6]. The iongel possesses a comparable CO_2 permselectivity to the $[C_2mIm^+][TFSA^-]$-based SILM, although it melts below 80°C. They also reported a high-toughness iongel with 10 wt% triblock copolymer, which was prepared by cross-linking reactions in the IL [10]. The electrical conductivity is about 2/3 of that of the neat IL because the ionic mobility is obstructed by the non-conductive part in their iongel. Kamio et al. reported a CO_2/N_2 separation membrane using poly(vinyl-prrolidone)-based iongels containing 50–70 wt% amino acid IL and the iongel shows compression breaking stress of 1 MPa at 70 wt% IL content [8]. They demonstrated that both CO_2 permeability and selectivity are significantly improved with an increase of the IL content. In our recent study, we have proposed high toughness iongels with low polymer concentration, i.e., tetra-armed poly(ethylene glycol) (TetraPEG) iongels [11, 12]. The TetraPEG iongels can be prepared by AB-type cross-end coupling of two symmetrical TetraPEGs in typical aprotic ILs (aILs). The electrical conductivity measurement for the TetraPEG iongel shows that the diffusivity of ionic species in the gel is almost comparable to that in the neat IL. It also shows high mechanical properties even with much lower polymer contents, for example, the maximum breaking strength by compression reaches 18 MPa (83.5% strain) at 6 wt% polymer content. The excellent mechanical properties originate from a homogeneous polymer network strucuture [12]. In addition, the TetraPEG $[C_2mIm^+][TFSA^-]$ gel is thermally stable up to 300°C. It is thus expected that the TetraPEG iongel is a promising material for CO_2 separation membrane. In this work, I show the CO_2 separation performance of the TetraPEG iongel membrane in a wide temperature range up to 100°C. Furthermore, I also made a new trial to directly evaluate the CO_2 absorption capacities of the TetraPEG iongel at pressures up to 3 MPa.

7.2 Experiment

7.2.1 Material

TetraPEG-NH_2 and TetraPEG-NHS were purchased from Nippon Oil Fat and Co (Japan). The molecular weight (M_w) of both TetraPEGs was 20000 g mol^{-1}. The aIL, [C_2mIm^+][$TFSA^-$], was synthesized according to conventional methods [13, 14]. Water content in the aIL was checked by Karl Fisher titration to be less than 50 ppm. The protic IL (pIL), [C_2ImH^+][$TFSA^-$], was prepared by mixing equimolar amounts of HTFSA and C_2Im in acetonitrile [15]. The acetonitrile solution was dried in vacuum at room temperature for 1 day to obtain [C_2ImH^+][$TFSA^-$]. The C_2Im was dried with molecular sieves (3A) and purified by distillation. The HTFSA was kept in a glovebox and used without further purification. Water content in the pIL was checked by Karl Fisher titration to be less than 100 ppm.

7.2.2 Preparation of iongel membrane

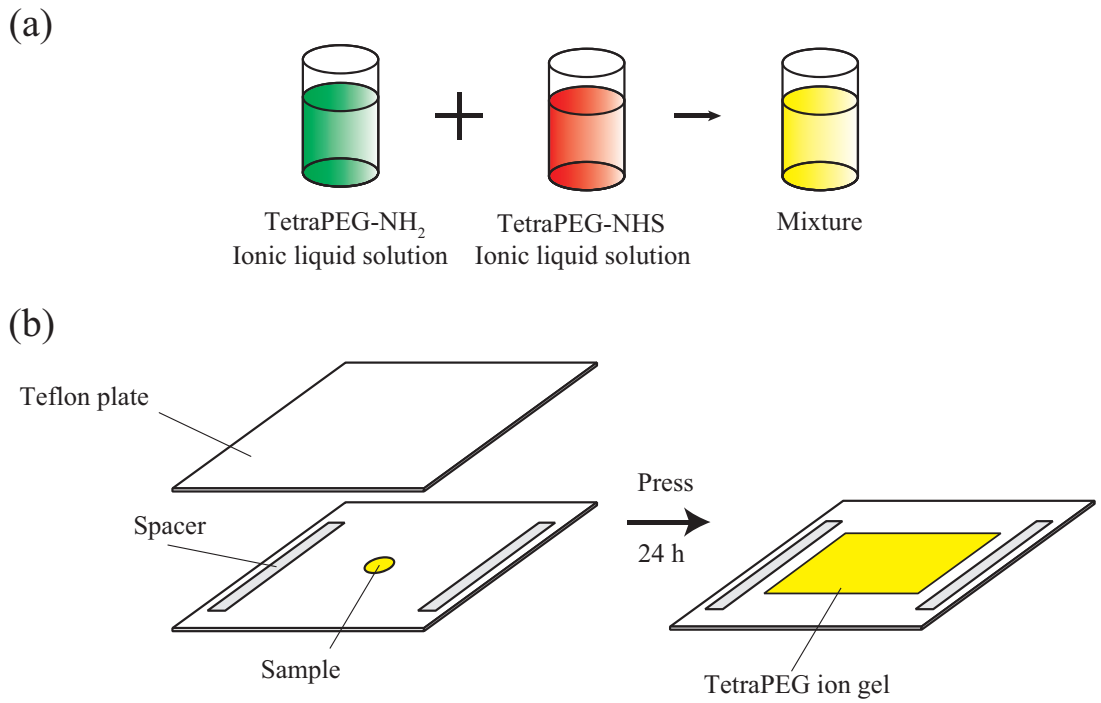

Figure 7.1. Preparation of TetraPEG iongel membrane.

TetraPEG iongel membranes were prepared as illustrated in Figure 7.1. (a) 6 wt%

TetraPEG-NH_2 and TetraPEG-NHS prepolymers were dissolved in [C_2mIm$^+$][TFSA$^-$] aIL with 3 mol dm^{-3} [C_2ImH$^+$][TFSA$^-$] pIL. The solutions were mixed during 30 min at room temperature. (b) The mixture was cast on a Teflon plate with 1 mm silicon spacers, and then pressed by another plate from the upper-side at room temperature for 24 h. After that we obtained the free-standing TetraPEG iongel membrane.

7.2.3 Gas separation measurements

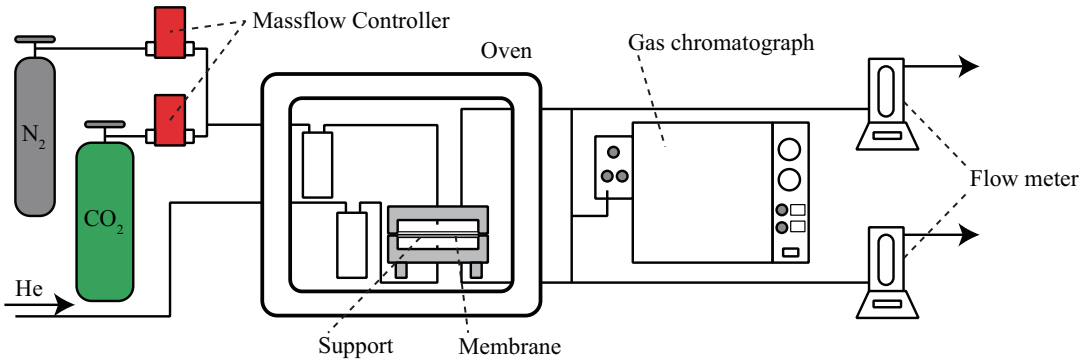

Figure 7.2. Schematic illustration of the experimental apparatus for the gas separation measurement.

The experimental apparatus for the gas separation measurements is illustrated in Figure 7.2. The TetraPEG iongel membrane (25 mm in diameter) was placed on a stainless steel cell with a porous hydrophobic PTFE filter (Advantec Co., T010A025A) as the support. The PTFE filter has a pore size of 0.1 μm, porosity of 68%, and thickness of 70 μm. The effective surface area was 3.40 cm^2 and a thickness of the membrane was measured with a micrometer. Feed and sweep gases were a CO_2/N_2 mixture, of which the CO_2 composition was 50 mol%, and He, respectively. A total pressure of the mixture was 101 kPa (atmospheric pressure). The flow rates of the feed and sweep gases were 50 cm^3 min^{-1} and 12 cm^3 min^{-1}, respectively, and they were regulated using mass flow controllers (HORIBA STEC Inc., SEC-E40). Neither of the feed and sweep gases contained water in the present study. Temperature was controlled using an oven (ESPEC Co., SH-641). The permeabilities of CO_2 and N_2 were evaluated from a flow rate and a composition of the outlet sweep. The flow rate was measured by a film flow meter (HORIBA STEC Inc., SF-1U). The composition was determined using a TCD gas chromatograph (Shimadzu, GC-8A).

A SILM was prepared as follows. A hydrophilic PTFE membrane (Merck Millipore, JVWP02500) was dipped into [C_2mIm$^+$][TFSA$^-$] under vacuum at room temperature for 24 h. The PTFE filter has a pore size of 0.1 μm, porosity of 80%, and thickness of 30

μm. The excess IL on the filter surface was wiped up just before the measurement. The permselectivities for the SILM were obtained with the procedure described in the previous paragraph.

7.2.4 Volume expansion measurements

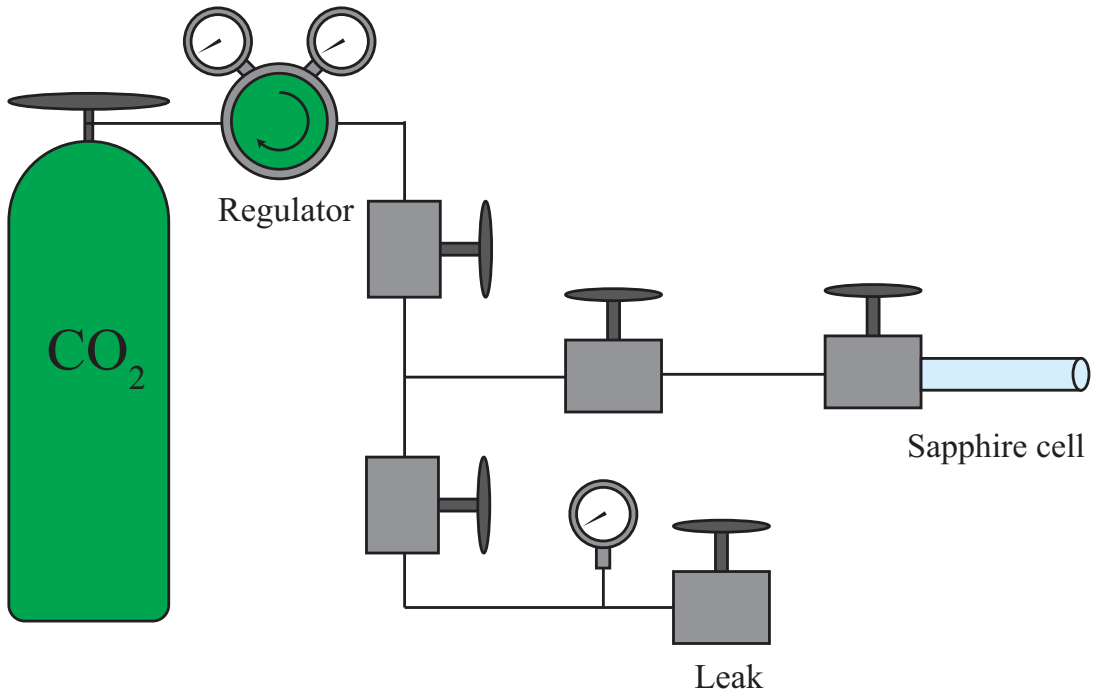

Figure 7.3. Schematic illustration of the experimental apparatus for the volume expansion measurement.

TetraPEG iongel was prepared in a capillary (1.4 mm in diameter). The cylindrical rod-like iongel thus obtained was placed in a pressure glass tube (NE-PCAV10-M, New Era Enterprises, Inc.) and then CO_2 gas was flowed into the pressure tube (~3 MPa). The diameter of the iongel was measured by using optical microscope (KEYENCE, VHX-900). By assuming an isotropic expansion of the iongel, the volume expansion, V/V_0 can be defined as a change of diameters between the iongel absorbing CO_2 (d) and its initial state without CO_2 (d_0), i.e., $V/V_0 = (d/d_0)^3$. The measurement was performed at room-temperature.

7.2.5 Stretching measurement

Uniaxial stretching tests were carried out for rectangular-shaped TetraPEG iongel (30 mm in length, 5 mm in width and 1 mm in thickness) using a universal testing apparatus (EZ-test, Shimadzu, Kyoto, Japan) at velocity of 10 mm/min.

7.3 Results and discussion

7.3.1 Preparation of iongel membrane

As reported in our previous work [11], the TetraPEG iongel can be prepared by mixing two TetraPEG prepolymers, i.e., tetra-amine-terminated and tetra-*N*-hydroxysuccinimide-terminated PEGs (TetraPEG-NH_2 and TetraPEG-NHS, respectively), in [C_2mIm^+][$TFSA^-$] aIL. The gelation time in the [C_2mIm^+][$TFSA^-$] was less than 60 s, which was too short to prepare an iongel membrane by a conventional method described in Experimental section.

Here, note that the gelation time of TetraPEG gel system strongly depends on the pH or concentration of H^+ in the solutions [16, 17]. In the hydrogel system, it has been established that (1) TetraPEG gelation undergoes as a simple second-order reaction kinetics ($-d$[-NH_2]/dt = k_{gel}[-NH_2][-NHS], k_{gel} : reaction rate constant) and (2) the gelation time is directly related to the acid-base reaction of the reactive NH_2 end-group within TetraPEG-NH_2 (TetraPEG-NH_2 + H^+ $\rightleftarrows$ TetraPEG-NH_3^+) [16, 17]. Thus, the concentration of NH_2 end-group, [-NH_2] decreases with a lower pH (= higher [H^+]), resulting in a longer gelation time. In aIL system, addition of H^+ sources is required for the gelation control, because there is no dissociative H^+ within both cation and anion in typical aILs. So, I focused on pILs as "non-volatile" H^+ sources. In this work, 1-ethylimidazolium bis(trifluoromethanesulfonyl)amide ([C_2ImH^+][$TFSA^-$]) that is analogous pIL of [C_2mIm^+][$TFSA^-$] aIL, was added into TetraPEG-NH_2/[C_2mIm^+][$TFSA^-$] and TetraPEG-NHS/[C_2mIm^+][$TFSA^-$] solutions with 6 wt% prepolymer content. The molecular weight was 20,000 for both prepolymers. After mixing them, the gelation reaction was investigated by rheological measurements to estimate the gelation time.

Figure. 7.4 shows typical results of the storage (G') and loss (G'') moduli for the TetraPEG gelation in [C_2mIm^+][$TFSA^-$] with varying the [C_2ImH^+][$TFSA^-$] concentration. Both G' and G'' gradually increased with the reaction time for all the systems, and the intersection of the G' and G'' profiles corresponding to the gelation point was clearly observed. The gelation times were 775, 2660 and 62375 s for 4.6, 5.0 and 6.0 mol dm^{-3} [C_2ImH^+][$TFSA^-$] solutions, respectively.

Figure 7.5 shows the gelation time (t_{gel}) plotted against the concentration of [C_2ImH^+][$TFSA^-$] (c_{pIL}). It was found in this figure that I can successfully control the gelation time as a function of pIL concentration, enabling easy preparation of gas separation membranes containing a large amount (94 wt%) of IL. I point out here that acid-base reactions

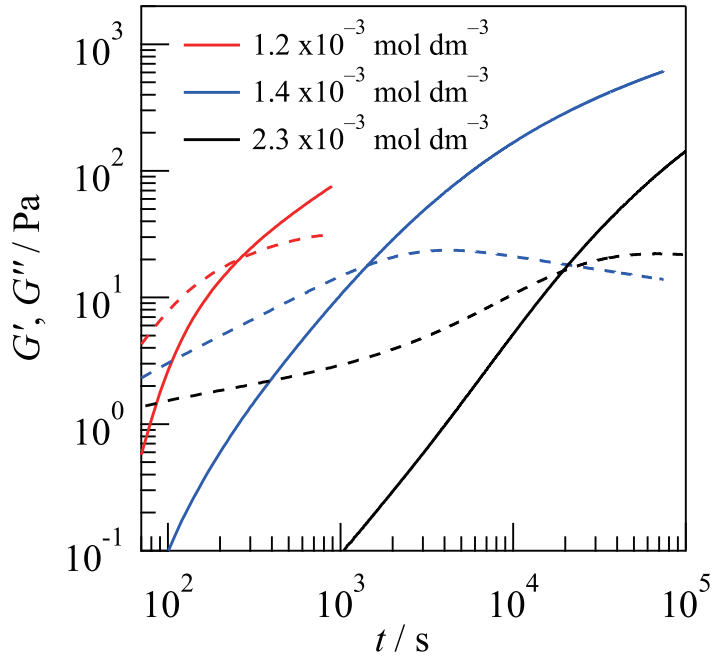

Figure 7.4. Dynamic moduli, G' (solid line) and G'' (broken line) plotted aginst reaction time, t, for the gelation of TetraPEG in $[C_2mIm^+][TFSA^-]$ with varying the concentration of pIL, $[C_2ImH^+][TFSA^-]$.

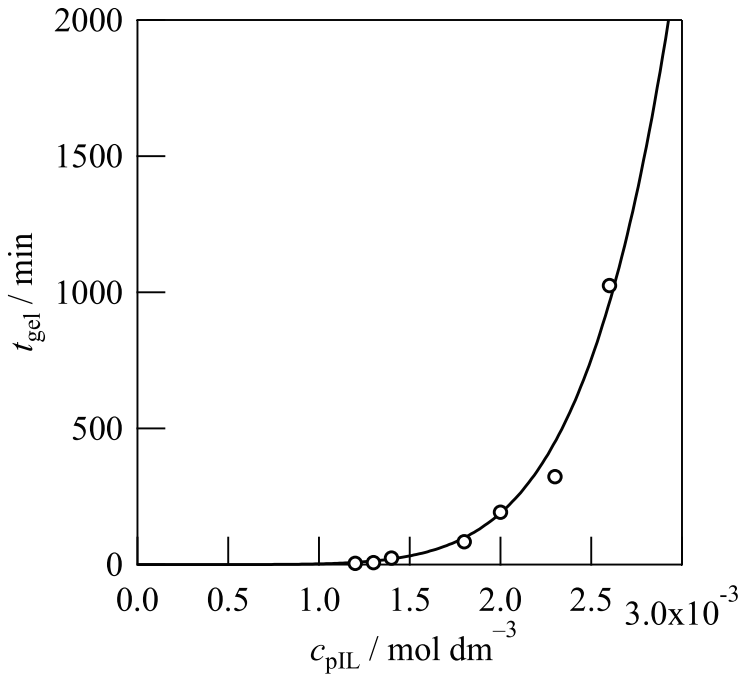

Figure 7.5. Gelation time (t_{gel}) determined by intersection of G' and G'' (rheological measurements) as a function of protic IL concentration (c_{pIL}). The arrows show the experimental points described in Figure 7.4.

of the terminal NH_2 group within TetraPEG in [C_2mIm$^+$][TFSA$^-$] aIL significantly affect the gelation time, which has been investigated by potentiometric titration in our recent work [15, 18]. The mechanical properties of the TetraPEG iongel obtained in this work were evaluated by stretching test, which is shown in Figure 7.6 (stretching stress-elongation curve).

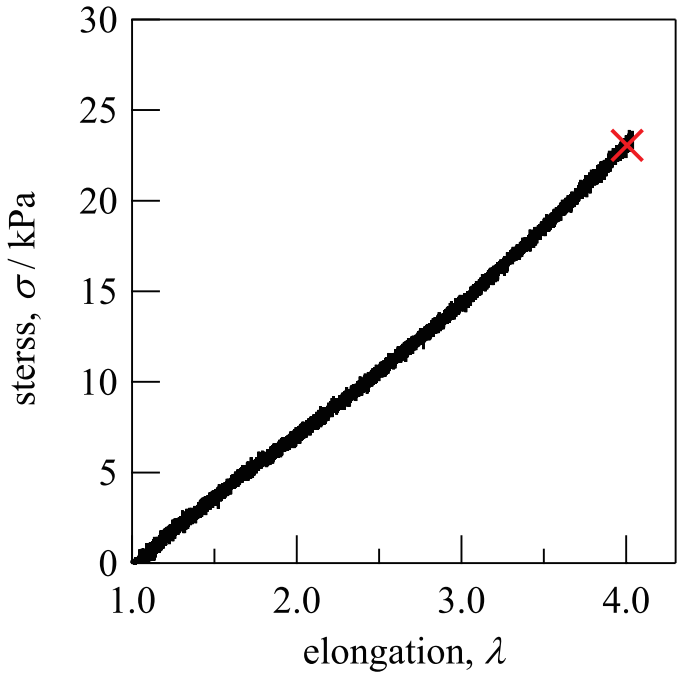

Figure 7.6. Stretching stress-elongation curve obtained for 6 wt% TetraPEG iongel. The (×) mark shows the breaking point.

The maximum breaking elongation, λ_{max} was over 4.0, which is larger than the high toughness iongels reported recently [10, 11]. The breaking stress was 24 kPa at $\lambda = 4.0$, and the elastic modulus was estimated to be 3.6 kPa.

7.3.2 CO_2 permselectivity

Figure 7.7 (a) shows the CO_2 permeability P_{CO_2} for the iongel membrane with varying temperature, together with those for the SILM of porous hydrophilic Teflon film filled with [C_2mIm$^+$][TFSA$^-$]. The CO_2 permeability for the TetraPEG iongel was 877 barrer at 25 °C and the value is approximately 1.4 times larger than that for the SILM. This might be ascribed to the difference of the cross-sectional area where gas molecules contact with IL, or the thickness change of the iongel during the measurement. The CO_2 permeability monotonically increased with rising temperature, indicating the increase of the CO_2 diffusion in the IL medium. Figure 7.7 (b) shows the CO_2/N_2 selectivity estimated from the permeabilities of

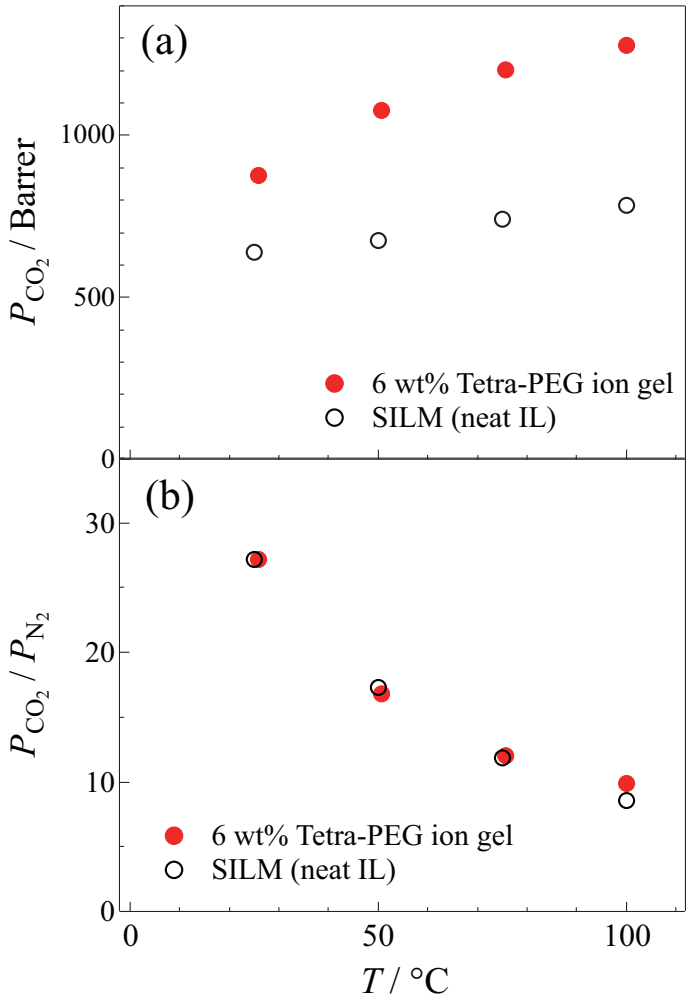

Figure 7.7. Temperature dependences of (a) the CO_2 permeabilty P_{CO_2}, and (b) the CO_2/N_2 selectivity P_{CO_2}/P_{N_2} for the 6 wt% TetraPEG + $[C_2mIm^+][TFSA^-]$ iongel, together with those for the corresponding SILM.

CO_2 and N_2, P_{CO_2}/P_{N_2}. The selectivity for the TetraPEG iongel decreased with increasing temperature, and the values at each temperature were almost similar to those for the SILM. According to a solution-diffusion transport mechanism, an ideal selectivity between two different gases (i, j) mainly depends on solubilities (S) and diffusion coefficients (D), i.e., $P_i/P_j = (S_i/S_j)(D_i/D_j)$. The result obtained here implies that both solubilities and diffusion coefficients of CO_2 and N_2 in the TetraPEG iongel are almost the same as those in the neat IL. I thus concluded that the support polymer, TetraPEG, does not hinder the gas separation performance at the temperatures examined because of the same selectivity in both iongel and SILM systems.

In order to obtain deeper insight on CO_2/N_2 permselectivity of TetraPEG iongel mentioned above, I extended our study to CO_2 absorption properties under high-pressure conditions. As

far as I know, this is the first report on the gas absorption for iongel under high pressures. Firstly, I carried out the volume expansion measurement for the TetraPEG iongel prepared in a capillary (diameter : 1.4 mm) by using an optical microscope. The volume expansion, V/V_0, was defined as a change of diameters between the iongels absorbing CO_2 (d) and without CO_2 (d_0), that is, $V/V_0 = (d/d_0)^3$. I assumed that the iongel isotropically expands with the absorption of CO_2.

7.3.3 CO_2 absorption selectivity

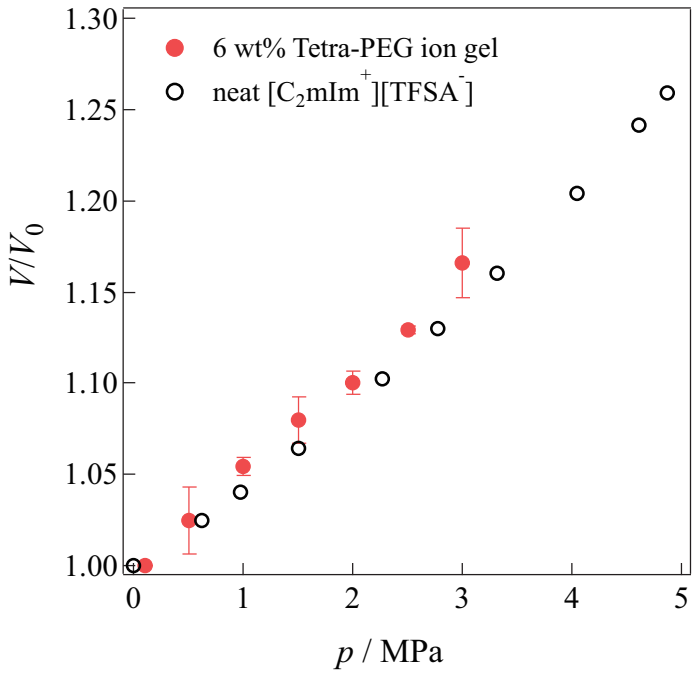

Figure 7.8. Volume expansion V/V_0 plotted against pressure p for the 6 wt% TetraPEG iongel + CO_2 (filled circles) and the corresponding neat IL + CO_2 (open circles) [19] systems.

Fig. 7.8 shows the V/V_0 as a function of CO_2 pressure at 298 K for the 6 wt% TetraPEG iongel. It was found that the TetraPEG iongel expands without solvent seeping-out of the gel even at the high-pressure examined. The V/V_0 for the iongel linearly increased with increasing pressure (the amount of CO_2 absorbed), and it is practically equal to that for the neat $[C_2mIm^+][TFSA^-]$ [19].

Figure 7.9 shows the pressure dependence of the CO_2 solubility (molarity scale) at 298 K. The experimental apparatus and procedure were described elsewhere [20]. The TetraPEG iongel can absorb CO_2 physically as much as the corresponding neat IL [19]. These results suggest the followings: (1) Liquid-like CO_2 absorption occurs in the solid-state iongel

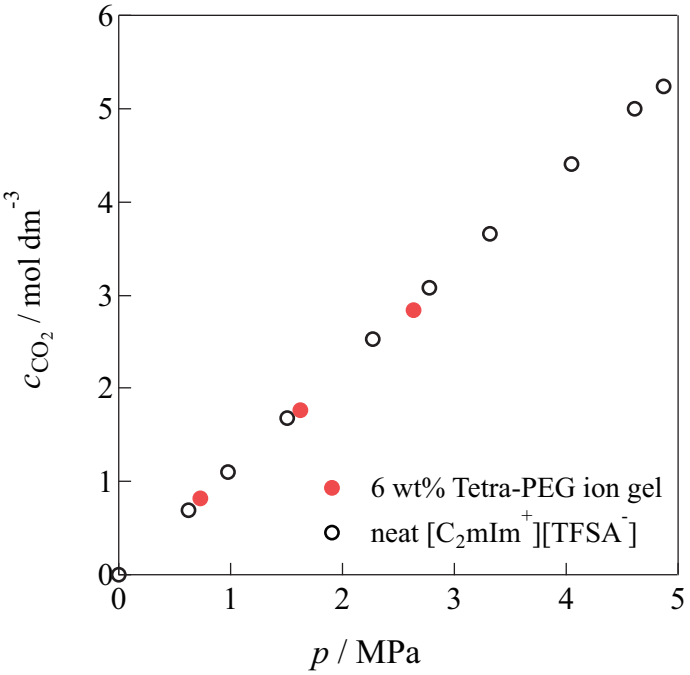

Figure 7.9. CO_2 solubilities cCO_2 plotted against pressure p for the 6 wt% TetraPEG iongel + CO_2 (filled circles) and the corresponding neat IL + CO_2 (open circles) [19] systems.

containing 94 wt% [C_2mIm$^+$][TFSA$^-$]; (2) TetraPEG as a support network does not interfere CO_2 absorption due to its low content in the iongel. I thus propose that the TetraPEG iongel shows the maximum CO_2 physical-absorption among polymer-IL composite materials, because IL physical absorbents without polymers absorb the largest amount of CO_2. A similar behavior was observed for the ionic conductivity in our previous work, that is, the conductivity of the TetraPEG iongel with low polymer contents was nearly equal to that of the neat IL [11].

7.4 Conclusion

High toughness TetraPEG iongel was prepared by controlling gelation time with addition of the protic IL to give the iongel membrane with a largest amount of IL (94 wt%) than any of polymer-IL membrenes in the literature. I demonstrated that the TetraPEG iongel membrane shows comparable CO_2/N_2 permselectivity to the corresponding SILM even in the high temperature range without any degradation. This exellent performance is derived from the good CO_2 absorption and diffusion properties, which are almost the same as those for the neat IL. The TetraPEG iongel absorbs CO_2 without solvent seeping under the pressure conditions up to 3 MPa. Again, the TetraPEG allows one to prepare a high toughness and thermally stable iongel membrane even with very low polymer concentrations. The low

polymer content in iongels is a key to maximize the potential of IL membranes. The present study may open up new possibilities for gas separation membrane under a wide range of temperatures and pressures. For practical use, much thinner membranes than the present one are required. Such trial to prepare thinner and tougher TetraPEG iongels can be achieved by optimizing the condition of the acid-base reaction, i.e., control of the gelation time and mechanical properties of iongel using pH-buffering method.

Reference

[1] L. A. Blanchard, D. Hancu, E. J. Beckman, and J. F. Brennecke. *Nature*, Vol. 399, pp. 28–29, 1999.

[2] J. E. Bara, T. K. Carlisle, C. J. Gabriel, D. Camper, A. A. Finotello, D. L. Gin, and R. D. Noble. *Ind. Eng. Chem. Res.*, Vol. 48, pp. 2739–2751, 2009.

[3] P. Scovazzo, J. Kieft, D. A. Finan, C. Koval, D. Dubois, and R. Noble. *J. Membr. Sci.*, Vol. 238, pp. 57–63, 2004.

[4] J. E. Bara, S. Lessmann, C. J. Gabriel, E. S. Hatakeyama, R. D. Noble, and D. L. Gin. *Ind. Eng. Chem. Res.*, Vol. 46, pp. 5397–5404, 2007.

[5] J. E. Bara, C. J. Gabriel, E. S. Hatakeyama, T. K. Carlisle, S. Lessmann, R. D. Noble, and D. L. Gin. *J. Membr. Sci.*, Vol. 321, pp. 3–7, 2008.

[6] Y. Gu and T. P. Lodge. *Macromolecules*, Vol. 44, pp. 1732–1736, 2011.

[7] P. Li, K. P. Pramoda, and T.-S. Chung. *Ind. Eng. Chem. Res.*, Vol. 50, pp. 9344–9353, 2011.

[8] S. Kasahara, E. Kamio, T. Ishigami, and H. Matsuyama. *Chem. Commun.*, Vol. 48, pp. 6903–6905, 2012.

[9] L. C. Tomé, D. Mecerreyes, C. S. R. Freire, L. P. N. Rebelo, and I. M. Marrucho. *J. Membr. Sci.*, Vol. 428, pp. 260–266, 2013.

[10] Y. Gu, S. Zhang, L. Martinetti, K. H. Lee, L. D. Mcintosh, C. D. Frisbie, and T. P. Lodge. *J. Am. Chem. Soc.*, Vol. 135, pp. 9652–9655, 2013.

[11] K. Fujii, H. Asai, T. Ueki, T. Sakai, S. Imaizumi, U. Chung, M. Watanabe, and M. Shibayama. *Soft Matter*, Vol. 8, pp. 1756–1759, 2012.

[12] H. Asai, K. Fujii, T. Ueki, S. Sawamura, Y. Nakamura, Y. Kitazawa, M. Watanabe, Y.-S. Han, T.-H. Kim, and M. Shibayama. *Macromolecules*, Vol. 46, pp. 1101–1106, 2013.

[13] K. Fujii, R. Kanzaki, T. Takamuku, Y. Kameda, S. Kohara, M. Kanakubo, M. Shibayama, S. Ishiguro, and Y. Umebayashi. *J. Chem. Phys.*, Vol. 135, p. 244502, 2011.

[14] K. Fujii, T. Nonaka, Y. Akimoto, Y. Umebayashi, and S. Ishiguro. *Anal. Sci.*, Vol. 24, pp. 1377–1380, 2008.

[15] K. Hashimoto, K. Fujii, and M. Shibayama. *J. Mol. Liquids*, Vol. 188, pp. 143–147, 2013.

[16] K. Nishi, K. Fujii, Y. Katsumoto, T. Sakai, and M. Shibayama. *Macromolecules*, Vol. 47, pp. 3274–3281, 2014.

[17] K. Nishi, K. Fujii, M. Chijiishi, Y. Katsumoto, U. Chung, T. Sakai, and M. Shibayama. *Macromolecules*, Vol. 45, pp. 1031–1036, 2012.

[18] K. Fujii, K. Hashimoto, T. Sakai, Y. Umebayashi, and M. Shibayama. *Chem. Lett.*, Vol. 42, pp. 1250–1251, 2013.

[19] T. Makino, M. Kanakubo, Y. Masuda, T. Umecky, and A. Suzuki. *Fluid Phase Equilib.*, Vol. 362, pp. 300–306, 2014.

[20] T. Makino, M. Kanakubo, T. Umecky, and A. Suzuki. *Fluid Phase Equilib.*, Vol. 357, pp. 64–70, 2013.

Chapter 8

Summary

The gelation process of homogeneous network prepolymer in ionic liquid was investigated from the view point of acid-base equilibrium in ionic liquids (Chapter 2,3 and 4) and gelation kinetics (Chapter 5, 6) to prepare high-toughness iongel with homogeneous network, which was successfully applied to a CO_2 separation study (Chapter 7). Through these investigation, I clearly elucidate (i) acidity and basicity in IL, (ii) the gelation mechanism in IL and (iii) CO_2 separation properties of iongels with ideal network. As mentioned in Chapter 1, solidification of ILs is one of the important subjects in application of ILs. Thus, TetraPEG iongel with ideal model network prepared by the control of the gelation proposed in this study is meaningful for further development of novel iongels. In addition, the knowledge of acid-base reaction in ILs including pH-buffering IL, suggested in this dissertation, is also useful to comprehend fundamental reactions in ILs, which essentially differs from those in conventional solvent systems. The details of the respective chapters are summarized below.

Chapter 2

The autoprotolysis reaction of $[C_nImH^+][TFSA^-]$ with $n = 2$ and 4 was investigated by potentiometric titration to directly and experimentally estimate the equilibrium constant, pK_s. The pK_s was appreciably larger than the corresponding ΔpK_a calculated by two pK_as for HA and HB^+ in aqueous system, which differs from the result for other pIL systems such as $[C_2NH_3{}^+][NO_3{}^-]$ etc. reported until now. From temperature dependence of the potentiometric titration, the reaction enthalpy in the autoprotolysis was determined in $[C_2ImH^+][TFSA^-]$. It was found that the reaction endothermerically undergoes and the enthalpy value is smaller than that for $[C_2NH_3{}^+][NO_3{}^-]$. To obtain more insight into the acid-base properties of pILs, the pK_s data should be accumulated in various pILs and discussed from thermodynamic aspect.

Chapter 3

The acid-dissociation constant, pK_a for $BuNH_3^+$ in aprotic [C_2mIm^+][$TFSA^-$] was successfully determined directly by using ISFET electrode to be 16.6(1). This value was significantly larger than the corresponding value for water (10.6), indicating that the $BuNH_2$ in aprotic ILs acts as a stronger Brønsted base than that in water. The value was compared with pK_a values in other non-aqueous solvents. However, there is no obvious relation between pK_a and conventional solvent parameters. To obtain more insight into the acid-base properties of solutes in IL systems, further knowledge of the thermodynamic and structural aspects of solvation in ILs is thus required.

Chapter 4

The solvation structures of $BuNH_2$ and $BuNH_3^+$ in [C_2mIm^+][$TFSA^-$] were investigated by HEXTS experiments and MD simulations and quantitatively discussed in terms of structural parameters such as distance, orientation, and coordination number for inter- and intramolecular interactions in the solutions to elucidate large pK_a value of $BuNH_3^+$. The experimental radial distribution functions, $r^2[G^{MD}(r) - 1]$, were well reproduced by theoretical ones derived from MD simulations for all of the systems examined here. It was found that the $BuNH_2$ and $BuNH_3^+$ molecules are preferentially solvated with the $TFSA^-$ anion rather than the C_2mIm^+ cation. We pointed out that the hydrogen bond between O_A (anion) and H_N ($BuNH_2$ or $BuNH_3^+$) is predominant in the solute–IL interaction due to a localized negative charge within four oxygen atoms of the anion. After protonation, the coordination number of $TFSA^-$ anion increased from 2 to 3, resulting in the large stabilization energy. Eventually, we concluded that drastic change of solvation structure results in large pK_a value.

Chapter 5

The gelation reaction of TetraPEG in [C_2mIm^+][$TFSA^-$] aIL was investigated in terms of gelation time, acid-base reaction of terminal NH_2 group of TetraPEG, and reaction efficiency. The gelation behavior of TetraPEG strongly depends on the [H^+] in the solution. We thus control the gelation reaction by adding [C_2ImH^+][$TFSA^-$] pIL as a proton source, in this work. The gelation time of TetraPEG in aprotic [C_2mIm^+][$TFSA^-$] can be successfully controlled by the pIL concentration, c_{pIL}, suggesting that the acid-base properties of terminal group of TetraPEG and pIL play a key role on in the gelation reaction. The acid dissociation constant, pK_a of protonated TetraPEG-NH_3^+ and C_2ImH^+ (pIL cation) is quantitatively determined in [C_2mIm^+][$TFSA^-$] aIL. The pK_a value for the TetraPEG-NH_3^+ (16.4) is

significantly larger than that of the C_2ImH^+, which indicates that most of H^+ in the system preferentially are bound to the NH_2 group within TetraPEG. The TetraPEG-$NH_3{}^+$ cannot react with TetraPEG-NHS to give the unreactive terminal groups. We thus conclude that the reaction efficiency or the extent of defects in the polymer network in TetraPEG iongel is essentially dominated by the concentration of TetraPEG-$NH_3{}^+$ depending on $[H^+]$ (or cpIL) in the solvent $[C_2mIm^+][TFSA^-]$.

Chapter 6

We proposed a "pH-buffering ionic liquid," i.e., an $[C_2mIm^+][TFSA^-]$ aIL solution with $[C_2ImH^+][TFSA^-]$ pIL (proton source) and its conjugated base, C_2Im, and applied it to the reaction field of homogeneous TetraPEG network formation. We demonstrated that the pH-buffering IL with $[C_2ImH^+][TFSA^-]/C_2Im$ = 1:10 exhibits a successful pH-buffering effect during the gelation reaction to give a constant solution pH ($\sim$ 16.2). From the kinetic aspect, the TetraPEG gelation reaction in the pH-buffering IL was characterized, and we found that (1) the gelation reaction proceeds as a second-order reaction, (2) the reaction rate constant ($k_{gel} = 7.8 \times 10^{-2}$ (mol dm^{-3})$^{-1}$ s^{-1}) is two orders of magnitude smaller than that in the corresponding hydrogel system, and (3) the gelation mechanism is likely a reaction-limited, rather than a diffusion-limited, process because of the much smaller k_{gel} value in the IL system than in the water system. The reaction efficiencies, the p values, corresponding to the extent of defects in the polymer network, were estimated to be 98% and 92%, as obtained by mechanical stretching tests and UV-vis spectroscopy, respectively. Note that these values are near ideal (i.e., 100%). We thus conclude that a pH-controlled reaction field, i.e., the pH-buffering IL proposed in this work, is essential to prepare a defect-free TetraPEG network iongel. This yields a high-toughness iongel with a low polymer concentration, good handling properties, and high performance, for use in applications such as electrochemical devices and gas-separation membranes.

Chapter 7

High-toughness Tetra-PEG iongels were prepared by controlling gelation time with addition of the protic IL to give the iongel membrane with a largest amount of IL (94 wt%) than any of polymer-IL membranes in the literature. We demonstrated that the Tetra-PEG iongel membrane shows comparable CO_2/N_2 permselectivity to the corresponding SILM even in the high temperature range without any degradation. This excellent performance is derived from the good CO_2 absorption and diffusion properties, which are almost the same as those for the neat IL. The Tetra-PEG iongel absorbs CO_2 without solvent sweeping under

the pressure conditions up to 3 MPa. In addition, the Tetra-PEG allows one to prepare a high toughness and thermally stable iongel membrane even with very low polymer concentrations. The low polymer content in iongels is a key to maximize the potential of IL membranes. The present study may open new possibilities for gas separation membrane under a wide range of temperatures and pressures. For practical use, much thinner membranes than the present one are required. Such trial to prepare thinner and tougher Tetra-PEG iongels can be achieved by optimizing the condition of the acid-base reaction, i.e., control of the gelation time and mechanical properties of iongel using pH-buffering method.

Publication List

Original Papers

1. K. Hashimoto, K. Fujii and M. Shibayama, ”Acid-Base Property of Protic Ionic Liquid, 1-Alkylimidazolium Bis(trifluoromethanesulfonyl)amide Studied by Potentiometric Titration”, *J. Mol. Liq.*, 188, 143 (2013) (Chapter 2)

2. K. Fujii, K. Hashimoto, T. Sakai, Y. Umebayashi and M. Shibayama, ”Brønsted Basicity of Solute Butylamine in an Aprotic Ionic Liquid Investigated by Potentiometric Titration”, *Chem. Lett.*, 42, 1250 (2013) (Chapter 3)

3. K. Hashimoto, K. Fujii, K. Nishi, T. Sakai, N. Yoshimoto, M. Morita and M, Shibayama, ”Gelation Mechanism of Tetra-Armed Poly(ethylene glycol) in Aprotic Ionic Liquid Containing Nonvolatile Proton Source, Protic Ionic Liquid”, *J. Phys. Chem. B.*, 119, 4795 (2015) (Chapter 5)

4. K. Hashimoto, K. Fujii, K. Nishi, T. Sakai and M, Shibayama, ”Nearly Ideal Polymer Network Iongel Prepared in pH-buffering Ionic Liquid System”, *Macromolecules*, accepted (2016). (Chapter 6)

5. K. Fujii, T. Makino, K. Hashimoto, T. Sakai, M. Kanakubo and M. Shibayama, ”Carbon Dioxide Separation Using a High-toughness Ion Gel with a Tetra-armed Polymer Network”, *Chem. Lett.*, 44, 17 (2015) (Chapter 7)

The contents in this doctoral dissertation are based on the original papers listed above.

Other Publications

1. K. Nishi, T. Hiroi, K. Hashimoto, K. Fujii, Y. S. Han, T. H. Kim, Y. Katsumoto and M. Shibayama ”SANS and DLS Study of Tacticity Effects on Hydrophobicity and Phase Separation of Poly(*N*-isopropylacrylamide)”, *Macromolecules*, 46, 6225 (2013)

2. T. Kusano, K. Fujii, K. Hashimoto and M. Shibayama ”Water-in-Ionic Liquid Microemulsion Formation in Solvent Mixture of Aprotic and Protic Imidazolium-Based Ionic Liquids”, *Langmuir*, 30 11890 (2014)

3. K. Hirosawa, K. Fujii, K. Hashimoto, Y. Umebayashi, and M. Shibayama ”Microscopic Solvation Structure of Glucose in 1-Ethyl-3methylimidazolium Methylphosphonate Ionic Liquid”, *J. Phys. Chem. B.*, 119, 6262 (2015)

Acknowledgements

This thesis is based on the study carried out in the research group of Professor Mitsuhiro Shibayama at Department of Advanced Materials Science, Graduate School of Frontier Sciences, The University of Tokyo from 2011 to 2016.

First of all, I would like to express my sincere gratitude to **Professor Mitsuhiro Shibayama** for giving many chances and research environment throughout my life in laboratory. Especially, he taught me attitudes towards science. I really appreciate his instruction.

I am deeply grateful to thank **Associate Professor Kenta Fujii** for guiding me into solution chemistry and ionic liquid science. With his helps, I could accomplish this study. His vast knowledge on chemistry and positive attitude on research and life always encourage and help me. I am very pleased with his promotion and consistent enthusiasm for research.

I would like to thank **Dr. Takashi Makino** and his colleagues at AIST for collaborative research on CO_2 separation experiments. The results for these experiments owe to his support and knowledge about CO_2 separation study.

I would like to thank **Associate Professor Takamasa Sakai** and members of Tei and Sakai laboratory for the kind advices on synthesis and characterization of Tetra-PEG gel. I am very grateful for their kind help.

I would like to thank **Dr. Hanako Asai**, **Dr. Nishi Kengo** and **Dr. Takumi Kusano** for the kind advices on both experments and life in my laboratory. They taught me how to perform experiments and presentations as a researcher, and I am very grateful for that.

I would also like to thank my colleagues of all present and past members of Shibayama laboratory and all the staff of the Institute for Solid State Physics, the University of Tokyo, for their kind cooperation.

March, 2016
Kei Hashimoto